AD-A138 296 METASTABLE TRANSITION METAL ALLOYS PRODUCED BY RAPID 1/2
QUENCHING: STRUCTURE..(U) NORTHEASTERN UNIV BOSTON MA
BARNETT INST OF CHEMICAL ANALYSIS.. B C GIESSEN JAN 84
UNCLASSIFIED N00014-76-C-0820 F/G 11/2 NL

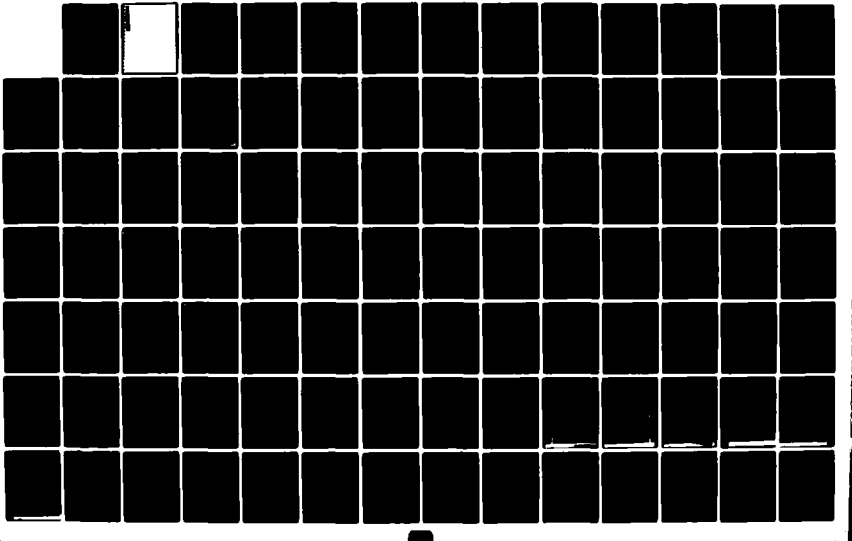

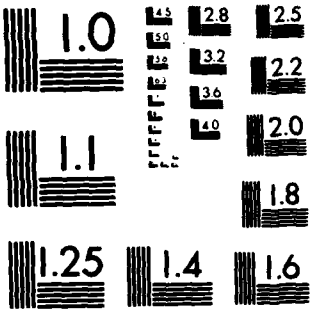

Unclassified

SECURITY CLASSIFICATION OF THIS PAGE (When Data Entered)

REPORT DOCUMENTATION PAGE		READ INSTRUCTIONS BEFORE COMPLETING FORM
1. REPORT NUMBER N 0014-76-C-0820-F	2. GOVT ACCESSION NO. AD A138296	3. RECIPIENT'S CATALOG NUMBER
4. TITLE (and Subtitle) METASTABLE TRANSITION METAL ALLOYS PRODUCED BY RAPID QUENCHING: STRUCTURE AND PROPERTIES		5. TYPE OF REPORT & PERIOD COVERED Final Apr. 1, 1976 to June 30, 1980 6. PERFORMING ORG. REPORT NUMBER
7. AUTHOR(s) Bill C. Giessen		8. CONTRACT OR GRANT NUMBER(s) N00014-76-C-0820
9. PERFORMING ORGANIZATION NAME AND ADDRESS Barnett Institute of Chem. Anal. & Maters. Sci. Northeastern University Boston, Massachusetts 02115		10. PROGRAM ELEMENT, PROJECT, TASK AREA & WORK UNIT NUMBERS NR 039-131
11. CONTROLLING OFFICE NAME AND ADDRESS Leader, Materials Division Office of Naval Research, Code 431 800 N. Quincy St., Arlington, VA 22217		12. REPORT DATE January 26, 1983 13. NUMBER OF PAGES 111
14. MONITORING AGENCY NAME & ADDRESS (if different from Controlling Office)		15. SECURITY CLASS. (of this report) Unclassified 15a. DECLASSIFICATION/DOWNGRADING SCHEDULE

16. DISTRIBUTION STATEMENT (of this Report)

Reproduction in whole or in part is permitted for any purpose of the United States Government. Distribution of this document is unlimited.

17. DISTRIBUTION STATEMENT (of the abstract entered in Block 20, if different from Report)

18. SUPPLEMENTARY NOTES

19. KEY WORDS (Continue on reverse side if necessary and identify by block number)

Rapid Solidification Processing, Rapid Quenching, Melt Spinning, Amorphous Metals, Metallic Glasses, Glass Formation in Alloys, Transition Metal Alloys, Metastable Alloys, Alloy Phases, Refractory Metals, Thermal Analysis, Electrical Conductivity, Magnetism, Crystallization, Mechanical Properties

20. ABSTRACT (Continue on reverse side if necessary and identify by block number)

Metastable transition metal alloys, primarily, metallic glasses, were prepared by rapid solidification processing (melt spinning and arc-furnace hammer-and-anvil quenching); appropriate properties of these alloys were investigated.

Specifically, glassy alloys containing transition metals such as Ti,Zr,Nb, Ta,Ni,Rh and Ir, as well as metals such as U,Ca and Cu and non-metallic additives such as O were studied; many of these glasses were prepared in this program for the first time. Properties studied included thermal stability (glass transition temperature and crystallization temperature), elastic-

Cont'd

DD FORM 1 JAN 73 1473 EDITION OF 1 NOV 65 IS OBSOLETE
S/N 0102-014-6601

Unclassified

SECURITY CLASSIFICATION OF THIS PAGE (When Data Entered)

20. (cont'd)
modulus (measured by a newly adapted dynamic technique of impulse induced resonance), microhardness, and electrical transport (resistivity and thermoelectricity). Alloy constitution was studied. Rules for the prediction of ready glass formation based on alloy properties were formulated; a universal correlation between microhardness and elastic modulus was described. A new multilayer melt spinning technique was implemented.

Nineteen publications resulted from this program and are listed in the report.

A-1

Report Number: N 0014-76-C-0820-F

Final Report

to

Office of Naval Research

Contract No. N 0014-76-C-0820

Metastable Transition Metal Alloys Produced by Rapid Quenching: Structure and Properties

B. C. Giessen

Barnett Institute of Chemical Analysis and Materials Science
and
Department of Chemistry
Northeastern University
Boston, Massachusetts 02115

SUMMARY OF RESEARCH PROGRAM AND RESULTS

The principal objective of this program was the systematic determination of the formation and thermal, mechanical and electronic properties of several groups of new metallic glasses containing transition metals prepared by rapid solidification processing. The focus was on properties that could be related to the bonding character of the glasses; this includes studies of thermal stability (both with respect to glass transition and crystallization), mechanical strength, as expressed by elasticity (Young's modulus) and plasticity (microhardness), electrical transport (resistivity and thermoelectricity) as well as other associated properties. Ready glass formation (RGF) upon quenching is an alloy property important in this context; it was studied exhaustively in several systems. RGF was shown to be related to bond strength via a relationship with the heat of formation and atomic size ratio which was developed in the course of this program. Alloy constitution studies were carried out; novel processing and property measurement techniques were developed.

Results of the program are documented in the appended list of Publications credited to this program. Highlights of these research results are given in the following:

New families of metallic glasses containing transition metals were investigated and their properties were established; alloys studied fell into four main categories:

Alloys containing actinide metals,especially uranium (1,14);

Alloys containing refractory metals (3);

Alloys containing simple (alkaline earth) metals (4);

Alloys containing intertransition metal combinations (5,7).

Special emphasis was placed on mechanical properties: elastic modulus measurements were carried out using a new dynamic pulse technique (IIR method) (8,9), and plastic properties (microhardness) were determined and correlated

with elastic properties (17).

Electronic properties measured included the magnetism of rare earth alloy glasses (11) and thermoelectric power (12,16).

The effect of oxygen additions on glass stability was investigated (2).

Alloy constitution and alloy phase structure were studied (6,10,18).

A novel method of rapid solidification processing for thick ribbons was described (13).

Fundamental models of ready glass forming ability were formulated and investigated (15).

PUBLICATIONS

1. B.C. Giessen and R.P. Elliott: Properties of Metallic Glasses Containing Actinide Metals: I. Thermal Properties of U-M Glasses (M = V, Cr, Mn, Fe, Co and Ni), in Rapidly Quenched Metals III, Vol. 1, B. Cantor, ed., The Metals Society, London, p. 406 (1978).

2. D.E. Polk, C.E. Dube and B.C. Giessen: The Effect of Oxygen Additions on the Properties of Amorphous Transition Metal Alloys, in Rapidly Quenched Metals III, Vol. 1, B. Cantor, ed., The Metals Society, London, p. 220 (1978).

3. S. Davis, M. Fischer, B.C. Giessen and D.E. Polk: Formation and Properties of Refractory Metal Glasses II: T_5- T_3 Glasses (T_5 = Nb, Ta; T_3 = Rh, Ir) in Rapidly Quenched Metals III, Vol. 2, B. Cantor, ed., The Metals Society, London, p. 425 (1978).

4. B.C. Giessen, J. Hong, L. Kabacoff, D.E. Polk, R. Raman and R. St. Amand: Compositional Dependence of the Thermal Stability and Related Properties of Metallic Glasses I: T_g for $Ca_{.65}M_{.35}$ and $Zr_{.475}Cu_{.475}M_{.05}$ Glasses, in Rapidly Quenched Metals III, Vol. 1, B. Cantor, ed., The Metals Society, London, p. 249 (1978).

5. R. St. Amand B.C. Giessen: Easy Glass Formation in Simple Metal Alloys: Amorphous Metals Containing Calcium and Strontium, Scripta Met., 12, 1021 (1978).

6. B.C. Giessen, J.C. Barrick and L. Tanner: Formation and Structure of a New η Phase, $Ti_3Be_3(O,N)_x$, Mater. Sci. Eng., 38, 211 (1979).

7. A.J. Kerns, D.E. Polk, R. Ray and B.C. Giessen: Thermal Behavior of Zr-Cu Metallic Glasses, Mater. Sci. Eng., 38, 49 (1979).

8. S.H. Whang, L.T. Kabacoff, D.E. Polk and B.C. Giessen: Measurement of Young's Modulus on Small Samples of Amorphous Metals Using the Impulse Induced Resonance Technique, Met. Trans. A, 10A, 1789 (1979).

9. S.H. Whang, L.T. Kabacoff, D.E. Polk and B.C. Giessen: A Technique for the Measurement of Young's Modulus of Small Metallic Glass Samples, J. Mat. Sci., 15, 247 (1980).

10. B.C. Giessen, N.J. Grant, D.P. Parker, R.C. Manuszewski and R.M. Waterstrat: The Niobium (Columbium) Palladium Constitution Diagram, Met. Trans. 11A, 709 (1980).

11. B.C. Giessen, W.A. Hines and L. Kabacoff; Magnetic Properties of Amorphous $RE_{.65}Al_{.35}$ Alloys, Proc. 18th IEEE International Magnetics Conference, Boston, AIP Conference Proceedings, in IEEE Transactions on Magnetics, MAG-16, p. 1203 (1980).

12. S. Basak, S.R. Nagel and B.C. Giessen: Thermoelectric Power of Magnetic and Nonmagnetic Amorphous Metals, Phys. Rev. B, 21, 4049 (1980).

13. B.C. Giessen, S. Davis, S. Whang and B.H. Kear: Preparation of Metallic Glasses in Thick Ribbons by a Multi-Layer Melt Spinning Process, in: Rapid Solidification Processing, Vol. II, R. Mehrabian, B.H. Kear and M. Cohen, Eds., Claitor's Publ. Div., Baton Rouge, LA, p. 237 (March 1980).

14. R.O. Elliott, D.A. Koss and B.C. Giessen: On the Characteristics of Amorphous U-Fe Alloys Formed by Liquid Quenching vs. Irradiation Techniques, Scripta Met., 14, 1061 (1980).

15. B.C. Giessen and S.H. Whang: Formation and Characterization of Amorphous Metals, Proc. 4th Int. Conf. on Liquid and Amorphous Metals, (LAM 4) Grenoble, Journal de Physique - Colloque C-8, 41, p. C8-95 (1980).

16. J.P. Carini, S. Basak, S.R. Nagel, B.C. Giessen and C.L. Tsai: The Thermoelectric Power of the Metallic Glass $Ca_{0.8}Al_{0.2}$, Phys. Letters, 81A(9), 525 (1981).

17. S.H. Whang, D.E. Polk and B.C. Giessen: Hardness vs. Young's Modulus of Metallic Glasses, in Proc. Fourth Internat. Conf. on Rapidly Quenched Metals, Sendai, (1981), Vol. 2, T. Masumoto and K. Suzuki, eds., The Japan Institute of Metals, Sendai, p. 1365.

18. R. Waterstrat and B.C. Giessen, Alloy Chemical Comparison of the Refractory Metal - Noble Metal Phase Diagrams T_5-T_{10} (T_5 = V, Nb, Ta; T_{10} = Pd, Pt), in Alloy Phase Diagrams, Mater. Res. Soc. Symp. Proc. Vol. 19, L.H. Bennett, T.B. Massalski, and B.C. Giessen, eds., North Holland, N.Y., p. 423 (1983).

19. B.C. Giessen, Crystal Chemistry of Metastable Alloy Phases, in Alloy Phase Diagrams, Mater. Res. Soc. Symp. Proc. Vol. 19, L.H. Bennett, T.B. Massalski, and B.C. Giessen, eds., North Holland, N.Y., p. 263 (1983).

From Rapidly Quenched Metals III, Vol.1,
B. Cantor, ed., The Metals Society, London,
(1978).

(C27)

PROPERTIES OF METALLIC GLASSES CONTAINING ACTINIDE METALS:

I. THERMAL PROPERTIES OF U-M GLASSES (M = V, Cr, Mn, Fe, Co, and Ni)

B.C. Giessen[+] and R.O. Elliott[*]

[+] Department of Chemistry, Northeastern University, Boston, Massachusetts, USA 02115

[*] University of California, Los Alamos Scientific Laboratory, Los Alamos, New Mexico, USA 87545

Introduction

On the basis of alloy chemical factors found to be active in metallic glass formation[1] there was reason to expect that binary alloys consisting of one or more of the actinide metals Th, U, Np and Pu on the one side and suitable addition elements such as transition metals (M) from the V, Cr, Mn, Fe, Co, and Ni groups on the other would form glasses upon rapid quenching from the melt at moderately high cooling rates. The previously reported metallic glasses containing Th, such as Th-Fe,[2] and glasses rich in U, such as U-Cr and U-V[3] provided examples for this family of amorphous metals. More recently metallic glasses have been prepared in thirteen additional actinide alloy systems, among them the first ones to be reported that contain Np or Pu.[4] In that report, nearest neighbor distances deduced from XRD patterns were given and factors active in actinide glass formation were discussed. Glass formation in alloys of U, Np and Pu was ascribed[4] to the low melting points T_m of these elements (compared to their boiling points);[5] the low T_m values in turn are thought to be related to the f-electron bonding present in these metals.[6] It was also observed[4] that metallic glasses containing U form more readily than the corresponding Pu glasses; this difference was ascribed to the lower concentrations of M at the eutectic compositions in the Pu-M alloy systems.[7]

In the present paper the results of a preparative and calorimetric study forming part of a continuing investigation of the new actinide glasses are reported. Specifically, lower bounds for the composition limits of glass formation (G.F.) at moderate cooling rates have been obtained for the U-M (M = Mn, Fe, Co, Ni) systems and the thermal stabilities of glasses in these four systems as well as for a U-V glass and a U-Cr glass have been surveyed.

The four U-M phase diagrams for M = Mn, Fe, Co, and Ni are quite similar to each other; all contain peritectically melting U_6M phases on the U-rich side and relatively more stable, congruently melting Laves phases UM_2 on the M-rich side; in addition, the U-Co and U-Ni systems contain additional phases such as UCo and UNi_x, respectively, in the central composition range which is of interest here.[4,7] The U-V and U-Cr systems are simpler; their constitution diagrams show eutectics formed by γ-U and V or Cr, respectively.[7]

Experimental Methods

The preparative techniques used have been discussed in Ref. 4; they included arc-melting and arc furnace quenching in glove box systems, followed by XRD examination (Cu K_α radiation) and DSC studies in a Perkin-Elmer DSC-2 calorimeter, carried out at 40 K/min. Some glass transitions were tentatively identi-

fied; their temperatures were obtained by the onset method rather than the mid-point method.[8]

XRD studies of the alloys after various stages of heat treating in the DSC unit have been delayed by the need for precautions required in the handling of samples prepared and treated in radioactively "hot" equipment; however, such studies are in progress.

Results

Table 1 lists the structures of the rapidly quenched alloys and the thermal effects observed; the latter are plotted for the four systems U-M with M = Mn, Fe, Co, and Ni in Fig. 1.

Glass Forming Ranges

Table 1 shows that the U-rich limit of the region of easy G.F. for the U-Mn and U-Fe systems is at < 20 at.pct. for either Mn or Fe; for the U-Co and U-Ni systems the U-rich limit lies between 20 and 27 at.pct. for either Co or Ni. (However, a small amount of amorphous material sufficient in quantity to obtain thermal data was also retained at 20 at.pct. Co or Ni.) The upper limits of the region of easy G.F. lie above 35.3 at.pct. Mn and 40 at.pct. Fe, Co, and Ni, respectively. For the remaining two systems, U-V and U-Cr, glass formation had been reported to occur between 20 and 40 at.pct. V and Cr;[3] however, in the present study the alloy at 27 at.pct. V was found to contain only small amounts of glass. The alloy at 27 at.pct. Cr was *amorphous, as reported.* In several of the alloys which were not completely amorphous (Table I), crystalline phases were found that were not among the known equilibrium phases; it would be of interest to identify these along with any transition phases forming in the course of the crystallization of the glasses. In the U-Fe and U-Co systems, metastable extensions of the intermediate U_6M phases (M = Fe, Co) were found, indicating metastable composition ranges of these phases of $\gtrsim$6 at.pct. M, up to >20 at.pct. M.

Thermal Data Given by System

The most important results of the present work concern the thermal stabilities of the glasses in the six binary U alloy systems studied. In the number of exothermic effects and the composition dependence of the T_c values, the U-Fe and U-Co glasses show very similar behavior. The U-Mn and U-Ni systems, however, have thermal characteristics different from those of the other two. For the systems U-V and U-Cr in which only one composition has been studied to date, the thermal characteristics are again similar. We briefly discuss these systems, following their order in the periodic table.

For $U_{.73}V_{.27}$ and $U_{.73}Cr_{.27}$, there are single strong exotherms, which presumably correspond to the reaction: glass → α-U + M (M = V, Cr), in accordance with the absence of intermediate phases in these systems. As the quenched $U_{.73}V_{.27}$ alloy also contains a large amount of metastable γ-U(V) solid solution, transformation of γ may be involved in this reaction.

The U-Mn alloys show two major exotherms: the first one, T_{c1}, occurs between 578 and 605 K with no clear composition dependence; the second, T_{c2}, occurs at temperatures which increase rapidly with increasing Mn content.

Both the U-Fe and U-Co systems show single exotherms for the more U-rich glasses and double exotherms for the glasses less rich in U; as observed frequently in such cases,[9,10] there are continuous transitions between both regimes, occurring approximately at $U_{.67}Fe_{.33}$ and $U_{.73}Co_{.27}$, respectively. In the U-Co system there are, in addition, weak exotherms at 20 and 27 at.pct. Co.

Besides the exotherms, endotherms were seen for the $U_{.73}Fe_{.27}$ and $U_{.67}Co_{.33}$ glasses; however, additional study will be required to distinguish whether these endotherms correspond to glass transitions or whether they are artifacts related to possible exothermic relaxation effects occurring at lower temperatures.

The U-Ni glasses were characterized by double and, at lower U contents, triple crystallization effects. As the alloy $U_{.88}Ni_{.28}$ was largely crystalline, the data collected for this alloy (Table 1) are not included in Fig. 1.

Discussion

Composition Dependence of Thermal Stability

In three of the four systems where comparisons of different compositions were possible (U-Fe, U-Co, and U-Ni), the thermal stabilities increase with increasing contents of the alloying elements M; only for U-Mn the present data are inconclusive in this regard. The results for the three systems are in line with observations on many binary metal-metal[10,11] and metal-metalloid glasses,[9,11] where the thermal stability generally increases with increasing contents of the component having the smaller size and higher elastic constant.

Further, the U-Fe and U-Co systems permit an extrapolation of the crystallization temperature to unalloyed uranium, obtained as $T_c(U) \sim 530 \pm 20$ K. This value, however, would apply only for a hypothetical U glass with a structure comparable to those of the binary U-M glasses.

Dependence of Thermal Stability on Alloying Element M

Perhaps the most interesting result contained in the present data concerns the change of T_{c1} with M. The T_{c1} for $U_{.73}M_{.27}$ glasses are presented in Fig. 2. The curve shows a stability maximum for glasses with M = Cr and a minimum for glasses with M = Fe and Co.

It is of interest to try to find correlations of the thermal stability (a) with other properties of the glass itself, (b) the phase diagram, and (c) properties of the alloying elements M, the latter especially with a view toward finding relations having a predictive quality. However, the existence of such correlations is uncertain for crystallization temperatures, as the crystallization products change discontinuously from system to system. [As pointed out,[9,12] such correlations are more likely to exist for glass transition temperatures; however, it is not clear whether T_g data can be collected for actinide glasses, (see above).]

We review the correlations of types (a) - (c) which were obtained for the present data on U glasses. As to (a), other property measurements, e.g. elastic moduli, are not yet available for the U glasses. Regarding (b), phase diagram features, the best-fitting correlation seen in analogous families of glass forming systems (such as those containing Ca[10] or refractory metals[13]) is that between T_{c1} and T_E, the lowest eutectic temperature in the glass forming region; a straight line relation with a ratio $T_{c1}/T_E \sim 0.56$ has been observed in such systems. While the crystallization temperatures for M = Fe, Co, and Ni lie close to this line (see the values for T_{c1}/T_E given in Table 1), for the $U_{.73}Cr_{.27}$ glass and the $U_{.73}Mn_{.27}$ glass (by interpolation) T_c lies above the straight line and for the $U_{.73}V_{.27}$ glass T_c lies below it.

The positive departure of T_c for the U-Cr glass from the straight line is probably related to the low T_E of U-Cr alloys relative to the melting point of Cr; the low T_E is primarily due to the absence of the intermetallic phases common to the other U-M systems with M = Mn, Fe, Co and Ni. [We comment parenthetically that the high T_{c1} and low T_g of U-Mn combine to produce a small supercooling

interval T_E-T_{c1} for alloys near the eutectic composition, thus providing a rationale for the observed, rather good G.F. ability of U-Mn glasses.] The negative departure of T_c for the U-V glass from the straight line, on the other hand, may be due to a too large value for the T_E which is due to the extensive solid solubility of V in γ-U, as compared to the other U systems. This solid solubility is made possible by the relatively small size difference between U and V.

As to (c), correlations of T_{c1} with elemental properties, a correlation of T_{c1} with elastic constants of the constituents and the atomic volume of M was tentatively identified. Figure 2 shows a plot of $\bar{E} \cdot V_M$, where $\bar{E}$ is the weighted average of the Young's moduli of the constituents and V_M is the atomic volume of M. [The V_M used here are those appropriate for the transition elements M = Mn, Fe, Co, and Ni in dilute solutions or in intermetallic phases with a low content of these M metals; these V_M differ from the elemental values which contain magnetic contributions.[14]]

Both sets of points plotted in Fig. 2 are similar in their overall change with M, suggesting a relationship between T_{c1} and $\bar{E} \cdot V_M$. However, while there is reason to expect some such relationship to exist,[15] the origin of the expression $\bar{E} \cdot V_M$ found to be usable here is not clear; this relation may not be confirmed if further data are considered and can therefore not be generalized at this time.

Conclusions

The ease of glass formation in actinide alloy systems suggests that comparative studies extending that reported here and including mechanical properties will be fruitful in leading to an understanding of the factors active in this particular category of metallic glasses.

Acknowledgement

One of us (B.C.G.) acknowledges support of this work by the Department of Energy under subcontract with the Lawrence Livermore Laboratory. We thank Dr. D.E. Polk for helpful discussions.

References

1. D.E. Polk and B.C. Giessen, in *Metallic Glasses*, J.J. Gilman and J.H. Leamy, Eds., p. 1, 1978, Metals Park, OH, Amer. Soc. Metals.
2. M. Segnini, Ph.D. Thesis, 1972, Boston, MA, Northeastern University.
3. R. Ray and E. Musso, U.S. Patent No. 3,981,722, September 1976.
4. R.O. Elliott and B.C. Giessen, Acta Met., submitted.
5. B. Johansson, in Proc. 2nd Intl. Conf. Electron Structure of the Actinides, p. 49, 1977, Wroclaw, Poland, Ossolineum.
6. E.A. Kmetko and H.H. Hill, J. Phys. 1976, F 6, 1025.
7. M. Hansen, Constitution of Binary Alloys, 2nd ed., 1958, New York, NY, McGraw-Hill.
8. A.J. Kerns, D.E. Polk, R. Ray and B.C. Giessen, Mater. Sci. Eng., submitted.
9. R. Ray, R. Hasegawa, C.P. Chou and L.A. Davis, Scripta Met. 1977, 11, 973.
10. R. St.Amand and B.C. Giessen, Scripta Met., submitted.
11. H.S. Chen and J.T. Krause, Scripta Met. 1977, 11, 761.
12. B.C. Giessen, J. Hong, L. Kabacoff, D.E. Polk, R. Raman, and R. St.Amand, in Proc. 3rd Intl. Conf. on Rapidly Quenched Metals (Brighton, 1978).
13. S. Davis, M. Fischer, B.C. Giessen, and D.E. Polk, in Proc. 3rd Intl. Conf. on Rapidly Quenched Metals (Brighton, 1978).
14. W.B. Pearson, The Crystal Chemistry and Physics of Metals and Alloys, p. 156, New York, NY, Wiley-Interscience.
15. B.C. Giessen and F. Spaepen, to be published.

Table 1

Results of Differential Scanning Calorimetry of Arc-Quenched U-M (M = V, Cr, Mn, Fe, Co, and Ni)
(Heating rate $\dot{T}$ = 40 K/min)

Composition (at.pct. M)		Structure after Arc-Quenching[a]	Equilibrium Structure	Exothermic Effects (K) and Est. ΔH (% of total $\Delta H_{cryst.}$) 1.	2.	3.	Endothermic Effect (K) (Tentative)	T_E (K)	$T_E - T_{C1}$ (K)	T_{C1}/T_E
27	V	γ-U s.s.+A.M.(minor) + α-U (?)(minor)	γ-U+V	658 (100);	-	-	-	1313	655	0.50
27	Cr	A.M.	γ-U+Cr	684 (100);	-	-	-	1132	448	0.60
20	Mn	A.M.+α-U+U_6Mn(trace)	U_6Mn+UMn_2	578 (24)[b];	642 (76)[b];	-	-	989		
25.5	Mn	A.M.+U_6Mn(?)+U.P.(trace)	"	605 (46)[b];	695 (54)[b];	-	-	"	384	0.61
30	Mn	A.M.+U.P.(trace)	"	605 (75)[b];	677 (25)[b];	-	-	"		
35.3	Mn	A.M.+U.P.(trace)	"	593 (50)[b];	745 (50)[b];	-	-	"		
20	Fe	A.M.+U_6Fe s.s.(minor)	U_6Fe+UFe_2	553 (100);	-	-	541	998		
27	Fe	A.M.+U_6Fe s.s.(minor)	"	560 (100);	-	-	527	"	438	0.56
33	Fe	A.M.+U_6Fe s.s.(trace)	"	566 (100);	-	-	-	"		
40	Fe	A.M.+U.P.(trace)	"	560 (32);	584 (68);	-	-	"		
20	Co	U_6Co s.s.+A.M.(minor)	U_6Co+UCo	545 (85);	575 (5) ;	585 (10)	-	1007		
27	Co	A.M.+U_6Co s.s.(trace)	"	554 (55);	593 (13);	578 (30)	527	"	452	0.55
33	Co	A.M.+U.P.	"	554 (40);	573 (60);	-	533	"		
40	Co	A.M.+U.P.	"	555 (25);	588 (75);	-	536	"		
20	Ni	α-U+U.P.(trace)+ A.M.(trace)	U_6Ni+UNi_x	613 (21)[b,d];	645 (79)[b,d];	-	593	1013		
27	Ni	A.M.+α-U(minor)	"	577 (-)[c];	632 (-)[c];	693 (-)[c]	-	"	436	0.57
33	Ni	A.M.+U.P.(trace)	"	599 (20);	641 (38);	677 (42)	-	"		
40	Ni	A.M.+U.P.(minor)	"	613 (15);	663 (75);	683 (12)	-	"		

Notes: a s.s. = solid solution; U.P. = unidentified crystalline phase; A.M. = amorphous metal.
b Averages of two measurements.
c ΔH_3 and hence ΔH_{total} not obtained; $\Delta H_1/\Delta H_2$ = 38/62.
d Alloy largely crystalline; exotherms not plotted in Fig. 1.

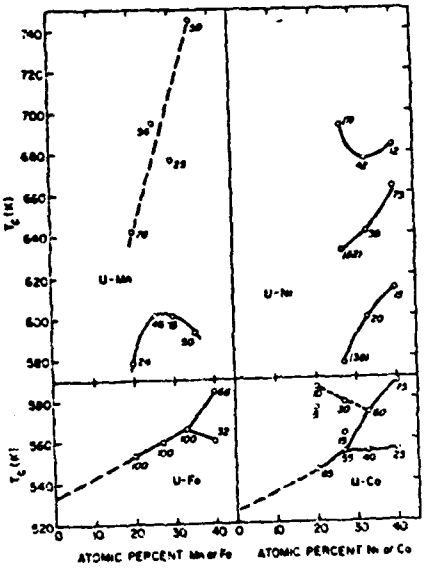

Figure 1. Temperatures of major exothermic effects as a function of composition for U-M glasses, where M=Mn, Fe, Co, and Ni (Numbers near each data point show estimated percentages of ΔH_{cryst}).

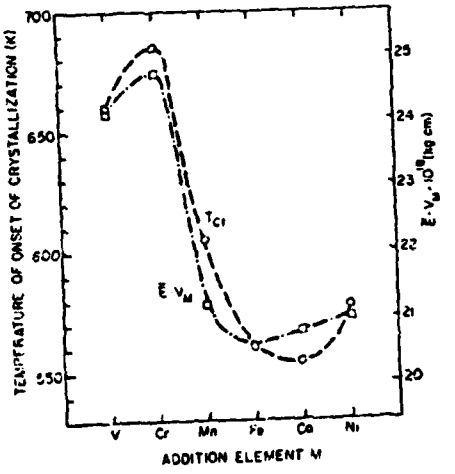

Figure 2. Onset temperatures of first exotherm, T_{c1}, for $U_{.73}M_{.27}$ glasses (from Table 1; left scale) and $\bar{E} \cdot V_M$ (see text; right scale) shown plotted against the transition metal additive M arranged in order of increasing atomic number.

From Rapidly Quenched Metals III, Vol. 1,
B. Cantor, ed., The Metals Society, London
(1978)

(C3)

THE EFFECT OF OXYGEN ADDITIONS ON THE PROPERTIES OF AMORPHOUS TRANSITION METAL ALLOYS

D.E. Polk,[+] C.E. Dube[•] and B.C. Giessen[+•]

[+] Institute of Chemical Analysis, Applications and Forensic Science, Northeastern University, Boston, Massachusetts, USA 02115

[•] Department of Chemistry, Northeastern University, Boston, Massachusetts, USA 02115

Introduction

Oxygen contamination is a potential problem in the study of amorphous metals because of the highly reactive nature of some of the constituent elements of metallic glasses and because of the processing techniques which are used to produce this metastable state. Oxygen is frequently present already in the starting materials, e.g. rare earth elements or early transition metals; further, oxygen present as an impurity in the gaseous atmosphere may be incorporated during alloy preparation (e.g. arc melting) or during the quench process (especially during thermal evaporation or sputtering or during splat quenching using the gun technique). Since these materials are generally studied as thin foils, further heat treating of the amorphous metal can also lead to a significant oxygen contamination. Nitrogen contamination may be a similar problem under these circumstances, but this impurity was not studied at the present time.

Effects of oxygen on the formation of and/or the behavior of amorphous metals have been noted previously. In sputtering or vapor deposition, the presence of oxygen has been shown to enhance the formation of an amorphous structure from unalloyed metals; for example, it has been shown[1,2] that a nickel film deposited by electron-beam evaporation onto a substrate held at 4 K is crystalline when optimum ultra-high vacuum conditions are used while the inclusion of gaseous impurities at a level of ~0.7% leads to an amorphous deposit with a crystallization temperature of ~50 K.[1] Other films of "amorphous Ni" have been reported to crystallize at much higher temperatures, e.g. 530 K,[3] undoubtedly due to higher levels of contamination by, at least in part, oxygen. Oxygen contamination can also readily stabilize the amorphous phase in films prepared by sputtering from a high purity nickel target.[4] Further, a noncrystalline structure was observed in thin, electron transparent regions of nickel foils produced by gun-technique splat quenching of initially unalloyed nickel onto a room temperature substrate;[5] the high T_c = 425 K of this material was attributed to oxygen contamination.[5]

It is clear that the presence of oxygen in amorphous metals can also affect the crystalline phases which form on crystallization as well as the thermal stability of the alloy. It has been observed, for example, that a new crystalline phase (η carbide, W_3Fe_3C type) formed upon heat treating of amorphous Ti-Be alloys in a calorimeter[6] and is found in a Ti-Be-O alloy due to its stabilization by the presence of oxygen and/or nitrogen.[7]

In this study, oxygen has been added to three binary inter-transition metal alloys already known to form a glass upon rapid liquid quenching. The effect of

oxygen upon the glass forming ability, the glass transition behavior, the ductility of the glasses and their crystallization products has been characterized.

Experimental

Alloys were prepared by melting together the pure metals and, for oxygen containing alloys, pressed pellets of copper oxide powder and nickel oxide powder (86 w/o Cu and 75.2 w/o Ni; Alfa Products, Ventron Corporation) in an arc-melting furnace. $Zr_{.50}Cu_{.50}$, $Nb_{.50}Ni_{.50}$ and $Ti_{.667}Ni_{.333}$ were selected as the basic binary alloy compositions to be studied; oxygen additions to these alloys were then made such that the metal ratio was kept constant. Alloys were not analyzed chemically after melting; indicated compositions are those calculated from the initial weights of the components. Rapid liquid quenching was accomplished using an arc-melting hammer and anvil apparatus and also, for the Zr-Cu-O alloys, melt spinning from a fused silica crucible onto the inside of a rotating cup. Standard X-ray diffractometer procedures with filtered CuKα radiation were used for structural characterizations. A Perkin-Elmer DSC2 (with 99.996% argon gas as protective atmosphere) was used for all thermal treatments; data was recorded on a two pen recorder so that the DSC2 output could be gathered at two different sensitivities.

Results and Discussion

Data on glass formation and thermal stability for the alloys which were studied are given in Table 1.

Compositions which form a glass.

For the $Zr_{.50-x/2}Cu_{.50-x/2}O_x$ alloys, glasses were obtained with up to 8 a/o oxygen by using the arc-melting quench unit; attempts to obtain the amorphous phase for alloys containing $\geq$ 10 a/o oxygen were unsuccessful. Results of the hammer-and-anvil quench process were not fully reproducible from splat to splat; some splats have a higher yield of metallic glass than others since the foil thickness and hence quench rate can vary from splat to splat. This observation can be used to qualitatively judge the relative glass forming ability of different alloys by quenching each composition several times and comparing the results. While binary $Zr_{.50}Cu_{.50}$ forms a glass readily upon arc quenching, it was found that the addition of oxygen progressively reduces the glass forming ability so that alloys containing 8 a/o and, to a lesser extent, 6 a/o oxygen could be made amorphous only with great difficulty.

$Zr_{.50}Cu_{.50}$ could be readily melt spun to a glass in vacuum. However, all $Zr_{.50-x/2}Cu_{.50-x/2}O_x$ alloys, even with only 1 a/o oxygen, were partially crystalline when melt spun under similar conditions. Ribbons from alloys of low oxygen content appeared amorphous on the substrate side but were partly crystalline on the top surface; they exhibited a crystalline pattern superimposed on a broad amorphous peak. This is consistent with our experience that the arc-melting hammer-and-anvil quench method produces higher quench rates than we could achieve by melt spinning. The results from melt spinning are discussed further in the section on crystalline phases.

For $Nb_{.50-x/2}Ni_{.50-x/2}O_x$, a glass was obtained upon quenching in the arc-melting unit with 2.9 and 5.7 a/o oxygen; alloys containing $\geq$ 8.6 a/o oxygen could not be made fully amorphous.

$Ti_{.667}Ni_{.333}$ could be quenched to a fully amorphous condition in the arc-melting unit. However, repeated attempts to produce fully amorphous Ti-Ni-O samples containing even only 1 or 2 a/o oxygen by this method were unsuccessful.

Thermal behavior by calorimetry: T_g and T_c.

Fig. 1 illustrates the DSC2 thermograms obtained for the amorphous Zr-Cu-O samples. Data in Fig. 1 was gathered from samples weighing ~9 mg at a heating rate of 80 K/min; one pen, having a full-scale deflection sensitivity of 5 mcal/sec, was appropriate for investigating the glass transition for the selected mole fraction and heating rate and the 50 mcal/sec sensitivity of the other pen was selected so that the full crystallization exotherm could be observed.

It can be seen in Fig. 1 that the $Zr_{.50}Cu_{.50}$ alloy, as observed previously,[8,9] exhibits a well defined thermal manifestation of the glass transition, i.e. a ΔC_p, and that the specific heat has "levelled off" at the higher value associated with the undercooled liquid.[10] The value of ΔC_p observed for $Zr_{.50}Cu_{.50}$, 4.6 cal/mole K, is typical of that measured for other metallic glasses where the "levelling off" is seen. The addition of 2 a/o oxygen raises T_g by 21 K though crystallization now beings sooner, relative to T_g, than in the oxygen free alloy so that the "levelling off" of C_p at the higher value is therefore not observed. It appears that, with increasing oxygen content, T_g moves to higher temperatures faster than T_c, i.e. $(T_c - T_g)$ decreases, such that only part of the ΔC_p is seen for the 4 a/o oxygen alloy and no ΔC_p is seen for the 6 and 8 a/o oxygen glasses. In general, a ΔC_p may or may not be seen for any given oxygen-free amorphous metal since $(T_c - T_g)$ varies as the composition varies.[11]

It had been noted previously[11] that metallic glasses can be prepared more readily by rapid liquid quenching, i.e. with lower quench rates, as their $(T_c - T_g)$ increases. Since the atomic mobility increases rapidly for $T > T_g$,[12] alloys of higher $(T_c - T_g)$ possess relatively higher atomic mobilities before crystallization occurs; the higher resistance to crystallization near the glass transition temperature thus appears to extend throughout the entire temperature range corresponding to the undercooled liquid. Thus, the fact that $(T_c - T_g)$ of the present alloys decreases as the oxygen content increases is consistent with the finding noted in the previous section that the ease of glass formation decreases as oxygen is added.

At temperatures preceding any glass transition and crystallization effects, all of the samples are seen to exhibit a broad exothermic "relaxation" effect over a temperature interval of about 200 K; this effect was previously noted for Pd-Si alloys[13] and for Zr-Cu alloys.[9] In Fig. 1, comparison of the amorphous curves with the curves taken for the samples after crystallization makes this effect apparent.

The crystallization exotherm is seen to broaden significantly at oxygen contents above 2 a/o. As mentioned, the onset temperature moves to higher temperatures as the oxygen content increases with a maximum increase of T_c of ~40 K at 6 a/o oxygen before it decreases for the 8 a/o oxygen alloy.

For the interpretation of the present results it is of major importance to decide whether or not: (1) the oxygen was in fact uniformly distributed throughout the amorphous phase and (2) the composition of the glass was as calculated from the initial components, e.g. whether or not oxygen was lost during melting.

As to the first point, the strongest argument that the oxygen is dissolved uniformly (on a microscopic scale) is the marked and smooth change in the glass transition behavior as a function of the nominal oxygen content (Fig. 1). We base an argument for local homogeneity on the reproducibility and compositional dependence of the thermal features for binary Zr-Cu glasses. We have found the "shape" of the glass transition for $Zr_{.50}Cu_{.50}$, determined by the relative temperatures of T_g and the onset of crystallization, to be quite reproducible

for alloys of this composition which were prepared, quenched and characterized on different occasions, using both the arc-quench method and melt spinning. Further, the "shape" of the glass transition is relatively constant in the vicinity of $Zr_{.50}Cu_{.50}$ as the ratio of Zr to Cu is changed.[9] Thus, the observed changes in the glass transition behavior can not be due, e.g., to the segregation of the oxygen into more zirconium rich regions, leaving behind the bulk of the material as a glass richer in copper than the $Zr_{.50}Cu_{.50}$ alloy.

As to the second point, the weight losses occurring upon preparation of the alloys containing oxygen in the arc-melting furnace were typical of the less than 1 w/o loss experienced for nominally oxygen-free alloys. Further, after crystallization the amorphous alloys from the initial pellets containing oxygen contained significant amounts of phases which were different from those found for the nominally pure alloys and which are known to be stabilized by oxygen; this is discussed in more detail in the subsequent section on crystal phases.

Finally, the data are found to be internally consistent with good reproducibility. Different splats of nominally the same composition generally had T_c's within ± 5 K (presumably due to compositional fluctuations between the ~50 mg alloy pieces chipped from the master alloy and then used for arc-quenching) of the average value and had similar glass transition behavior, i.e. the "shape" of the C_p change or the absence of such a change.

T_c values for Nb-Ni alloys are given in Table 1. Upon scanning amorphous $Nb_{.50}Ni_{.50}$ at 80 K/min, no crystallization exotherm was observed below 1000 K, the temperature limit of the DSC2. Upon scanning at 10 K/min, however, a crystallization exotherm was observed; accordingly, the Nb-Ni-O glasses were also run at a heating rate of 10 K/min. For the oxygen-containing alloys, a second peak appeared at lower temperatures; i.e. in contrast to the Zr-Cu alloys, the presence of oxygen caused crystallization to occur at a lower temperature. The first peak accounted for ~38% of the heat of crystallization in the alloy with 2.9 a/o oxygen and ~47% of the heat of crystallization in the alloy with 5.7 a/o oxygen. For a scan rate of 10 K/min and the available amount of sample, it was not possible to determine the C_p behavior of these alloys immediately before crystallization in detail.

Heating rate dependence of crystallization and isothermal annealing.

A more detailed comparison of the crystallization behavior of the binary $Zr_{.50}Cu_{.50}$ glass and a ternary Zr-Cu-O glass was desired. For such studies, melt-spun ribbons would be desirable in order to avoid any small variations possible between nominally identical glasses prepared by arc quenching; this is necessary since experiments for the determination of the activation energy for crystallization involve only small changes in the crystallization temperature. However, the inability to produce fully amorphous melt-spun Zr-Cu-O ribbons hampered this comparison.

Portions of an amorphous $Zr_{.50}Cu_{.50}$ ribbon were scanned at heating rates of 10 K/min to 160 K/min; the qualitative features of the crystallization exotherm did not change. The crystallization temperatures obtained in these runs are given in Table 1. In order to determine the activation energy for crystallization ΔE_c, $\ell n\ T_p/\alpha$ vs. $1/T_p$ was plotted;[14] however, rather than a straight line, a "smooth", curved line was obtained. The tangent to the portion of the curve obtained at low heating rates (10 to 20 K/min) resulted in a value of ΔE_c = 96 Kcal/mole and that for high heating rates (80 to 160 K/min) gave ΔE_c = 75 Kcal/mole. Because the sample may not track the indicated temperatures at the high rates exactly and because of the results of isothermal annealing experiments given below, the value derived from the lower heating rates is preferred.

Isothermal runs, where the rate of evolution of heat as a function of time was measured, were also conducted. As illustrated in Fig. 2, a single peak was observed for $Zr_{.50}Cu_{.50}$. Isothermal data were recorded from 690 K to 715 K at intervals of 5 K. A plot of ℓn(time) (both for times corresponding to the maximum rate of heat evolution and for times corresponding to 1/5 of this maximum rate) vs. 1/T gave a straight line with a slope corresponding to a ΔE_c = 97 Kcal/mole for both stages of crystallization, in good agreement with the value quoted above determined from variation of the heating rate.

Since data for oxygen-containing alloys had to be obtained from splats, only the heating rate variation method (which can be done with smaller amounts of sample so that one splat can be used for several runs) was practical, given the small variations between splats of nominally identical composition. Sections of one splat of amorphous $Zr_{.49}Cu_{.49}O_{.02}$ were run at different heating rates. As for $Zr_{.50}Cu_{.50}$, the shape of the crystallization exotherm was unchanged by changes in the heating rate though the exotherms for the 2 a/o oxygen alloy have a distinct shoulder on the low temperature side, unlike that for $Zr_{.50}Cu_{.50}$. The ΔE_c = 95 Kcal/mole calculated from the variation of T_p for the 2 a/o oxygen glass is essentially identical to that found for $Zr_{.50}Cu_{.50}$ though this ΔE_c value is associated with the main peak; the shoulder may be due to the formation of the η phase (see below) which may have a different ΔE_c.

In contrast to the thermal scans, the 2 a/o oxygen alloy behaves markedly different from the $Zr_{.50}Cu_{.50}$ alloy upon isothermal annealing. Fig. 2 also illustrates the thermogram from a 2 a/o oxygen foil annealed at 700 K; while some variation between different samples was observed, these thermograms generally show two peaks. X-ray diffraction measurements of a sample after the first peak show the first peak to be associated with ~20% of the sample forming a microcrystalline η phase (W_3Fe_3C type) (see below). The second peak corresponds to the crystallization of the remaining amorphous phase to α-ZrCu.

The difference in the crystallization behavior of the binary and ternary alloys, including the formation of the η phase (W_3Fe_3C type) which is often stabilized by the presence of oxygen,[15] is a further indication that the oxygen has remained in solution in the alloy.

Crystalline phases.

For $Zr_{.50}Cu_{.50}$, the α-ZrCu phase is found both in the as-cast alloy and after the DSC scan of the initially amorphous sample. For Zr-Cu-O samples, both α-ZrCu and an η phase (W_3Fe_3C type) form in the single exotherm seen in the DSC scan with, as expected, the relative proportion of the η phase increasing as the oxygen content increases.

After crystallization during the DSC scan, the $Nb_{.50}Ni_{.50}$ alloy did not have the hexagonal μ phase structure expected from the phase diagram[15] and present in the alloy before quenching. Instead a more complex XRD pattern was found, the principal lines of which (in the forward reflection region) could be tentatively indexed with an orthorhombic unit cell corresponding to the M phase type found as an equilibrium phase in the Nb-Ni-Al system[16] and other ternary Nb-Ni alloys.[17] The M phase had earlier been observed in an isothermally annealed, splat cooled Nb-Ni glass.[18] Further annealing tests would be required to determine whether the observed M phase is a metastable binary phase or whether it was being stabilized by unknown low-level impurities. In any case, the effect of oxygen additions at levels of $\geq$ 2 at.pct. is different: for both Nb-Ni alloys which initially contain oxygen, the low temperature exotherm was associated with the formation of a ternary phase, reported earlier as an equilibrium phase,[19] that has the η phase (W_3Fe_3C type) structure and coexists with the remaining amorphous phase; the second exotherm is due to the crystallization of the remaining amorphous material to the M-phase. The relative amounts of η and the amor-

phous phases indicate that, if the oxygen is totally concentrated in the η phase of equal Nb and Ni content, the η phase would have a composition near $Nb_3Ni_3O_x$ with $x \sim 0.5$.

This crystallization behavior of the Nb-Ni-O alloys is similar to the two-step crystallization of $Zr_{.49}Cu_{.49}O_{.02}$ upon isothermal annealing which was discussed previously. Thus, in both systems, segregation takes place during crystallization, with oxygen migrating from the glass to form a metal-rich, oxygen stabilized ternary phase.

As confirmed in this study where $Ti_{.667}Ni_{.333}$ was arc-quenched into a fully amorphous foil, it had been noted previously[20] that a glass could be made at the composition of the intermetallic phase Ti_2Ni. This equilibrium compound has a structure[21] which is closely related to the W_3Fe_3C structure discussed above. For Ti-Ni alloys, however, oxygen additions even as low as 1 a/o resulted in splats which were <u>partly</u> crystalline, suggesting oxygen segregation during the processing, apparently due to additional stabilization of this phase by oxygen.

Fig. 3 shows the diffraction pattern obtained from the crystallized $Zr_{.49}Cu_{.49}O_{.02}$ foils superimposed on the broad first peak characteristic of the glass. The two main peaks at ∿37° and ∿40° are from α-ZrCu (though the intensity of the peak at ∿37° would be relatively higher in a non-textured sample); the peak between them is at the position of the main peak of the η phase (W_3Fe_3C type) in the Zr-Cu-O alloys; while there is overlap with a peak from α-ZrCu and possibly β-ZrCu at the same location, it may indicate the presence of the η phase even in the 2 a/o oxygen alloy.

In general, the major diffraction peaks for any intermetallic phase having a composition near that of the glass, as well as the first reflection of a hypothetical fcc or bcc structure of appropriate atomic volume, occur near the center of the broad peak. As seen in Fig. 3, this is the case for a fcc $Zr_{.50}Cu_{.50}$ structure which maintains the elemental atomic volumes; it is also the case for the α-ZrCu and the closely related Zr_7Cu_{10} structure as well as the oxygen stabilized η phase which has been found here in the ternary system.

In contrast, the major peaks of the ZrO_2 phases are found at much larger d values and lower 2θ, as indicated in Fig. 3. The peak seen at 2θ of ∿28° in the crystalline pattern from $Zr_{.49}Cu_{.49}O_{.02}$ is in fact due to monoclinic ZrO_2. The atmosphere in the DSC2 was not sufficiently clean to prevent some oxidation of the sample during the runs, and some "blackening" of the surface is generally visible to the eye. After longer annealing times and/or higher temperatures, the ZrO_2 lines become more intense, including the well defined, second most intense reflection of monoclinic ZrO_2 and a reflection from tetragonal ZrO_2. In each case, these lines ascribed to ZrO_2 disappear upon a light polishing of the surface of the annealed sample.

In analogy with other inorganic oxide glass systems (e.g. the SiO_2 system[22]), it is expected that the broad first peak of an amorphous phase having short range order similar to that in monoclinic ZrO_2 would occur at about 28°. This statement is of interest since broad peaks at about this location have been observed in previous studies of Zr-Cu alloys.[23,24] In a transmission electron microscopy study[23] of foils heat treated so as to initiate crystallization, regions within the foil which were associated with a broad halo at k values corresponding approximately to the crystalline peak of ZrO_2 mentioned above were found. This phase was labelled the "transformed amorphous phase" and was generally found at the boundary between growing crystals and the amorphous matrix.[23] In view of the small relative difference in the scattering powers of Zr and the Cu, it is not considered possible that an amorphous (or crystalline) structure based only on Cu and Zr would have significant values of the interference function (or structure factor) at the observed low k values, i.e. that it would have a halo

at such a low angle. Even amorphous pure Zr would presumably have a broad peak centered at an angle not lower than .34°. Thus, it is suggested that the "transformed amorphous" material is likely to be rich in oxygen, formed either by the expulsion of oxygen from crystallizing regions or by contamination during annealing.

A pattern similar to the "transformed amorphous" pattern with a broad inner halo has also been observed in thermally evaporated amorphous $Zr_{.66}Cu_{.66}$ but not in sputtered amorphous $Zr_{.66}Cu_{.66}$.[24] This is presumably due to a relatively high level of oxygen contamination in the thermally evaporated sample.

The extent of the conditions under which this (presumably) amorphous ZrO_2-like phase will form is not clear. It had been hoped that such a peak would be seen in our as-prepared or annealed Zr-Cu-O alloys, but the so-far limited studies of these alloys generally produced either an oxygen-stabilized η phase internally or crystalline ZrO_2 phases on the surface. Possibly, higher oxygen contents are necessary in an internal region to produce the amorphous ZrO_2-like phase.

As noted previously, the $Zr_3Cu_3O_x$ phase (η phase, W_3Fe_3C type) was found by X-ray diffraction measurements on the top surface of some melt spun Zr-Cu-O ribbons. However, in other melt spun ribbons of 1, 2 and 4 a/o oxygen, a different, unidentified phase was observed; the reason for this difference is not known. Similar patterns and variability were observed for partly crystalline Zr-Cu-O splats.

Ductility.

It is known that many of the metallic glasses produced by rapid liquid quenching are very ductile, i.e. that they will deform plastically on bending and that foils can even be bent back sharply to form a V-shape without fracturing. This is also true of the binary Zr-Cu, Ti-Ni and Nb-Ni glasses which were prepared in this study. However, it is also known that other amorphous metals do not share this feature and that embrittlement can be caused by annealing, e.g. Ref. 25, while the material appears to remain amorphous. The cause of this brittleness remains a point of controversy.

This study demonstrates clearly that the inclusion of oxygen into the amorphous T-T alloys which were studied enhances brittleness, with increasing O contents causing increasing brittleness. Some amorphous Zr-Cu samples with 2 a/o oxygen were partly brittle; the 4 a/o oxygen alloys were generally partly brittle; amorphous alloys with 6 and 8 a/o oxygen were always brittle, i.e. they would fracture readily on bending with no plastic deformation, and they could not be sheared with scissors. However, it is not yet known if this is an intrinsic property of a homogeneous alloy, i.e. one in which the oxygen is fully dissolved, or whether it is due to the presence of a minute amount of oxygen-induced precipitates; transmission electron microscopy would be required to resolve this point.

Since the ductility of the $Zr_{.49}Cu_{.49}O_{.02}$ alloy varied somewhat from splat to splat, presumably because of a different temperature-time history for each, thermal annealing studies of this alloy were of interest to study this embrittlement. However, this study was hampered by the inability to spin oxygen-containing Zr-Cu alloys to a fully amorphous state to give initially identical samples for annealing studies. Limited studies on splats were therefore made which are thus far inconclusive. Annealing at 700 K for a time corresponding to the first peak in Fig. 2, i.e. corresponding to the formation of a fine-crystalline η phase embedded in the amorphous matrix, produced a very brittle sample; however, annealing for only 5 min at this temperature did not cause embrittlement. Further studies will be necessary to determine whether or not embrittlement can be induced before the fine, oxygen content induced precipitates are apparent to a XRD.

It is noted that a sputtered amorphous Zr-Cu film, nominally 50 a/o Zr, is also very brittle.[26] Whether or not this is due to the presence of gaseous impurities is not yet known.

While no detailed study of the ductility of the Nb-Ni-O glasses was made, the as-prepared glasses were also found to be partly brittle.

Comments on the observation of T_g.

To unambiguously determine whether or not a given amorphous metal displays a glass transition, one must balance the sample size, scanning rate and DSC sensitivity to give a sufficiently large deflection for the ΔC_p. The task of determining ΔC_p is made more complex by the curvature which is generally present in the baseline of the instrument, the "relaxation" which often occurs in the region preceding crystallization, and the need to be sure of the location of the baseline which can shift from run to run due to different thermal configurations of the sample pan and the platinum sample pan cover of the DSC2. For example, the thermogram for the $Zr_{.47}Cu_{.47}O_{.06}$ glass, taken at high sensitivity, qualitatively appears to show a glass transition; however, a careful comparison to the DSC trace for the crystallized material shows that the observed curvature is due primarily to the end of the relaxation effect. Further, any endothermic rise in C_p should be quantized in order to assist in assessing whether or not the "full" ΔC_p is likely to have been observed and thus whether or not the T_g measured from such a trace is in fact accurate.

Because of the high thermal stability of $Nb_{.50}Ni_{.50}$, it could not be determined with the DSC2 whether or not this alloy exhibits a glass transition. However, $Nb_{.40}Ni_{.60}$ was found to exhibit the characteristic relaxation (maximum depth of ~1.7 cal/mole K) followed by a rise of ~1.1 cal/mole K above the crystalline specific heat, when heated at 80 K/min, although without any indications of a "levelling off". Thus, a glass transition can be seen to begin in amorphous $Nb_{.40}Ni_{.60}$ although the onset of crystallization occurs before the full ΔC_p is achieved.

The sputtered amorphous Zr-Cu behaves similarly[26] to the liquid-quenched $Nb_{.40}Ni_{.60}$. Thus, a relaxation is observed, followed by a ~1.3 cal/mole K rise above the crystalline value and then crystallization with a T_c = 758 K and T_p = 769 K for a 80 K/min scan. (A careful comparison with T_c for a liquid quenched alloy of the same Zr-Cu composition must await an accurate compositional analysis of the sputtered sample.) Since all liquid quenched alloys in this broad compositional region show a well-defined T_g, one might speculate that gaseous impurities in the sputtered film may preclude the observation of the full glass transition. From Fig. 1, it can be seen that about 4 a/o oxygen would produce such behavior in a liquid quenched amorphous $Zr_{.50}Cu_{.50}$.

Acknowledgment. This work was supported by the Office of Naval Research; we thank them for their support. Melt-spun ribbons were kindly produced by Ms. Juli Hong.

References

1. M.R. Bennett and J.G. Wright, phys. stat. sol. (a), 1972, 13, 135.
2. P.K. Leung and J.G. Wright, Phil. Mag., 1974, 30, 995.
3. K. Tamura and H. Endo, Phys. Letters, 1969, 29A, 52.
4. H. Matsueda and B.L. Averbach, Mat. Sci. Eng., 1976, 23, 131.
5. H.A. Davies and J.B. Hull, Mat. Sci. Eng., 1976, 23, 193.
6. L.E. Tanner and R. Ray, Scripta Met., 1977, 11, 783.
7. B.C. Giessen, J.C. Barrick and L.E. Tanner, to be published.
8. A.J. Kerns, Ph.D. Thesis, Northeastern University, Boston, Massachusetts, 1974.
9. R.V. Raman, Ph.D. Thesis, Northeastern University, Boston, Massachusetts, 1977.
10. H.S. Chen and D. Turnbull, J. Chem. Phys., 1968, 48, 2560

11. D.E. Polk and H.S. Chen, J. Non-Cryst. Solids, 1974, 15, 165.
12. F. Spaepen and D. Turnbull, in Metallic Glasses, pp. 114-127, 1978, Metals Park, Ohio, ASM.
13. H.S. Chen and E. Coleman, Appl. Phys. Letters, 1976, 28, 245.
14. H.O.K. Kirchner, P. Ramachandrarao and G.A. Chadwick, Phil. Mag., 1972, 25, 1151.
15. Constitution of Binary Alloys, Second Supplement, p. 191, 1969, New York, McGraw Hill.
16. C.B. Shoemaker and D.P. Shoemaker, Acta Cryst., 1967, 23, 231.
17. B.C. Giessen and D. Szymanski, to be published.
18. R.C. Ruhl, B.C. Giessen, M. Cohen and N.J. Grant, Acta Met., 1967, 15, 1693.
19. H.H. Stadelmaier, H. Holleck and F. Thummler, Monatsh. Chemie, 1967, 98, 133.
20. D.E. Polk, A. Calka and B.C. Giessen, Acta Met., 1978, 26, 1097.
21. H.H. Stadelmaier, in Developments in the Structural Chemistry of Alloy Phases, pp. 141-180, 1969, New York, Plenum Press.
22. R.L. Mozzi and B.E. Warren, J. Appl. Cryst., 1969, 2, 164.
23. J.M. Vitek, J.B. Vander Sande and N.J. Grant, Acta Met., 1975, 23, 165.
24. M.Scott, Mater. Sci. Eng., 1977, 30, 219.
25. L.A. Davis, R. Ray, C.-P. Chou and R.C. O'Handley, Scripta Met., 1976, 10, 541.
26. D.E. Polk and C.F. Cline, unpublished results.

Table 1. Thermal Characteristics of Amorphous Samples

Alloy Composition	Heating Rate K/min	T_c^*, K	T_p^*, K	Comments
$Zr_{.50}Cu_{.50}$	80	735	742	T_g^*=681
$(Zr_{.50}Cu_{.50})_{.98}O_{.02}$	80	754+	760	T_g^*=702
$(Zr_{.50}Cu_{.50})_{.96}O_{.04}$	80	764	771	
$(Zr_{.50}Cu_{.50})_{.94}O_{.06}$	80	767	781	
$(Zr_{.50}Cu_{.50})_{.92}O_{.08}$	80	761	771,790	
$Nb_{.50}Ni_{.50}$	10	961	973	
$(Nb_{.50}Ni_{.50})_{.971}O_{.029}$	10	915,956	926,972	
$(Nb_{.50}Ni_{.50})_{.943}O_{.057}$	10	911,956	920,972	
$Nb_{.40}Ni_{.60}$	10	918,~947,~964	928,958,981	
"	80	950,~985	962, -	
$\sim Zr_{.50}Cu_{.50}$	80	758	769	sputtered[26]
$Zr_{.50}Cu_{.50}$	10	722.0	726.0	melt spun
"	20	728.5	733.5	"
"	40	736.0	741.0	"
"	80	745.5	750.5	", T_g^*=693
"	160	754.0	760.5	"

* T_g and T_c are defined as the onset temperatures obtained from the intersections of the extrapolated curve preceding crystallization and the steepest tangent to the ΔC_p and the exotherm, respectively. T_p is the temperature at which the crystallization exotherm reaches its maximum.

+ the "shoulder" for this alloy has a T_c=749 K.

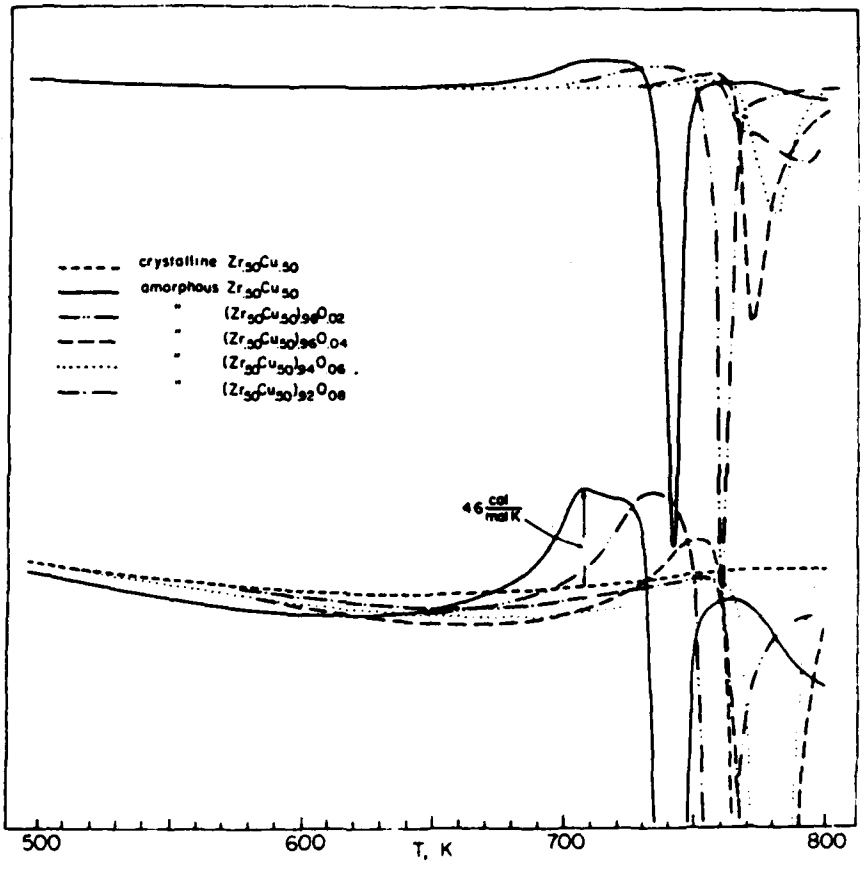

Figure 1. Thermograms measured with a Perkin Elmer DSC2 at 80 K/min for ~9 mg samples of Zr-Cu-O amorphous metals. The lower set of traces shows the specific heat behavior preceding crystallization; the upper set of traces, recorded at 1/5 of the sensitivity of the lower set, shows the full crystallization exotherm.

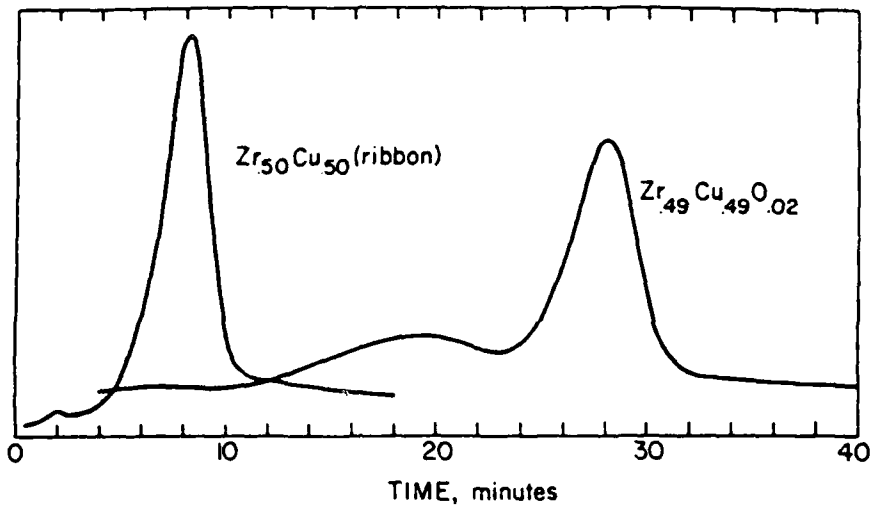

Figure 2. DSC thermograms showing rate of heat evolution as a function of time for indicated samples when annealed at 700 K (displaced zeros). Very small peak at ~2 minutes for the melt spun ribbon is reproducible and may be due to trace amounts of oxygen in this nominally oxygen-free alloy.

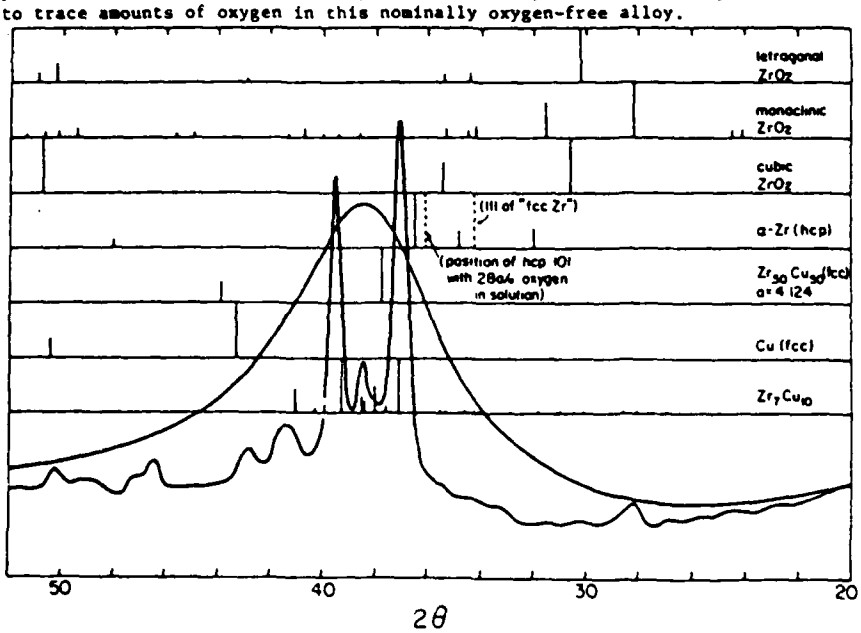

Figure 3. X-Ray diffraction patterns (CuKα radiation) for various phases. The smooth curve is the first broad peak of the pattern obtained from $Zr_{.50}Cu_{.50}$. The crystalline trace is from a crystallized foil of $Zr_{.49}Cu_{.49}O_{.02}$ which contains primarily the α-ZrCu phase.

From Rapidly Quenched Metals III, Vol. 2,
B. Cantor, ed., The Metals Society, London
(1978)

(G24)

FORMATION AND PROPERTIES OF REFRACTORY METAL GLASSES II: T_5-T_9 GLASSES (T_5=Nb, Ta; T_9=Rh, Ir)

S. Davis, M. Fischer, B.C. Giessen and D.E. Polk

Department of Chemistry and Institute of Chemical Analysis,
Applications and Forensic Science
Northeastern University, Boston, Massachusetts, USA 02115

Introduction

There is an increasing amount of evidence[1,2] that the thermal and mechanical behavior of metallic glasses containing only transition metals (or rare earth metals and actinides) is closely related to the corresponding properties of the constituent elements. (This is in sharp contrast to glasses containing B-metals such as Al as a major alloying constituent or as a minor additive;[2] here the stabilizing and strengthening effect is frequently far in excess of the inherent stability of the additive.) Among inter-transition metal systems, then, high strength and thermal stability would be expected to be found in glasses formed by the combination of transition metals having high elastic moduli and/or high melting points.[3]

It is likely that the strongest and most stable metallic glasses will not be binary metal-metal alloys but will contain one or more refractory metal(s) as well as metalloid additions. However, there is an interest in the systematic study of the properties of glasses formed by binary combinations of refractory metals; for instance, such alloys can give indications of the correlations existing between the thermal and mechanical parameters of the glass and its components. Such a study is reported here for the four possible combinations of the T_5 metals Nb and Ta on the one side and the T_9 metals Rh and Ir on the other.

The first amorphous T_5-T_9 metal alloys to be prepared were Nb-Rh glasses, characterized as microcrystalline at the time of their initial preparation.[4] Electronic properties of the Nb-Rh glasses, especially their superconductivity, were investigated.[4] The preparation of all four of the possible T_5-T_9 glasses (as well as some other refractory metal glasses) was recently reported;[3] some approximate crystallization temperatures obtained by isothermal annealing and microhardnesses (lower limits) had also been given.[3]

In the present study, the glass forming (G.F)) composition ranges of all four systems have been determined; the crystallization temperatures T_c and microhardnesses H_v have been determined for four glasses with the composition $(T_5)_{.55}(T_9)_{.45}$. T_c values were determined from measurements of the electrical resistivity; the resistivities and their changes with temperature will be discussed in a different context elsewhere.[5]

The Ta-Rh constitution diagram[6] is given schematically in Fig. 1; many features of it are typical of those of the other T_5-T_9 systems.[7] There is a central eutectic region in all four systems which contains the G.F. range; it is bounded on the left at ~40 a/o T_9 by a σ phase and on the right by phases with 12-coordinated close-packed structures at ~52 a/o T_9. Both Rh systems

show high-temperature phases (α_3 for Ta-Rh) of unknown structures.

Experimental

The procedure used to prepare refractory metal glasses has been discussed in Ref. 3 together with design features of the arc furnace quenching unit which was used. Amorphous samples were selected from the quenched foils on the basis of the presence of the typical "amorphous" diffraction pattern.

Electrical resistivities were determined by a four-point ac technique using a Keithley 503 Milliohmmeter. The samples were heated in a fused silica tube held at high vacuum. The temperature was determined using a chromel-alumel thermocouple. Upon crystallization the electrical resistivity showed a decrease of 20 to 30% of the value for the amorphous sample; T_c was taken as the onset temperature (steepest tangent method) for this decrease. In the vicinity of T_c, heating took place at rates of $\dot{T}$ = 8 K/min for $Nb_{.55}Rh_{.45}$, 3 K/min for $Nb_{.55}Ir_{.45}$, 3 K/min for $Ta_{.55}Rh_{.45}$, and 1 K/min for $Ta_{.55}Ir_{.45}$; i.e., the heating rates decreased with increasing T_c.

To obtain a cross-check on the resistometrically determined values, T_c was also determined by DSC in a Perkin-Elmer DSC 2 unit for a $Nb_{.55}Rh_{.45}$ sample at a heating rate $\dot{T}$ = 10 K/min; this composition was the only one of the four alloys studied which crystallized below the temperature limit of 1000 K for this unit. The agreement of the two values (see Table 2) was excellent.

The microhardness values were measured with a Kentron microhardness tester using a 100 g load.

Results and Discussion

Glass Formation: The structures of the quenched T_s-T_g alloys are listed in Table 1; G.F. ranges of about 12 a/o were found in all four systems. Among the crystalline phases that were found there were several that had not yet been reported as an equilibrium phase for their respective binary system;[6] for the systems with Rh, these phases may be the high temperature phases. The extent of the G.F. ranges can be somewhat correlated with features of the constitution diagram: on the T_s-rich side, G.F is limited by the position of the σ phase field (i.e. crystallization to the σ phase occurs, preventing G.F.); on the T_g-rich side, crystallization to the high-temperature phase(s) may be suppressed in favor of G.F. (e.g., for Nb-Rh) while, on the other hand, the low-temperature phases tend to form, preventing G.F., as the T_g content increases.

Crystallization Temperatures: The crystallization temperatures T_c for the $(T_s)_{.55}(T_g)_{.45}$ glasses are listed in Table 2. In Fig. 2a the T_c values are plotted against the eutectic temperature T_E and the averaged melting temperatures $\bar{T}_M$ of the components. The straight line shown for T_c vs. T_E passes through the origin and is represented by $T_c/T_E = 0.550$. While the plot of T_c vs. T_E shows some scatter, all T_c/T_E values (Table 2) lie within 0.03 (≈5%) of the straight-line value. This ratio agrees closely with those found for many other metal glasses[2,9] and gives encouragement to attempts[2,11] to link the crystallization temperatures of the glass and the eutectic melting temperatures of the solid, even though the latter is two phase at the G.F. composition. T_c also correlates well with $\bar{T}_M$; the straight line shown in Fig. 2 corresponds to $T_c = 0.61(\bar{T}_M - 900)$; as is obvious, this relation cannot be generalized with these parameters to all metallic glasses.

Considerations of the atomic motions required for crystallization suggest that a relation exists between the elastic properties and thermal stability, measured only as T_c in the present systems, of a glass. In the absence of elas-

tic data for the glass itself, one can examine the correlation of T_c with $\bar{E}$, the averaged Young's modulus of the components, or $\overline{EV}/\bar{V}$, where $\bar{V}$ is the mean atomic volume and $\overline{EV}$ is the weighted average of E·V. Both quantities correlate well with T_c (Fig. 2b), although again the resulting equations for the straight lines cannot be general for all metallic glasses.

Microhardness Data: The microhardness values H_V are given in Table 2 and are plotted vs. T_c and $\bar{E}$ in Fig. 3. The thermal and mechanical behavior of each glass are closely coupled; by the relations between T_c and T_E or $\bar{T}_M$ treated in the previous section, H_V is thus also related to T_E and $\bar{T}_M$. The solid line indicated in Fig. 3 for H_V as a function of T_c is given by $H_V = 1.04\cdot(T_c-200)$ kg $mm^{-2}K^{-1}$; a dash-dotted line through the origin is also shown. For H_V vs. $\bar{E}$, the fit to a smooth curve is excellent. Since one might expect $H_V \to 0$ as $\bar{E} \to 0$, a dashed straight line through the origin is again also shown; this one such line, $H_V/\bar{E} = 0.0320$, is correct for the stronger glasses (Table 2) but predicts lower values of H_V for the weaker ones than are observed. Like the thermal stability, the mechanical strengths of the glasses are again strongly correlated with the elastic moduli of the constituents.

As mentioned before,[3] the present glasses possess good bend ductility; some of the alloys even possess a certain degree of toughness in the crystalline state.

Conclusion

Probably due to the considerable similarity in the atomic size and periodic table position of their constituents, the thermal and mechanical properties of the present glasses possess a high degree of correlation (a) with each other, (b) jointly with features of the phase diagram, and, most interestingly, (c) jointly with pertinent properties of the constituents.

Acknowledgement

The present work was supported by the Department of Energy through a subcontract with the Lawrence Livermore Laboratory. One of us (B.C.G.) also acknowledges support by the Office of Naval Research.

References

1. H.S. Chen and J.T. Krause, Scripta Met., 1977, 11, 761.
2. B.C. Giessen, J. Hong, L. Kabacoff, D.E. Polk, R. Raman, and R. St.Amand, in Proc. 3rd Intl. Conf. on Rapidly Quenched Metals (Brighton, 1978).
3. M. Fischer, D.E. Polk and B.C. Giessen, in Rapid Solidification Processing: Principles and Technologies, p. 140, 1978, Baton Rouge, LA, Claitors Publishing Division.
4. W.L. Johnson and S.J. Poon, J. Appl. Phys., 1975, 46, 1787.
5. M. Fischer and B.C. Giessen, to be published.
6. B.C. Giessen, H. Ibach, and N.J. Grant, Trans. Met. Soc. AIME, 1964, 230, 113.
7. F.A. Shunk, Constitution of Binary Alloys, Second Supplement, 1969, New York, NY, McGraw-Hill Book Co.
8. D.L. Ritter, B.C. Giessen, and N.J. Grant, Trans. Met. Soc. AIME, 1964, 230, 1259.
9. D.E. Polk and B.C. Giessen, in Metallic Glasses, J.J. Gilman and H.J. Leamy, Eds., p.1, 1978, Metals Park, OH, American Society for Metals.
10. B.C. Giessen and F. Spaepen, to be published.
11. C.P. Chou, L.A. Davis and M.C. Narasimhan, Scripta Met., 1977, 11, 417.

Table 1: Glass Formation Upon
Arc Furnace Quenching in T_5-T_9 Alloy Systems

Alloy Composition	Equilibrium Structure at T_E	Extent of Central Two Phase Field at T_E and at 300 K (at.pct. T_9)	Structure after Rapid Quenching	Minimum G.F. Range in T_5-T_9 System (at.pct. T_9)
$Nb_{.65}Rh_{.35}$	σ		σ	
$Nb_{.60}Rh_{.40}$	$\sigma + \alpha_1$		A.M.	
$Nb_{.55}Rh_{.45}$	$\sigma + \alpha_1$	39 to 46.5 39.5 to 51.5	A.M.	< 40 to > 51
$Nb_{.50}Rh_{.50}$	α_1		cryst. (α_1?)	
$Nb_{.485}Rh_{.515}$	α_1		A.M.	
$Ta_{.65}Rh_{.35}$	σ		σ	
$Ta_{.60}Rh_{.40}$	σ		A.M.+tr.cryst.	
$Ta_{.55}Rh_{.45}$	$\sigma + \alpha_3$	40 to 49 ~38 to ~54	A.M.	~ 40 to ~ 50
$Ta_{.50}Rh_{.50}$	α_3		A.M.+tr.cryst.	
$Ta_{.485}Rh_{.515}$	α_3		cryst.	
$Ta_{.45}Rh_{.55}$	α_3		cryst.	
$Nb_{.63}Ir_{.37}$	σ		σ	
$Nb_{.575}Ir_{.425}$	$\sigma + \alpha_1$		A.M.+tr. cryst.	
$Nb_{.55}Ir_{.45}$	$\sigma + \alpha_1$	41.5 to 52.0 ~41 to 52	A.M.	~ 43 to < 55
$Nb_{.50}Ir_{.50}$	$\sigma + \alpha_1$		A.M.	
$Nb_{.45}Ir_{.55}$	α_2		A.M.+cryst. (major)	
$Ta_{.65}Ir_{.35}$	σ		σ	
$Ta_{.625}Ir_{.375}$	σ		A.M.+tr.cryst.	
$Ta_{.60}Ir_{.40}$	σ	41 to 50.4	A.M.+tr.cryst.	~ 38 to ~ 52
$Ta_{.55}Ir_{.45}$	$\sigma + \alpha_1$	~35 to ~51.5	A.M.	
$Ta_{.50}Ir_{.50}$	α_1		A.M.	
$Ta_{.475}Ir_{.525}$	α_1		A.M.+tr.cryst.	

Table 2: Properties of $(T_5)_{.55}(T_9)_{.45}$ Transition Metal Glasses

Alloy	T_c (K)	$T_c/\bar{T}_m$	T_c/T_E	H_V (kg/mm^2) (Vickers)	$\bar{E}\cdot10^6$ (kg/cm^2)	$H_V/\bar{E}\cdot10^2$
$Nb_{.55}Rh_{.45}$	973 ± 10 980[a] ± 2	0.387	0.549	780 ± 40	2.30	3.39
$Ta_{.55}Rh_{.45}$	1118 ± 10	0.399	0.529	890 ± 50	2.72	3.27
$Nb_{.55}Ir_{.45}$	1133 ± 10	0.415	0.563	970 ± 50	3.01	3.22
$Ta_{.55}Ir_{.45}$	1283 ± 10	0.425	0.577	1100 ± 70	3.44	3.20

(a) by DSC, at 10 K/min.

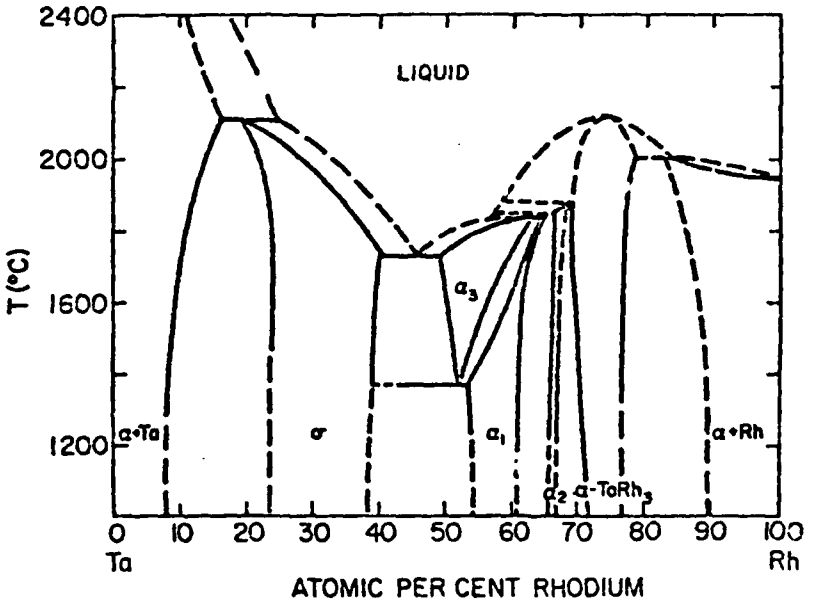

Figure 1. The Ta-Rh constitution diagram.[6]

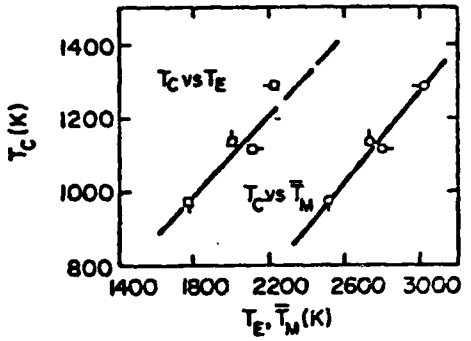

Figure 2. (a) Crystallization temperature T_c of glass vs. eutectic temperature T_E (□) and averaged melting point of the components $\bar{T}_M$ (o).
●● = $Nb_{.55}Rh_{.45}$; ●-○ = $Nb_{.55}Ir_{.45}$;
▲▲ = $Ta_{.55}Rh_{.45}$; ▲-○ = $Ta_{.55}Ir_{.45}$

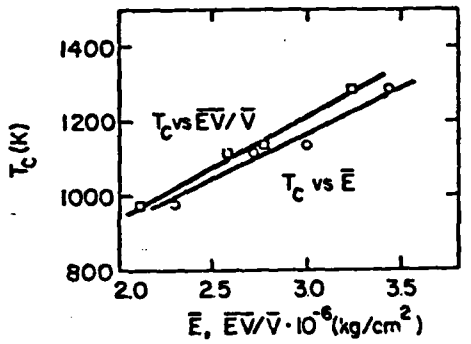

(b) T_c vs. the averaged elastic (Young's) modulus of the components $\bar{E}$ (o) and $\overline{EV}/\bar{V}$ (□) (see text).

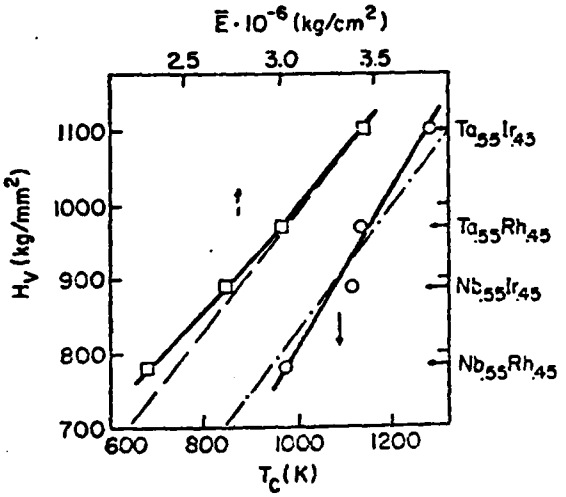

Figure 3. Vickers microhardness H_V vs. T_c and $\bar{E}$ for $(T_5)_{.55}(T_9)_{.45}$ glasses.

From Rapidly Quenched Metals III, Vol. 1,
B. Cantor, ed., The Metals Society, London
(1978)

(C6)

COMPOSITIONAL DEPENDENCE OF THE THERMAL STABILITY AND RELATED PROPERTIES OF METALLIC GLASSES I: T_g FOR $Ca_{.65}M_{.35}$ AND $Zr_{.475}Cu_{.475}M_{.05}$ GLASSES

B.C. Giessen, J. Hong, L. Kabacoff, D.E. Polk, R. Raman* and R. St.Amand**

Department of Chemistry and Institute of Chemical Analysis,
Applications and Forensic Science
Northeastern University, Boston, Massachusetts, USA 02115

* Present Address: Dept. of Materials Science and Engineering, M.I.T., Cambridge, MA 02139

** Present Address: R&D Dept., Engelhard Industries Div., Engelhard Min. and Chem. Corp., Menlo Park, Edison, NJ 08817

INTRODUCTION

The stability of metallic glasses at ambient and elevated temperatures is a property of considerable practical as well as theoretical importance. Consequently, the thermal effects occurring on heating of metallic glasses are among their most commonly determined characteristics.[1,2] As for the phase transformations (especially melting) of most crystalline metals and alloys, however, the understanding of these effects, especially their correlation with other properties, is not yet well developed, although progress has been made in individual cases.[1,3-5]

One may distinguish two types of thermal effects: exothermic (crystallization, recrystallization, relaxation) and endothermic (glass transition). Of these, the former are complex in that they pertain to reactions involving more than one phase at the same time; accordingly, they generally differ from glass to glass and can not be easily treated quantitatively. The latter, however, is a reversible effect which occurs within a homogeneous phase and should therefore be amenable to a general treatment. Such a treatment would then establish correlations of three types: (a) between the glass transition temperature T_g and related properties of the glass itself such as elastic moduli;[3-5] (b) between T_g and physical-chemical properties of the alloy system, such as phase diagram features[6] (e.g. the presence of intermediate phases and their melting points) and thermodynamic quantities of the system;[7] (c) between T_g and appropriate parameters of the constituent elements.[4,5] Relations of types (b) and (c) can be expected to have predictive character concerning T_g without the glass actually having been formed; relations of type (c) would be the most generally useful. (It should be pointed out that in the absence of T_g values, correlations of types (a) - (c) have been attempted for the crystallization temperatures T_c.[9-10])

To examine the validity of such correlations, one fruitful approach is to compare the T_g's of binary glasses in which one component and the stoichiometric ratio are held fixed while the other component is varied. Studies of T_g, however, are confronted with the difficulty that only a rather small number of binary glassy alloys display glass transitions, especially well pronounced ones [i.e. glass transitions with a sufficiently large interval $(T_c - T_g)$[11]]; these alloys include Pd-Si,[12] Zr-Cu,[3,4,13] and, Ca-Al and Ca-Zn glasses[6,14] which were discovered only recently. On the other hand, while glasses containing three or more components at substantial concentrations more frequently show glass transitions,[1] such alloys are also more likely to have more complex interactions of the components; at the present state of this field, they are therefore less suitable than binary glasses to examine such correlations.

There are two approaches, both involving ternary systems, by which additional T_g data usable for comparative studies can be obtained: (1) deduction of the T_g values for binary glasses from studies of suitable ternary systems[1,7] and (2) ternary additions (at levels from 0-20 at.pct.) to binary glasses displaying a glass transition.[15] In the work reported in the present paper, the first approach has been applied to $Ca_{.65}M_{.35}$ glasses; $Zr_{.475}Cu_{.475}M_{.05}$ glasses were studied as an example of the second approach.

$Ca_{.65}M_{.35}$ Glasses (M = Pd; Cu, Ag, Au; Mg, Zn; Al, Ga)

It had recently been reported that Ca readily forms binary glasses with a number of metallic elements M added at levels, depending on the system, of ~15 to ~60 a/o M;[6,14] the list of metals M includes A metals (Mg), transition metals (Ni, Pd), and B metals (Cu, Ag, Au, Zn, Al, and Ga).[6,14,16] The formation and alloy chemistry of many of these glasses have been discussed and a survey of their crystallization behavior has been given;[6] the crystallization sequences of some glassy Ca alloys were found to be quite complex, displaying up to five exothermic steps for some compositions.[14,16]

In this survey, well defined glass transitions were found in two binary Ca alloy systems, Ca-Zn and Ca-Al.[6,14] The glass transitions in the Ca-Al and Ca-Zn systems are observable for $0.30 \leq x_{Al} \leq 0.45$, and $0.20 \leq x_{Zn} \leq 0.60$, respectively; in all other Ca systems (with the possible exception of Ca-Au at relatively high Au concentrations[16]) T_g is masked by crystallization or other exothermic processes. At high Ca concentrations, the crystallization temperatures drop rapidly, masking T_g even in the Ca-Al system at $x_{Al} < 0.30$.[14]

The composition $Ca_{.65}M_{.35}$ was selected for a comparative study. To obtain the T_g values of interest despite the overlapping exothermic effects in the respective binary Ca systems, ternary alloys of the composition $Ca_{.65}(Al_{1-y}M_y)_{.35}$ were studied in the hope, first, of being able to retain ternary glasses at the desired composition $x_{(Al+M)} = 0.35$ over a wide range of y values and, second, to be able to determine T_g for binary $Ca_{.65}M_{.35}$ by extrapolation from the ternary $Ca_{.65}(Al_{1-y}M_y)_{.35}$ alloys. For M = Cu, alloys of composition $Ca_{.65}(Zn_{1-y}M_y)_{.35}$ were also studied.

$(Zr_{.50}Cu_{.50})_{0.95}M_{.05}$ Glasses (M = Sc, Ti, V, Cr, Mn, Fe, Co, Ni, Cu)

The second approach to providing interpretable T_g data, wherein the change in T_g upon the addition of alloying elements to glasses displaying glass transitions is determined, was used in a study of T_g for Pd-Si-M glasses;[12,15] it was also employed to examine the effect of alloying additions on T_c in Fe-C-P-M glasses (M = transition metals)[8] and in Mg-Zn-M glasses (M = B metals).[17] A corresponding study for Zr-Cu-M glasses has now been carried out[4] wherein the well pronounced glass transition of binary $Zr_{.50}Cu_{.50}$ glass[3,13] was utilized. The effect of ternary additions of first period transition metals M at a level of 5 at.pct. to form $Zr_{.475}Cu_{.475}M_{.05}$ glasses is reported here.

EXPERIMENTAL METHODS

All alloys were initially prepared by arc-melting using 99.9% pure starting materials (with the exception of Zr which was 99.7% purity reactor grade material). Weight loss analyses indicated agreement between the nominal and actual composition to ≤ 1 at.pct.

For Ca alloys, glasses were prepared by melt spinning[18] in a vacuum of ~50 μm Hg; ribbons of ~2 mm width and ~50 μ thickness were formed during solidification on the inside of a copper drum. For Zr-Cu alloys, amorphous foils were

prepared by arc furnace hammer-and-anvil quenching.[19] All ribbons or foils selected for thermal analysis exhibited no evidence of crystalline portions when examined by XRD (to the detection limit of this method, estimated at several %). Differential scanning calorimetry (DSC) was carried out on a Perkin-Elmer DSC2 at $\dot{T}$ = 80 K/min; the glass transitions reported here were determined by the midpoint method (point of inflection of the endotherm). Crystallization temperatures T_c were determined as onset temperatures (steepest tangent method).

RESULTS

T_g for $Ca_{.65}(Al_{1-x}M_x)_{.35}$ Glasses

The desired ternary glassy Ca alloys were prepared in eight systems which are reported here. $Ca_{.65}(Al_{1-y}M_y)_{.35}$ glasses, with M = Pd, Cu, Ag, Au, Mg, Zn, Ga, and $Ca_{.65}(Zn_{1-y}Cu_y)_{.35}$ glasses were prepared. Glasses in seven of these eight systems showed glass transitions up to $y \sim 0.75$; the exception was the $Ca_{.65}(Al_{1-y}Cu_y)_{.35}$ system, where T_g was observable only for $y \leq 0.25$. Instead of the latter system, $Ca_{.65}(Zn_{1-y}Cu_y)_{.35}$ glasses were therefore studied yielding T_g values up to y = 0.67. An example of the DSC results obtained on such ternary alloys is given in Figure 1 for the $Ca_{.65}(Al_{1-y}Au_y)_{.35}$ system. The multiple exothermic effects and the decrease of the initial T_c to values below T_g at $y \sim 0.35$ (thus masking T_g) can be seen. It is also apparent that the observed T_g have a parabolic dependence on y. T_g was therefore fitted to the expression:

$$T_g(y) = (1-y)T_g(Ca_{.65}Al_{.35}) + y \cdot T_g(Ca_{.65}M_{.35}) + \lambda \cdot y(1-y).$$

Expressions of this type have been used before for ternary glasses.[1,7] The fit with the experimental points was excellent (see Figure 1) and the values for $T_g(Ca_{.65}M_{.35})$ obtained by extrapolation are thought to be precise within the assumed functional relationship to ± 10 K. The resulting $T_g(Ca_{.65}M_{.35})$ are shown in Figure 2, where they are plotted together with the values obtained directly for the two binary glasses $Ca_{.65}Al_{.35}$ and $Ca_{.65}Zn_{.35}$ against the valence of the addition element M (see below).

A presentation and further discussion of the ternary data, especially of the interaction coefficients λ, will be given elsewhere.

T_g for $(Zr_{.50}Cu_{.50})_{.95}M_{.05}$ and T_c for $(Zr_{.50}Cu_{.50})_{.975}M_{.025}$ Glasses

$(Zr_{.50}Cu_{.50})_{1-x}M_x$ alloys (where M represents transition metals of the first long period from Sc to Ni) with M contents corresponding to 2.5, 5, and 10 a/o were studied.[6] Glasses were obtained at all levels for all of these additives, with the exception of the alloy containing Sc at x = .10 which was partly crystalline; further, glass transition temperatures could not be reliably determined for glasses containing V and Cr at this level.[6] At x = .05, however, glass transition temperatures could be obtained for all additives; these values as well as the crystallization temperatures of $(Zr_{.50}Cu_{.50})_{1-x}M_x$ glasses with x = .025 are reported and discussed here. Results on additional ternary alloys of this type, also including non-transition metal additives, will be reported subsequently.

Values for $\Delta T_g = T_g(Zr_{.475}Cu_{.475}M_{.05}) - T_g(Zr_{.50}Cu_{.50})$ were calculated, using a value of $T_g(Zr_{.50}Cu_{.50}) = 692$ K. The resulting ΔT_g are plotted against the periodic table position (group number) of M in Fig. 3a. From the measured temperatures of the onset of crystallization, values for $\Delta T_c = T_c(Zr_{.4875}Cu_{.4875}M_{.025}) - T_c(Zr_{.50}Cu_{.50})$ were calculated, using $T_c(Zr_{.50}Cu_{.50}) = 737$ K; these ΔT_c values are presented in Fig. 3b. The overall similarity of the curves for ΔT_g (presented here for x = .05) and ΔT_c (at

x = .025) as functions of M is apparent, indicating a similar effect of M in both transitions. (The similarity between ΔT_g and ΔT_c was somewhat less pronounced when both curves were taken at x = .05.) Further, for most of the addition elements M studied here, the curves of ΔT_g and ΔT_c vs x are not linear. This made it necessary to give ΔT_g and ΔT_c at a specific value of x rather than presenting the slope dT_g/dx, as is customary for linear changes of T_g with x;[1,7] the values of ΔT_g and ΔT_c given here are not quantitatively representative of the effect of M on T_g and T_c at other addition element concentrations.

DISCUSSION

Correlations of T_g with Other Alloy Parameters

It had been noted previously[3] that the thermal stability, and especially, T_g, of the metallic glasses which were studied correlates with their elastic properties; thus, T_g and the Young's modulus E both increase with increasing Cu content in amorphous Zr-Cu.[3,20] Further, the thermal stability of the glass has been related to the melting behavior of the corresponding crystalline alloy; thus, T_g (and T_c) often increases with increasing melting point T_m of the alloy, as suggested early by Mader[21] (for a review, see Ref. 22) and as confirmed recently for glasses containing actinides,[10] refractory metals,[9] and, now, Ca.[6]

These connections between T_g, T_m, and E suggest that the glass transition resembles the melting process in being related to the elastic properties of the solid. For crystalline alloys, such a connection is described by the Lindemann melting point formula,[23] which relates T_m to the Debye temperature Θ_D and/or E.[24-26] It has recently been considered that an analogous relation might hold for T_g, linking T_g to E, and, hence, to T_m.[5] This idea has considerable appeal: in some respects, a Lindemann-type equation may be more applicable to the glass transition than to the melting process; the atomic processes[27] thought to take place during the rearrangement of free volume at T_g appear to be more amenable to an analysis based on elastic forces, which underlies the Lindemann T_m formula, than the melting process. Furthermore, a fundamental criticism of the Lindemann T_m formula is that it is a "single phase" formula, i.e. an expression using only parameters of the solid, although it is applied to a two-phase process. The glass transition, on the other hand, occurs within a single phase; it does not involve the total rearrangement of the structure which occurs during the melting process, and it therefore comes much closer to the physical picture on which the Lindemann T_m formula is based.

In the following section we briefly review the Lindemann T_m formula and present modifications required for its application to T_g, with specific reference to metallic glasses having compositions typical of the two families of glasses treated here.

The Lindemann T_m Formula and its Modification for Application to T_g

The Lindemann formula for the melting point T_m of an element M is:[23-26]

$$T_m = L \cdot m_M \cdot \Theta_D^2 \cdot V_M^{2/3} \qquad (1)$$

where L is a constant (Lindemann constant), m_M is the atomic mass of M, Θ_D is the Debye temperature, and V_M is the atomic volume of M. From this expression, a relation to the elastic parameters can be derived[25] which yields:

$$T_m = L' \cdot E \cdot V, \qquad (2)$$

where E is the Young's modulus of M. For the first case of interest here, a

binary glass $A_{1-x}B_x$, an expression of the form

$$T_g = h(r_A/r_B) \cdot E \cdot V_B \qquad (3a)$$

can be derived, where E is the Young's modulus of the glass, V_B is the atomic volume of the smaller component, and $h(r_A/r_B)$ is a relatively slowly varying function of the atomic size ratio r_A/r_B. For the special case of relatively weakly interacting atomic species, the elastic constants may be assumed to be approximately additive; hence

$$E = \alpha \cdot \bar{E}$$

and

$$T_g = h(r_A/r_B) \cdot \alpha \cdot \bar{E} \cdot V_B \qquad (3b)$$

where $\bar{E}$ is the weighted averaged E of the components in their crystalline form and α is a constant factor ($\alpha \sim 0.7$)[28] relating E for a glass to that of the corresponding crystal or crystal mixture.

Using the solidus melting temperature T_S (frequently a eutectic temperature) for the glass forming composition and making the doubtful assumption that the melting mechanism is similar to that for the glass transition, one obtains

$$T_g = k_1 \cdot T_S, \qquad (3c)$$

as frequently (but notuniversally) found[22] (see below).

Turning to the second case of interest here, ternary additions M at level x_M to a binary glass $A_{1-y}B_y$, and again assuming weak interactions between M and A or B, one obtains

$$\frac{\partial \ln T_g}{\partial x_M} = F_{AB}(E_M, V_M, m_M) \qquad (4a)$$

where E_M, V_M and m_M are the Young's modulus, atomic volume, and atomic mass of the addition element M, respectively, and F_{AB} is a function dependent on the properties of the binary glass $A_{1-y}B_y$.

An especially simple relationship of this type for which there is some theoretical justification expresses $\Delta T_g(x_M)$ by

$$\Delta T_g(x_M) = A_M \cdot E_M \cdot V_M^{1/3}; \qquad (4b)$$

where A_M is a function of M that contains m_M. Substituting $T_m(M)$, the melting point of M, for its elastic modulus, using (2), one obtains from (4b)

$$\Delta T_g(x_M) = (A_M/L') \cdot T_m(M) V_M^{-2/3}. \qquad (4c)$$

T_g for $Ca_{.65}M_{.35}$ Glasses

We discuss the T_g values for these glasses presented in Fig. 2, and we review correlations of T_g with pertinent alloy parameters, beginning with those discussed in the preceding section and continuing with alternate variables such as compound melting points or alloy valence.

Elastic Modulus E: At present, E values for the $Ca_{.65}M_{.35}$ glasses as required in Eq. (3a) are not yet available; however, they are being determined.[20] Expressions such as (3b) which contain only the elastic constants of the components instead of E for the glass are not applicable to the present systems

because the components show significant interactions which vary from system to system; accordingly, T_g and $\bar{E}$ do not correlate.

Solidus Temperature T_S: A possible correlation of T_g with T_S, the solidus temperatures of the binary systems Ca-M at 35 at.pct. M, according to Eq. (3c), is tested in Figure 4. [For Ca-Au, T_S increases from 931 K for $x_{Au} < 0.333$ (Ca_2Au) to 1073 K for $x_{Au} > 0.333$; an averaged value $T_S \sim 1000$ K was therefore used to remove this discontinuity.] It is seen that T_g for M = Zn, Mg, Cu, Ag, and Au lies on or close to a straight line with $T_g/T_S = 0.58$; this value for T_g/T_S is in good agreement with other values observed for T_g/T_S.[22] The T_g values for the trivalent M elements Al and Ca (especially Al) do not follow this relation: for these elements T_g is either higher or T_S is lower than given by the correlation (or both). This suggests that both the melt and the glass are strongly stabilized with respect to the crystalline phase or phases in the Ca-Al and Ca-Ca systems. To explain the observed T_g values, further study of pertinent thermodynamic quantities would be useful, including an assessment of phase diagram features affecting T_S in these systems.

Melting Temperatures T_m of the Compound CaM_2: From the relations suggested by Eq. (3b) and (3c) we turn to a correlation of T_g with a phase diagram feature other than T_S. Inspection of the phase diagrams of the present Ca-M systems which form glasses in their Ca rich regions shows that in all of these systems, except Ca-Cu, the M rich regions contain CaM_2 phases. Four of these phases, in the systems with M = Mg, Zn, Al, and Ga, are Laves phases with relatively high melting points. To test for a possible correlation between the thermal stabilities of the glass and the CaM_2 phases, T_g was plotted against the melting points $T_m(CaM_2)$ (Figure 5). For the systems with Ag and Au, averages of the T_m for two phases adjacent to and more stable than CaM_2 were used; for Ca-Cu the liquidus at the composition $CaCu_2$ was used as an upper bound for T_m. With these provisos, a fair correlation of T_g and $T_m(CaM_2)$ was found, with $T_g/T_m(CaM_2) \sim .42$; existence of this correlation may reflect the consideration expressed earlier[5] that formation and stability of glasses in the Ca systems (and other similar systems) is related to the presence and stability of a Laves phase by complementary aspects of packing and bonding.

Relation of T_g with Other Parameters: The size ratio of the components in Ca-M glasses has been shown[5] to correlate well with the width of the glass forming range and might also be expected to affect glass stability, as reported, e.g., for Laves phases;[23] however, no correlation between T_g and $r_{1/2}(Ca)/r_{1/2}(M)$ is apparent.

T_g was also plotted against $\overline{\Delta H_c}$, the averaged cohesive energy of the glass components; a straight line relation including the origin was found, with a scatter comparable to that seen in Fig. 4. The principal departures from this straight line were observed for Cu and Ag, for which T_g was $\sim$ 100 K lower than predicted from their cohesive energies.

Alloy Valence: It is likely that better correlations than those presented here are not possible until measurements on the elastic properties of the Ca-M glasses are available or more thermodynamic information on the Ca-M alloy systems is available. In the meantime, it is instructive to consider the thermal stability of the Ca-M glasses in terms of the valence n of element M, or in terms of the average valence electron concentration (VEC) (Figure 2). The VEC also plays an important role in the Nagel-Tauc theory relating glass formation and stability to VEC $\sim$ 2 e/a.[10]

The plot shows the following features, discussed in order of decreasing valence of M:

a) Glasses of Ca with Si and Ge, n=4, would be expected to be very stable.

However, for chemical reasons, such glasses could not yet be prepared.

b) Al and Ga, n = 3, form stable glasses with Ca.

c) Mg and Zn, n = 2, form the least stable glasses with Ca prepared in this study.

d) For Cu, Ag and Au, n = 1, T_g increases again; this increase, however, is due to the bond strength inherent in these metals [due (for Cu) in roughly equal parts to conduction electron bonding and s-d hybridization[31]); this bond strength appears to be retained in the glass. A glass of Ca with a simple monovalent (alkali group) metal has not yet been prepared; it is assumed that its thermal stability would be lower than that of the Ca-Mg glass, as indicated for Na.

e) Pd, assigned n = 0, as frequently done in the classification of compounds formed by Ni group metals with simple metals such as Zn,[32] forms the most stable glass; this results mainly from the d - electron bonding contribution of Pd to the glass.

f) Besides its valence, the size of M plays a major role; for each group of M metals, T_g increases with increasing size of M (Zn → Mg; Cu → Au). T_g for Ca-Ag is especially interesting; although the size of Ag should place T_g near T_g(Ca-Au), the lower bond strength of Ag (expressed e.g. in its cohesive energy[33]), as compared to Au, moves T_g(Ca-Ag) down to T_g(Ca-Cu).

T_g for $Zr_{.475}Cu_{.475}M_{.05}$ Glasses

The ΔT_g data in Fig. 3a are discussed in terms of the elastic moduli E_M and atomic volumes V_M of the addition elements M (data from Ref. 35) and equations (4b) and (4c) are applied. Values for Zr and Cu considered as "ternary additions" are also included; these were derived from data on the binary Zr-Cu system.[4,13]

A similar study of the effect of transition metal additives from the second long period is now in progress.

Elastic Moduli and Atomic Sizes of M: The qualitative similarity of the plots for ΔT_g, ΔT_c, and E in Figure 3 (a-c) suggests that these quantities are indeed interrelated; the characteristic, bimodal appearance of all three plots is familiar from the plots of other properties of the first long period transition elements[33] (cohesive energy, bulk modulus) and its recurrence here is striking. In comparing the plots for ΔT_g and E in Fig. 3, disagreements in detail are seen, particularly for V and Cu; for both of these ΔT_g is considerably larger than suggested by E.

The quantitative connection established by the relation (4b) is tested in Figure 6, which shows a plot of ΔT_g vs. $E_M \cdot V_M^{1/3}$. There is a fairly good linear relationship between these two quantities, except for V and Cu which depart strongly from this relationship as noted already for T_m; both elements are more effective in stabilizing the Zr-Cu glass than is indicated by their elastic moduli and atomic sizes. The larger effect of Cu may be due to its B-metal character (see below); for V the melting temperature represents the stabilizing effect better than the low Young's modulus E (see below) or any of the other elastic moduli G or B.[13]

Melting Temperatures T_m(M): The previous section suggests that the present Zr-Cu-M glasses (M = transition metal) are largely additive in their elastic properties which affect T_g. It is therefore of interest whether the elastic constants of the addition elements can be replaced by the corresponding melting temperatures T_m(M) following Eq. (2).

The relation of ΔT_g to $T_m(M)$ given by Eq. (4c) is tested in Fig. 7, where ΔT_g is plotted against $T_m(M) \cdot V_M^{-2/3}$. For all transition metal additives, the ΔT_g values are seen to follow a common curve with relatively little scatter; only Cu departs from this curve, showing again a greater stabilizing effect than would be suggested by its melting point (see below). In contrast to the relation of ΔT_g with E_M, previously discussed, the value for V now follows the common curve, indicating that its glass stabilizing effect is more closely related to its melting point than its elastic modulus. The good overall fit of the ΔT_g data with Eq. (4c) strongly suggests that the glass stabilizing effect and the melting points of the transition metal additives in the present glasses are indeed interrelated.

Other Relations: We note that a fit of ΔT_g to the cohesive energies, even if evaluated in connection with an empirical volume factor, provides less overall agreement than the correlations with E_M and $T_m(M)$ discussed in the two previous sections; thus the observed stabilizing effect of Cr and the strong destabilizing effects of Sc and Ti are underestimated, and the (smaller) stabilizing effects of the late transition elements are overstimated.

Non-Transition Metal Additives: A comprehensive study of the effect of B-metal and metalloid additives on T_g for $Zr_{.50}Cu_{.50}$ is in progress.[34] Initial results[4] show that several non-transition metal addition elements have strong stabilizing effects; the magnitude of these effects, however, is not well correlated to their elastic properties and melting points but depends on other pertinent properties such as valence, again in combination with size. The effect of these addition elements thus resembles in some respects that of the B-metal and coinage metal components in the Ca-M glasses treated above; as for the latter, correlations of T_g with phase diagram features (compound formation and stability) may also exist for the Zr-Cu-M glasses. An example is Al which causes a thermal stabilization of the Zr-Cu glass larger than that produced by any of the T-metal addition elements at equal levels; the corresponding T_g value falls far above that given by either of the curves in Figure 6 and 7. The strengthening effect of Cu as an additive in Zr-Cu-M alloys noted above probably has the same origin as that of the other B metals.

We will not comment here on possible alloy chemical reasons for the difference between the effects due to the two groups of additives. In any case, it appears that for the non-transition metal additives the interactions between the additive and the transition metal combination forming the "basic" glass are no longer negligible as they seem to be for transition metal additives, and hence Eq. (3b), (3c), (4b), and (4c) do not apply.

CONCLUSION

Ternary alloy glasses have been studied to obtain T_g values for binary Ca glasses not displaying a glass transition. The results show that for $Ca_{.65}M_{.35}$ glasses T_g depends on alloy valence and size; some correlations to phase diagram features such as the solidus temperature and the melting points of the phase CaM_2 were also observed.

It was also shown that for first long period transition metal additives to a $Zr_{.50}Cu_{.50}$ glass the changes of T_g and T_c are closely related to each other and, jointly, to the elastic moduli and melting points of the additives; the changes of T_g are in general agreement with the predictions of an expression for T_g which is based on a modification of the Lindemann melting point formula appropriate for the glass transition.

The present results suggest that the properties controlling the thermal stability of glasses are additive when transition metal elements are added to

a binary glass such as Zr-Cu, while interaction terms must be considered for non-transition metal addition elements as well as for most Ca-M glasses.

The study of the thermal stability (and elastic properties) of metallic glasses may provide a general approach enabling one to determine the bonding effect of alloying additions at low and high levels without the restrictions on single phase formation imposed by the phase diagram.

ACKNOWLEDGEMENT

The study of the Ca alloy glasses was supported by the National Science Foundation and the study of the Zr-Cu-M glasses was supported by the Office of Naval Research. We thank both agencies for their sponsorship. We are also glad to acknowledge discussions with Prof. F. Spaepen.

REFERENCES

1. H.S. Chen and K.A. Jackson, in Metallic Glasses, J.J. Gilman and H.J. Leamy, Eds., p. 74, 1978, Metals Park, OH, Amer. Soc. Metals.
2. H.A. Davies, Phys. and Chem. of Glasses, 1976, 17.
3. H.S. Chen and J.T. Krause, Scripta Met., 1977, 11, 761.
4. R. Raman, Ph.D. Thesis, 1977, Boston, MA, Northeastern University.
5. B.C. Giessen and F. Spaepen, to be published.
6. R. St.Amand and B.C. Giessen, Scripta Met., submitted.
7. H.S. Chen, Acta Met., 1976, 24, 153.
8. M. Naka, S. Tomizawa, T. Masumoto, and T. Watanabe, in Proc. 2nd Intl. Conf. on Rapidly Quenched Metals, N.J. Grant and B.C. Giessen, Eds., p.273, 1976, Cambridge, MA, M.I.T. Press.
9. S. Davis, M. Fischer, D.E. Polk and B.C. Giessen, in Proc. 3rd Intl. Conf. on Rapidly Quenched Metals (Brighton, 1978).
10. R.O. Elliott and B.C. Giessen, in Proc. 3rd Intl. Conf. on Rapidly Quenched Metals (Brighton, 1978).
11. D.E. Polk and H.S. Chen, J. Noncryst. Solids, 1974, 15, 165.
12. H.S. Chen and D. Turnbull, Acta Met., 1969, 17, 1021.
13. A. Kerns, D.E. Polk, R. Ray and B.C. Giessen, Mater. Sci. Eng., submitted.
14. R. St.Amand, Ph.D. Thesis, 1978, Boston, MA, Northeastern University.
15. H.S. Chen, Acta Met., 1974, 22, 897.
16. J. Hong and B.C. Giessen, to be published.
17. A. Calka, D.E. Polk and B.C. Giessen, to be published.
18. S. Kavesh, in Metallic Glasses, J.J. Gilman and H.J. Leamy, Eds., p.36, 1978, Metals Park, OH, Amer. Soc. Metals.
19. M. Fischer, D.E. Polk and B.C. Giessen, in Rapid Solidification Processing, Principles and Technologies, R. Mehrabian, B.H. Kear and M. Cohen, Eds., p. 140, 1978, Baton Rouge, LA, Claitor's Publ. Division.
20. L. Kabacoff, J. Hong, D.E. Polk and B.C. Giessen, present results.
21. S. Mader, J. Vac. Sci. Technol., 1965, 2, 35.
22. B.C. Giessen and C.N.J. Wagner, in Liquid Metals, S.Z. Beer, Ed., p. 633, 1972, New York, NY, Marcel Dekker.
23. F.A. Lindemann, Physik. Z., 1910, 11, 609.
24. J.M. Ziman, Principles of the Theory of Solids, Sec. Ed., p. 65, 1972, Cambridge, Cambridge Univ. Press.
25. F.H. Herbstein, Adv. Phys., 1961, 10, 313.
26. N.H. March, Liquid Metals, p. 54, 1968, Oxford, Pergamon.
27. F. Spaepen, in Proc. 3rd Intl. Conf. on Rapidly Quenched Metals (Brighton, 1978).
28. T. Masumoto and R. Maddin, Mater. Sci. Eng., 1975, 19, 1.
29. G.M. Campbell, Met. Trans. 1977, 8A, 1493.

30. S. Nagel and J. Tauc, in Proc. 2nd Intl. Conf. on Rapidly Quenched Metals, N.J. Grant and B.C. Giessen, Eds., p. 337, 1976, Cambridge, MA, M.I.T. Press.
31. G.D. Gelatt, Jr., H. Ehrenreich, and R.E. Watson, Phys. Rev., 1977, B15, 1613.
32. W. Hume-Rothery and G.V. Raynor, The Structure of Metals and Alloys, p. 197, 1962, London, The Institute of Metals.
33. K. Gschneidner, Jr., Solid State Physics, 1964, 16, 275.
34. R. Raman and B.C. Giessen, to be published.

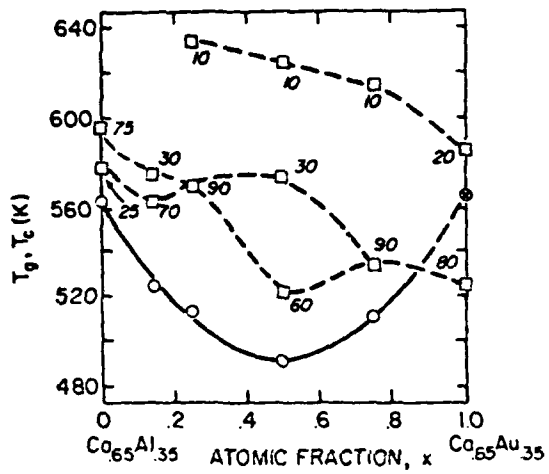

Fig. 1. Glass transitions T_g(o) and exothermic effects (□) in ternary $Ca_{.65}(Al_{1-x}Au_x)_{.35}$ glasses. The T_g values are fitted with the parabolic curve shown in solid line (see text) so as to determine T_g for $Ca_{.65}Au_{.35}$. The dashed connections of the exothermic effects are tentative; some connected exothermic effects may not correspond to related physical processes.

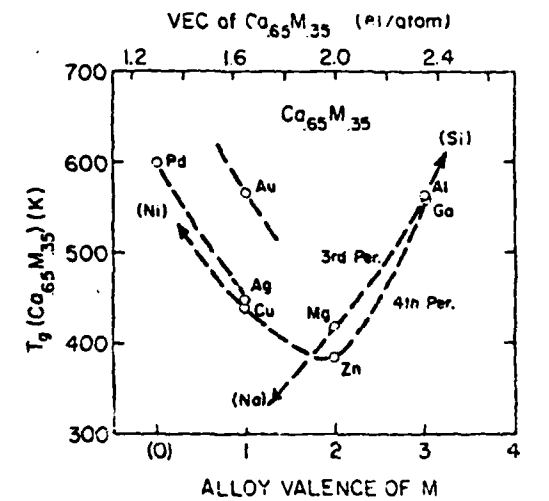

Fig. 2. Glass transition temperatures T_g for binary $Ca_{.65}M_{.35}$ glasses derived from binary or appropriate ternary systems (see text), plotted against the valence of M (bottom) and the average valence electron concentration (VEC) of the glass (top). Here, Pd is assumed to have a valence of zero.[32]

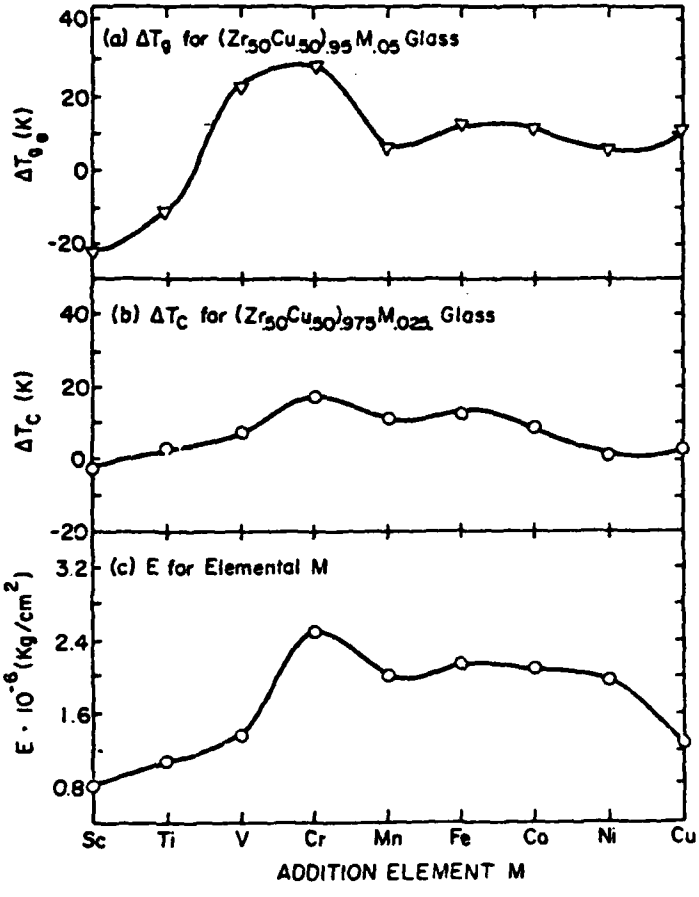

Fig. 3. Properties of Zr-Cu-M glasses (a,b) and crystalline M (c) plotted against M, transition elements from the first long period.
(a) $\Delta T_g(Zr_{.475}Cu_{.475}M_{.05}) = T_g(Zr_{.475}Cu_{.475}M_{.05}) - T_g(Zr_{.50}Cu_{.50})$
(b) $\Delta T_C^g(Zr_{.4875}Cu_{.4875}M_{.025}) = T_C(Zr_{.4875}Cu_{.4875}M_{.025}) - T_C(Zr_{.50}Cu_{.50})$
(c) Young's modulus E for crystalline, elemental M.

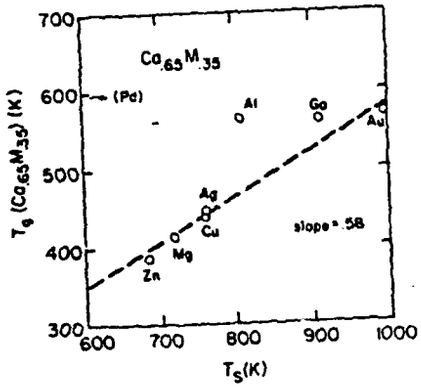

Fig. 4. Glass transition temperature T_g of $Ca_{.65}M_{.35}$ glasses plotted against the solidus temperatures T_S.[6]

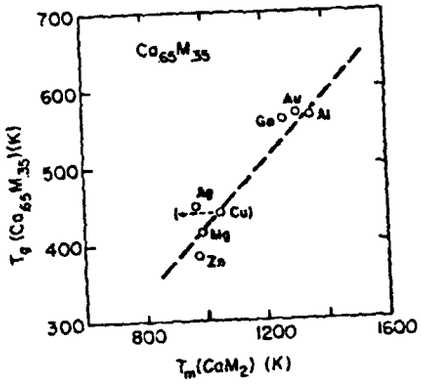

Fig. 5. Glass transition temperature T_g of $Ca_{.65}M_{.35}$ glasses plotted against T_m, the melting temperatures of CaM_2 (see text for explanation for M = Cu Ag, and Au).

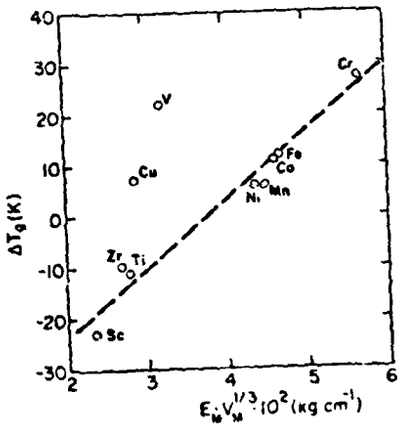

Fig. 6. ΔT_g for $(Zr_{.50}Cu_{.50})_{.95}M_{.05}$ glasses (as defined in Fig. 3) plotted against $E_M \cdot V_M^{1/3}$, where E_M = Young's modulus of M, V_M = atomic volume of M.

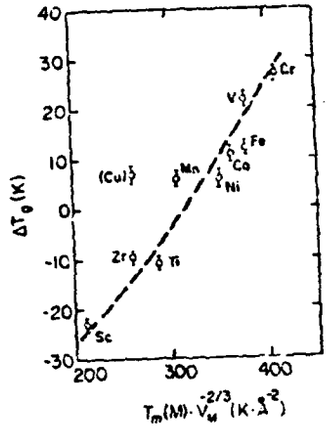

Fig. 7. ΔT_g for $(Zr_{.50}Cu_{.50})_{.95}M_{.05}$ glasses (as defined in Figure 3) plotted against $T_m(M)V_M^{-2/3}$ where $T_m(M)$ = melting temperature of M, V_M = atomic volume of M.

Scripta METALLURGICA Vol. 12, pp. 1021-1026, 1978 Pergamon Press, Inc.
Printed in the United States

EASY GLASS FORMATION IN SIMPLE METAL ALLOYS: AMORPHOUS METALS CONTAINING CALCIUM AND STRONTIUM

R. St.Amand and B.C. Giessen
Solid State Chemistry Laboratory, Department of Chemistry
Northeastern University, Boston, MA 02115

(Received August 7, 1978)
(Revised September 6, 1978)

Introduction

Most metallic glasses prepared by rapid quenching from the melt[1] contain one or more transition metals.[2] The only previously reported glass forming (G.F.) system containing only simple metals is Mg-Zn;[3] however, no other Mg glasses appear yet to have been made. It has also been found that the easily glass forming composition ranges in binary alloy systems are generally narrow (≤ 20 at.pct.);[2] the only known binary system with a G.F. composition range of ~50 at.pct. is Zr-Cu.[4,5]

We report in the following the preparation and some thermal properties of new metallic glasses in seven binary, simple metal alloy systems containing the alkaline earth metals Ca and Sr. Some of these alloys are characterized by high G.F. tendency,[2,6] broad G.F. composition ranges, interesting transformation behavior, and, at least in two cases, alloy chemical simplicity that allows the role of the size factor in glass formation[2] to be identified clearly.

The seven systems are listed in Table I. Phase diagrams[7,8] for two representative systems, Ca-Mg and Ca-Cu are given in Fig. 1 a and c, respectively. The Ca-Mg system is characterized by a $MgCu_2$ type Laves phase $CaMg_2$; the Ca-Zn and Ca-Al systems are similar to the Ca-Mg system in this respect but contain additional phases in the Ca rich region of the low melting eutectic at ~73 at.pct. Ca, as well as at low Ca contents. The Sr systems are similar to the corresponding Ca systems. In Ca-Cu, the Laves phase at AB_2 is replaced by the structurally related phase $CaCu_5$.[8]

Experimental Methods

Amorphous alloys were prepared using a melt spinning technique[9] (squirting of a thin liquid alloy jet onto the inside of a rotating Cu drum in a vacuum) under experimental conditions (e.g. squirt gas pressure, orifice size, melt superheat) that were kept constant as much as possible. This method yields alloy ribbons typically 30 μm thick, 2 mm wide, and 2-8 m long; glass formation or non-formation at a given composition is reproducible if smooth portions of equal thickness indicating similar cooling rates are compared. Alloy examination by XRD and DSC (Perkin Elmer DSC-2) was as customary.[2] Some amorphous alloys were characterized by an extremely broad, double-humped first diffraction maximum due to the large size differences of the components.

Results and Discussion

The results summarized in Table I show that (a) Ca and Sr alloys were easily retained as glasses by rapid quenching; (b) the G.F. composition ranges are between 20 and 50 at.pct. wide; (c) in some cases (e.g. Ca-Cu and Ca-Mg) a complex series of thermal effects occurs; and (d) the glass transition (T_g) or crystallization temperatures (T_c) lie between 383 and 585 K (for glasses $A_{.45}B_{.55}$). We discuss these features briefly in the following.

Glass Formation: Elemental properties or alloy constitutional factors that have been associated with ready glass formation are summarized in Ref. 2; these include: a favorable component size ratio[10] [$R_L/R_S > 1.15$,[2] where R_L and R_S are the 12-coordinated radii of the larger and smaller (and, generally, majority and minority) components, respectively]; a favorable valence electron concentration (VEC ~ 2 electrons/atom, Nagel-Tauc model);[11] strong chemical interactions of the constituents;[12] chemical and periodic table differences of the constituents;[2] a strong depression of the alloy melting point T_m below the values for the ideal solution, $T_{m,id}$[13] or the component average, $\bar{T}_m$.[2] The easy G.F. found e.g. in the Ca-Cu and Ca-Al systems argues against a dominant role of the valence electron concentration (easy glass formation was observed for 1.4 e/a < VEC < 2.4 e/a). Easy G.F. in Ca-Mg alloys argues against the effectiveness of several other factors considered, namely, the role of strong chemical interactions (the intermediate phase $CaMg_2$ has only a moderate heat of formation, see Table I), differences in chemical character and periodic table position (both elements are alkaline earth metals and vertical neighbors in their group), and a large melting point depression below the ideal solution value $T_{m,id}$[13] (at 27 at.pct. Mg the Ca liquidus is depressed only by 14% from $T_{m,id}$).

Concerning the chemical interactions in the liquid it may be noted that the integral enthalpies of mixing in the Ca-Mg system[14] can be separated into a (symmetric) regular solution portion and a slightly skewed excess portion; the latter quantity, however, has its maximum at $x_{Mg} = .54$, with only a considerably smaller value of the excess enthalpy in the glass forming range. The role of liquid interactions in G.F. remains unclear.

These considerations leave as factors to be considered for the present systems the depression of the melting point below the average component value [$\Delta T_{mr} = (\bar{T}_m - T_m)/\bar{T}_m = 32\%$ for Ca-Mg, i.e., in the G.F. range[2]] and the component size ratio ($R_L/R_S = 1.23$ for Ca-Mg[15]). [Some alloying elements B such as Ga or Al melt abnormally low in relation to their boiling points. For them the usual expression for the reduced melting point depression[2] $\Delta T_{mr} = (T_m - T_m)/T_m$ should be modified, e.g. by using a constant fraction of the boiling point of B instead of $T_m(B)$ to compute $\bar{T}_m$, since their alloy chemical behavior, e.g. the melting points of their intermetallic compounds with other elements, reflects their cohesive energies rather than their low melting points; the boiling points can then be used as a measure of the cohesive energies.]

As to the relative importance of these two factors, kinetic considerations[6] show that a critical viscosity generally due to a sizeable melting point depression is required for G.F. to occur; however, as the next paragraph shows, the size factor plays a major role in determining the width of the glass forming region and may also control glass formation, e.g. via the viscosity. Further, the melting point depression and the size factor were found to be inter-related in the present systems; there is a weak dependence of ΔT_{mr} on R_L/R_S.

Glass Forming Composition Ranges: The width of the G.F. ranges Δx_g generally depends on the cooling rate and can often be extended somewhat by a faster quenching method, such as splat cooling of thinner foils; however, the method of preparation used here resulted in approximately constant cooling rates and thus produced Δx_g values that permitted comparison and correlation with alloy chemical parameters. It was found that the Δx_g values for the present alkaline earth metal systems are well represented by a straight line, making Δx_g proportional to the component size ratios R_L/R_S, as shown in Fig. 2; however, a different functional relationship between Δx_g and R_L/R_S than the straight line would be expected to hold at high and low values of R_L/R_S. While $\Delta x_g \sim 0$ upon extrapolation to $R_L/R_S = 1$ for the present systems, general experience shows that Δx_g vanishes at values of $R_L/R_S > 1$, say, at $R_L/R_S \sim 1.05$. Also, while $\Delta x_g \approx 1.0$ upon extrapolation to $R_L/R_S \sim 2.0$, one expects that $\Delta x_g < 1$ for all values of R_L/R_S and actually decreases beyond a certain value of R_L/R_S. However, the observed dependence of Δx_g on R_L/R_S again emphasizes the crucial role of the size factor in G.F. A qualitative relation of the composition ranges of three vapor deposited amorphous phases to their component size ratios had been given previously by Nader.[16]

Thermal Effects: Table I shows that the transformation behavior differs widely from system to system and is often complex; details will be the subject of a future report. In most of the present systems, there are several thermal effects with different composition dependences, as shown for Ca-Al glasses in Fig. 3. Compared to some other Ca glasses, the thermal behavior of the Ca-Al glasses is relatively simple, with a glass transition T_g and three exothermic crystallization (or recrystallization) effect T_{c1}, T_{c2}, and T_{c3}. The glass transition is only observable at Al contents > 30 at.pct., being preceded by the crystallization effects T_{c1} and T_{c2} at lower Al concentrations. The different slopes of the T_g and T_c curves above 30 at.pct. Al suggest that the glass transition does not vanish below that Al concentration, but that there is a cross-over of the T_c and T_g curves, in agreement with the hypothesis[17] that every metallic glass will show a glass transition if crystallization or another irreversible effect does not occur before.

A thermal effect of special interest was found in the Ca-Cu system, where a hitherto unreported phenomenon, namely an ordering reaction in the glassy state (which is accompanied by a strong exothermic effect) is believed to exist.[18] In the Ca-Mg system, heating may result in phase separation[19] of a single glass into two glasses.[18] These observations will be reported in detail in a subsequent publication, as noted above.

Thermal Stability: Finally, we discuss correlations concerning the thermal stability of alkaline earth metal glasses having the composition $A_{.65}B_{.35}$ (Fig. 4; where there are several exothermic reactions involving amorphous alloys, temperature ranges showing the temperatures and approximate relative enthalpies of the respective processes are given). In general, such correlations are more likely to exist for T_c data than for the temperatures of the first crystallization or other exothermic effects which are apt to depend on constitutional details of the individual system; however, since both T_g and T_c effects reflect at least in part local atomic mobility and dynamics, T_c data are sometimes used in those systems where the absence of observed glass transitions restricts the data available for correlations involving T_g.[20,21] As shown in Fig. 4, the temperatures of the major exothermic effects lie within a broad band which correlates roughly with the temperatures T_E of the eutectics in the G.F. regions. The ratios T_{c1}/T_E lie between 0.58 (Mg-Zn) and 0.70 (Ca-Al); these values agree with the range of 0.44 (Au-Si) to 0.68 (Nb-Ni) typically found for metallic glasses.[22]

Fig. 4 also shows that the two observed T_g values (for Ca-Zn and Ca-Al) increase with T_E; a straight line connecting these T_g values (as a first approximation) lies in the middle of the range of crystallization temperatures. This suggests again that the reason for the failure to observe T_g in the other present systems is the low temperature at which exothermic effects (crystallization, phase separation, or ordering, see above) begin to occur in each of them.

The observed qualitative correlation of T_g, T_{c1}, and T_E suggests a microscopic similarity of glass transition, crystallization, and melting, involving common controlling factors, as suggested by a recently given expression[23,24] for T_g which is related to the Lindemann melting point formula.[25] There is also a monotonic correlation between the T_{c1} (and T_g) and the averaged cohesive energies $\overline{\Delta H_f}$ of the constituents; however, to be applicable to the systems with Cu and Ag, this correlation requires ΔH_f for these elements to be reduced by an amount roughly corresponding to the s/d hybridization contribution to ΔH_f.[26]

Other correlations that have been proposed or could be considered for the thermal stability, e.g. with the elastic moduli of the constituents,[27] alloy valence[5,21,23] or constituent size ratio were not found to be followed well in the present alloys.

Concluding Remarks

The foregoing observations show that alkaline earths easily form metallic glasses in combination with other simple metals; the data suggest a prime role of the component size ratio in G.F. and the width of the G.F. range. As the size ratio is also a dominant factor in the formation of the Laves phases present at the stoichiometry AB_2 in most of the present systems (Table I), formation of the amorphous simple metal alloys containing Mg, Ca and Sr which

center approximately around the composition A_2B may perhaps be seen as being due to a combination of favorable component size ratio and composition capable of forming amorphous "Anti-Laves-Phases" in that range. Further, there is a close relation between the thermal stability of these glasses and the eutectic melting temperatures of the corresponding alloys. It is hoped that further study of metallic glasses containing simple metals, such as the present ones, will aid in obtaining a broader understanding of the glassy state in metals.

Acknowledgement

This work was supported by the Office of Naval Research and the National Science Foundation. We are grateful to Prof. D. Turnbull for permission to use a DSC 2 calorimeter at Harvard University (supported by an NSF-MRL grant and ONR Contract No. N00014-77-C-0002). We thank Dr. D.E. Polk, Dr. A.Calka and Ms. J. Hong for discussions and assistance.

References

1. P. Duwez and R.H. Willens, Trans. Met. Soc. AIME, 227, 362 (1963).
2. D.E. Polk and B.C. Giessen, in Metallic Glasses, J.J. Gilman and J.H. Leamy, Eds., American Society for Metals, Metals Park, OH, p. 1 (1978).
3. A. Calka, M. Madhava, D.E. Polk, B.C. Giessen, H. Matyja, J. Vander Sande, Scripta Met. 11, 65 (1977).
4. A. Kerns, D.E. Polk, R. Ray, and B.C. Giessen, Mater.Sci. Eng., submitted.
5. R. Raman, Ph.D.Thesis, Northeastern University, Boston, MA (1977).
6. F. Spaepen and D. Turnbull, in Proc. Second Internat. Conf. on Rapidly Quenched Metals, Section I, N.J. Grant and B.C. Giessen, eds., M.I.T. Press, Cambridge, MA, p. 205 (1976).
7. M. Hansen, Constitution of Binary Alloys, McGraw-Hill, New York, NY (1958).
   R.P. Elliott, Constitution of Binary Alloys, First Supplement, McGraw-Hill, New York, NY (1965).
   F.A. Shunk, Constitution of Binary Alloys, Second Supplement, McGraw-Hill, New York, NY (1969).
8. W.G. Moffatt, Binary Phase Diagrams Handbook, General Electric, Schenectady, NY (1976).
9. R. Pond and R. Maddin, Trans. Met. Soc. AIME, 245, 2475 (1969).
10. D.E. Polk, Acta Met.,20, 485 (1972).
11. S.R. Nagel and J. Tauc, in Proc. Second Internat. Conf. on Rapidly Quenched Metals, Section I, N.J. Grant and B.C. Giessen, eds., M.I.T. Press, Cambridge, MA, p. 337 (1976).
12. H.S. Chen and B.K. Park, Acta Met.,21, 395 (1973).
13. M. Marcus and D. Turnbull, Mater. Sci. Eng., 23, 211 (1976).
14. F. Sommer, B. Predel, and D. Assmann, Z. Metallk., 68, 347 (1977).
15. W.B. Pearson, The Crystal Chemistry and Physics of Metals and Alloys, Wiley-Interscience, New York, NY, p.151 (1972).
16. S. Mader, J. Vac. Sci. Tech.,2, 35 (1965).
17. M.H. Cohen and D. Turnbull, J. Chem. Phys., 31, 1164 (1959).
18. R. St.Amand, Ph.D. Thesis, Northeastern University, Boston, MA (1978).
19. H.S.Chen and D. Turnbull, Acta Met., 17, 1021 (1969).
20. A. Calka, D.E. Polk and B.C. Giessen, to be published.
21. M. Naka, S. Tomizawa, T. Masumoto, and T. Watanake, in Proc. Second Internat. Conf. on Rapidly Quenched Metals, Section I, N.J. Grant and B.C. Giessen, Eds., M.I.T. Press, Cambridge, MA, p. 273 (1976).
22. B.C. Giessen and C.N.J. Wagner, in Liquid Metals, Chemistry and Physics, S.Z. Beer, Ed., Marcel Dekker, New York, NY, p. 633 (1972).
23. B.C. Giessen and F. Spaepen, to be published.
24. B.C. Giessen, J. Hong, L. Kabacoff, D.E. Polk, R.Raman and R. St. Amand, in Proc. Third Intl. Conf. on Rapidly Quenched Metals, Brighton, England (1978).
25. J.M. Ziman, Principles of the Theory of Solids, Sec. Ed., Cambridge Univ. Press, Cambridge, England, p. 65 (1972).
26. C.D. Gelatt, Jr., H. Ehrenreich, and R.E. Watson, Phys. Rev., B15, 1613 (1977).
27. H.S. Chen and J.T. Krause, Scripta Met. 11, 761 (1977).
28. K. Gschneidner, Jr., in Solid State Physics, 16, 275 (1964).
29. R. Hultgren, P.D. Desai, D.T. Hawkins, M. Gleiser, K.K. Kelley, Selected Values of the Thermodynamic Properties of Binary Alloys, American Society for Metals, Metals Park, OH (1973).
30. P.M. Robinson and M.B. Bever, in Intermetallic Compounds, J.H. Westbrook, Ed., Wiley, NY, p. 38 (1967).

Table 1
New Glass Forming Systems A-B with A = Ca, Sr and B = Cu, Ag, Mg, Zn, Al.

Alloy System	Composition Range	Thermal Effects in	Radius Ratio	Eutectic Temperature	Averaged Cohesive	Enthalpy of Formation for	Comments

Table I

New Glass Forming Systems A-B with A = Ca, Sr and B = Cu, Ag, Mg, Zn, Al.

Alloy System	Composition Range of Glass Formation (at.pct. B)[a]	Thermal Effects in $A_{.65}B_{.35}$ Alloys		Radius Ratio R_L/R_S[c]	Eutectic Temperature in G.F. Range(K)[d]	Averaged Cohesive Energy ΔH_{coh} (kJ/mole)[e]	Enthalpy of Formation for Highest Melting Compound ΔH_f (kJ/mole)[f]	Comments
		T_g(K)	$T_{exoth.}$ (K)[b]					
Ca-Cu	12.5 - 62.5	N.D.[g]	441, 65% 522, 22%	1.54	761	233	7.3 ($CaCu_5$)	first exotherm assumed to represent ordering of glass without crystallization
Ca-Ag	12.5 - 42.5	N.D.	438,100%	1.37	761	215	- ($CaAg_3$)	
Ca-Mg	22.5 - 42.5	N.D.	414, 28% 428, 18% 497, 35%	1.23	718	166	13.4 ($CaMg_2$)	Phase separation followed by two crystallization effects
Ca-Zn	17.5 - 62.5	389	407, 95%	1.42	664	160	13.0 ($CaZn_2$)	-
Ca-Al	12.5 - 47.5	563	585, 25%	1.38	818	227	73.2 ($CaAl_2$)	Crystallization of "Ca_2Al" in first exotherm
Sr-Mg	Not Determined	N.D.	383, 25% 480, 35%	1.35	699	159	- ($SrMg_2$)	-
Sr-Al	Not Determined	N.D.	490,100%	1.51	--[h]	220	- (SrAl)	Phase diagram not known
Mg-Zn[i]	25 - 35[i]	N.D.	390, 30%[i] 401, 65%	1.15	616	141	10.9 ($MgZn_2$)	Formation of disordered microcrystals assumed in first exotherm

a all values ± (≤ 2.5 at.pct.);
b major exothermic effects only ($\dot{T}$ = 80 K/min);
c Ref. 15;
d Ref. 7;
e Ref. 28;
f Refs. 29, 30;
g N.D. = Not detected;
h Not available;
i Refs. 3, 20.

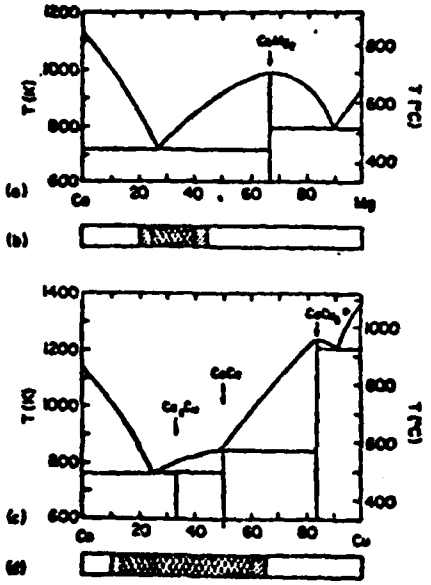

Fig. 1: The constitution diagrams (a) Ca-Mg[7] and (c) Ca-Cu[8] and (b,d) Δx_g, the corresponding composition ranges of easy glass formation (cross-hatched range: complete G.F. observed; hatched regions: G.F. possible).

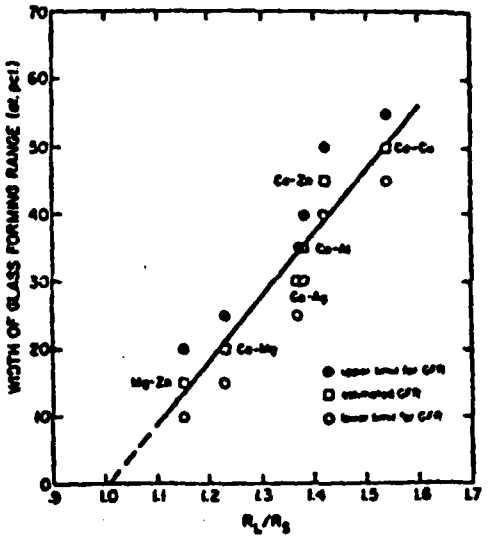

Fig. 2: Width of composition ranges of easy G.F., Δx_g, for five new G.F. systems containing Ca and for Mg-Zn,[20] plotted against the component size ratio R_L/R_S (see text).

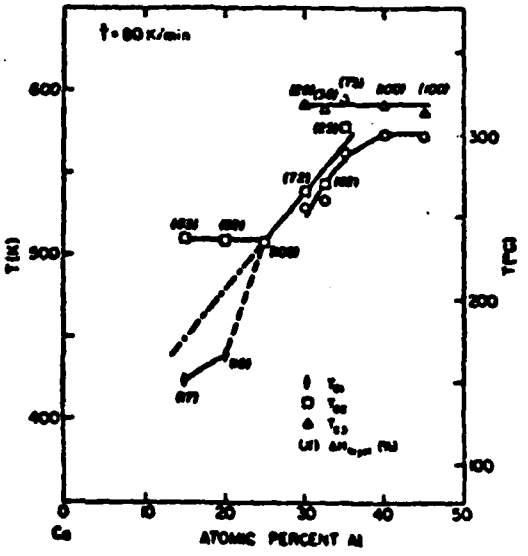

Fig. 3: Thermal effects observed on heating Ca-Al glasses at 80 K/min.

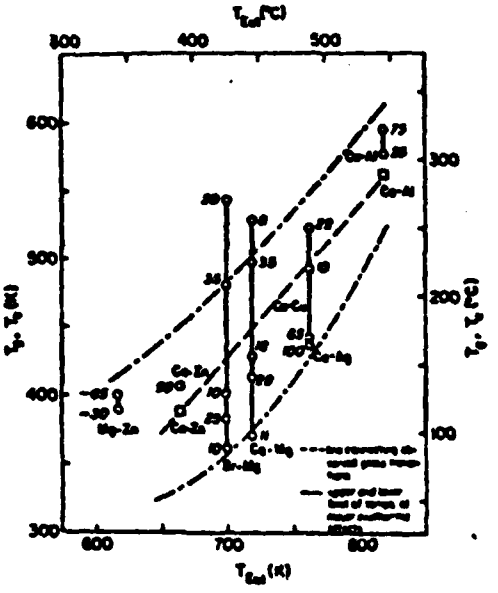

Fig. 4: Temperatures of glass transition, T_g, and exothermal effects, T_c, for glasses of composition $A_{.85}B_{.15}$ containing Ca and Sr, and Mg-Zn.[3,20]

Materials and Science Engineering 38 (1979) 211 - 216

Formation and Structure of a New η phase $Ti_3Be_3(O,N)_x$

B. C. GIESSEN and J. C. BARRICK*

Department of Chemistry and Material Science Division, Institute of Chemical Analysis, Applications and Forensic Science, Northeastern University, Boston, Mass. 02115 (U.S.A.)

L. E. TANNER**

Materials Research Center, Allied Chemical Corporation, Morristown, N.J. 07960 (U.S.A.)

(Received August 11, 1978)

SUMMARY

By heat treating amorphous Ti–Be alloys in the presence of oxygen and nitrogen an η phase $Ti_3Be_3(O,N)_x$ ($x \approx 0.5$) was prepared. Its structure was identified and its atomic parameters were refined. The η phase is cubic (W_3Fe_3C-$E9_3$ type) with $a_0 = 10.713$ Å; the titanium and beryllium atoms have nearly ideal positional parameters. $Ti_3Be_3(O,N)_x$ is the first reported η phase containing beryllium; its occurrence and alloy chemistry are discussed.

1. INTRODUCTION

The η phase structure type ($E9_3$ or $cF112$ type) [1, 2] with a range of compositions and two principal structures characterized by the prototypes W_3Fe_3C and Ti_2Ni is found relatively frequently in transition metal phases [1]. It has the general formula $T_tM_mX_x$, where T represents one or more early transition metal(s) from the scandium, titanium, vanadium or chromium groups, M stands for one or more late transition metal(s) from the manganese, iron, cobalt or nickel groups or B metal(s) such as copper, zinc or aluminum, and X is a metalloid such as carbon, nitrogen or oxygen. The stoichiometry of η phases is variable over a wide range both in the ratio t/m of the metal components, for which $1 \leq t/m \leq 2$, and in the amount of stabilizing metalloid [3, 4]; in some systems such as Ti_2Ni no metalloid is required for η phase formation.

To date η phases containing beryllium (*i.e.* M = Be) have not been described. In recent studies of the annealing behavior of amorphous Ti–Be and Ti–Zr–Be alloys [5, 6] a new phase was observed to form which was subsequently identified as $Ti_3Be_3(O,N)_x$ and which is designated η in the following. We report here its formation and structure.

The equilibration behavior of amorphous Ti–Be alloys [6] is fairly complex. It includes formation of the metastable transition phase m-TiBe (CsCl type) described previously [7].

2. EXPERIMENTAL METHODS AND DATA EVALUATION

Ti–Be metallic glasses were initially prepared by arc furnace splat quenching from the melt [8]; the resulting foils were 10 - 30 μm thick. Some ternary alloy glasses with zirconium were also produced at cooling rates of not less than 10^6 °C s^{-1} in the form of continuous ribbons 1 - 2 mm wide and about 30 μm thick. Differential scanning calorimetry (DSC) using samples encapsulated under a nominally pure argon atmosphere was carried out in a Perkin–Elmer DSC-2 calorimeter by heating at 20 °C min^{-1} up to about 700 °C and then cooling rapidly at 320 °C min^{-1}. Some samples were also examined at higher temperatures in a Mettler TA-1 differential thermal analysis unit (DTA) in nominally pure helium at heating and cooling rates of 15 °C min^{-1}. In addition a ternary Ti–Be–O alloy ($Ti_{0.50}Be_{0.40}O_{0.10}$) was prepared directly

*Present address: Department of Chemistry, Wilmington College, Wilmington, Ohio 45177, U.S.A.
**Present address: ManLabs, Inc., Cambridge, Mass. 02139, U.S.A.

TABLE 1

XRD powder pattern of η phase $Ti_3Be_3(O,N)_x$[a]

hkl	d (Å)		Intensity		
	Obs.[b]	Calc.	Obs.	Calc. (total)	Calc.
400	2.678(6)	2.678	201.0	208.5	208.5
331	2.456(4)	2.458	114.5	112.1	112.1
422	2.186(3)	2.186	184.0	200.6	200.6
511, 333	2.063(2)	2.061	291.0	298.7	180.2, 118.5
440	1.893(2)	1.894	98.0	109.6	109.6
531	1.810(4)	1.811	10.5	12.6	12.6
442	—	1.785	2.0	1.8	1.8
620	1.694(3)	1.694	11.0	17.2	17.2
444	1.548(5)	1.546	12.0	2.4	2.4
551, 711	1.4994(13)	1.5000	99.0	77.3	76.0, 0.7
553	1.3949(17)	1.3947	54.0	44.4	14.3
731					30.0
733	1.3088(14)	1.3087	51.0	46.7	46.7
822, 660	1.2624(7)	1.2625	150.0	132.8	94.4, 38.4
751, 555	1.2351(12)	1.2370	24.0	31.1	4.7, 25.7
662	—	1.2288			0.6
840	—	1.1977	1.0	0.6	0.6
911, 753	1.1743(24)	1.1759	8.5	8.6	3.3, 4.7
842	—	1.1688			0.6
664	1.1418(8)	1.1419	12.0	12.0	12.0
931	—	1.1230	1.0	0.4	0.4
844	—	1.0934	1.0	0.7	0.7
933, 771, 755	1.0767(9)	1.0767	35.0	34.6	16.8, 7.4, 10.4
10,20, 862	1.0504(7)	1.0505	36.0	34.7	14.2, 20.5
773, 951	1.0357(8)	1.0356	39.0	37.5	20.0, 16.1
10,22	—	1.0308			1.4
953	—	0.9989	4.0	1.1	1.1
10,42	0.9772(17)	0.9779	4.0	2.8	2.8
955, 11,31, 971	0.9364(12)	0.9360	17.0	16.7	14.9, 0.1, 1.2
10,44, 882	—	0.9324			0.4, 0.2
10,60, 866	0.9187(7)	0.9186	48.0	43.3	43.1, 0.2
11,33, 973	0.9091(6)	0.9086	13.0	14.8	2.6, 12.2
884, 12,00	0.8927(5)	0.8927	34.5	31.0	26.4, 4.6
11,51, 777	0.8836(3)	0.8836	35.5	38.7	34.2, 4.5
12,22, 10,64	0.8689(2)	0.8689	83.0	81.5	33.7, 47.8
975, 11,53	—	0.8605	—	—	—
12,40	—	0.8469	2.7	5.0	5.0
991	—	0.8391	2.1	1.7	1.7
12,42	—	0.8365	1.1	0.1	0.1

TABLE 1 (continued)

hkl	d (Å)		Intensity		
	Obs.[b]	Calc.	Obs.	Calc. (total)	Calc.
10,82	0.8260(7)	0.8265	11.8	10.2	10.2
11,71	0.8187(3)	0.8192	52.0	43.9	2.9
11,51					36.2
993					4.0
13,11					0.9

[a] The samples were prepared by heating glassy $Ti_{0.56}Be_{0.44}$ alloy to about 1000 °C in a DTA unit under nominally pure helium (see text).
[b] The numbers in parentheses are the standard deviations.

by arc melting a mixture of titanium, TiO_2 and beryllium.

The phases present in the as-quenched and transformed specimens were studied by X-ray diffractometry (XRD) using filtered copper K_α and molybdenum K_α radiation. The resulting powder patterns were internally calibrated with α-titanium lines; peaks due to α-titanium and $TiBe_2$ were subtracted to obtain the powder pattern of η which was readily indexed. The positional parameters of η were obtained by a least squares refinement carried out directly on the intensity data [9]; this was required because of the numerous systematic peak overlaps present in the powder pattern of a cubic substance such as η.

3. RESULTS

Glassy Ti–Be foils containing 40 - 45 at.% beryllium were heated through the devitrification temperature (about 400 °C) and through the temperature range (about 470 - 525 °C) where metastable m-TiBe forms and is then present together with equilibrium α-titanium (beryllium) solid solution up to about 700 °C [7]. Upon further heat treatment, *e.g.* heating to about 1000 °C (the eutectic temperature is 1030 °C), m-TiBe transforms, producing $TiBe_2$, additional α-titanium and up to 60% η. No attempt was made to determine the composition of η by quantitative XRD analysis; the composition $Ti_3Be_3(O,N)_x$ was inferred from the unit cell volume and the XRD intensity match discussed in the next paragraph. The η phase was also found in the ternary alloy $Ti_{0.50}Be_{0.40}O_{0.10}$ prepared by arc melting.

The crystal structure of η was unambiguously identified from its powder pattern (Table 1) and confirmed by the good match between observed and calculated line positions and intensities (fractional standard deviation $\Delta d/d = 10^{-3}$, residual $R_I = \Sigma(|I_{obs} - I_{calc}|)/\Sigma I_{obs} = 0.089$). The good agreement between the observed and calculated intensities in quenched foils and ribbons indicated that there is no preferred crystallization texture for these alloys in agreement with previous observations for m-TiBe [7]. In the following the standard deviations are given in parentheses.

The η phase $Ti_3Be_3(O,N)_x$ is cubic with the following properties: $Fd3m$ space group no. 227, W_3Fe_3C type [1 - 4], $a_0 = 10.713(1)$ Å. The 96 metal atoms are in the following positions (using the first setting (ref. 10, p. 340) with the origin at $\bar{4}3m$ ($\bar{1}/8, \bar{1}/8, \bar{1}/8$ from $\bar{3}m$)):

titanium in 48 (*f*): $x,0,0$ etc., with $x_f = 0.196(1)$;

beryllium in 32 (*e*): x,x,x etc., with $x_e = 0.829(12)$;

beryllium in 16 (*d*): 5/8, 5/8, 5/8 etc.

The oxygen and/or nitrogen atoms are in the following positions:

(O, N) in 16 (c): 1/8, 1/8, 1/8 etc.; occupation factor = 0.30(11), (≙ 4.8 O, N atoms);

(O, N) in 8 (*a*): 0,0,0 etc.; occupation factor = 0.37(14) (≙ 3.0 O, N atoms).

Owing to the low scattering power of beryllium the parameter x_e has a larger standard deviation than x_f. The least squares fit is quite sensitive to the amount of oxygen or nitrogen present and allowed an approximate determination of the metalloid content; owing to the low scattering power of beryllium the fit is more sensitive to the location and number of metalloid atoms than to the positional

parameters of the beryllium atoms. The residual R_I (see earlier) varies from 12%, if no metalloid content is assumed, through a minimum (best fit) of 8.9%, for about one-third occupancy of both (*a*) and (*c*), to 18% for full occupancy of these sites. Refinement with metalloid atoms occupying only one of the positions (*a*) or (*c*) increased R_I, *i.e.* resulted in a worse fit.

The best fit occupation factors given above yield 7.8 metalloid atoms per 96 metal atoms (7.5 at.% O,N) which corresponds to the formula $Ti_3Be_3(O,N)_{\sim 0.5}$. Considering the method of preparation, the oxygen and nitrogen present in the alloy was probably not homogeneously distributed and a further refinement of the occupancy parameters would not have been meaningful.

4. DISCUSSION

4.1. Metalloid content

Extended heating of the Ti–Be glass up to 1003 °C was necessary to prepare η; this shows that formation of η in this alloy was the result of a slow, diffusion-controlled process such as the uptake of oxygen and/or nitrogen. The critical lower limit of metalloid concentration required to form η was not determined. Metalloid atoms are generally needed for the formation of η-type phases as demonstrated by the tables of representatives of this type [1, 3] which show that only about 10% of the representatives given are binary intermetallic alloys.

The possible filling schemes for the metalloid (X) sites are reviewed in refs. 3 and 4. Examples exist for the filling of the (*a*) position, the (*c*) position and the simultaneous filling of (*a*) and (*c*); however, to date the latter case has only been observed for η type phases of composition T_2MX_x, where $x = 0.75$ [11].

4.2. Mean atomic volume and atomic positions

The mean atomic volume (MAV, taken per metal atom) of η is $\bar{V}_{T,M} = 12.81(2)$ Å^3; this closely matches the value of 12.71 Å^3 for m-TiBe [7] as well as the interpolated MAV for the binary equiatomic composition (Fig. 3 of ref. 7). This agreement also confirms the stoichiometry of η with respect to the ratio of titanium to beryllium.

The positional atomic parameters in η are very close to those found in prior studies on η carbides such as $x_t = 0.195$ and $x_e = 0.825$ for W_3Fe_3C [12]. Further, both sets of values are close to those required for spherical packing of T and M species: $x_t = 3/16 = 0.1875$ and $x_e = 1/2 - (231/512)^{1/2} = -0.172 \triangleq 0.828$ [3]. Parameters obtained with different settings or site occupation [13, 14] have been shown to be equivalent to the present values [3, 4, 15]. We may thus conclude that despite the large size ratio of the T and M components the geometry of the present η phase is determined by the same factors as that of other η phases.

4.3. Interatomic separations

The interatomic separations for η are as given in Table 2. These separations may be compared with the separations d(Ti–Be) = 2.546 Å and d(Ti–Ti) = d(Be–Be) = 2.940 Å in the isostoichiometric phase m-TiBe [7] and with the separations $2r_{12}$(Be) = 2.256 Å and $2r_{12}$(Ti) = 2.924 Å in the elements. Compared with m-TiBe, longer Ti–Be separations, slightly shorter Ti–Ti separations and much shorter Be–Be separations are observed in η; compared with the elements, the Be–Be separations are similar and both shorter and slightly longer Ti–Ti separations are observed.

Further, the metal–metalloid separations presented in Table 2 show that the oxygen and nitrogen atoms are located closer to the titanium atoms than the beryllium atoms; the Ti–O separations of 2.040 and 2.097 Å are slightly larger than those of 1.924 and 2.014 Å observed in TiO_2 (rutile).

4.4. Occurrence of η phase

$Ti_3Be_3(O,N)_x$ is the first example of an η phase $T_tM_mX_x$ with M = Be. The known η phases with T = Ti are shown in Fig. 1; it is seen that metalloid additions, especially oxygen, are required to form most of them. The maximum atomic contact for spherical atoms and close packing occurs for this type when the radius ratio $r_T/r_M \approx 1.22$ [3]; in the present case $r_{Ti}/r_{Be} = 1.30$ which probably places beryllium in $Ti_3Be_3(O,N)_x$ at the edge of the range of elements M capable of forming η phases with titanium (Fig. 1).

This size consideration may also supply the reason why corresponding η phases do not

TABLE 2

Interatomic separations in η phase $Ti_3Be_3(O,N)_x$

Atom	Number of neighbors	Neighbor	Separation (Å)
48 Ti(f)	2	Be(e)	2.60(13)
	2	Be(e)	2.69(13)
	2	Be(d)	2.696(7)
	4	Ti	2.801(3)
	4	Ti	2.097(9)
	14	metal atoms	
	0.60	O,N(c) (2 × 0.30)	2.040(3)
	0.37	O,N(a) (2 × 0.37)	2.097(9)
	≈1	metalloid atom	
32 Be(e)	3	Be(d)	2.30(13)
	3	Be(e)	2.41(18)
	3	Ti	2.60(13)
	3	Ti	2.69(13)
	12	metal atoms (no close metalloid atoms)[a]	
16 Be(d)	6	Be(e)	2.30(13)
	6	Ti	2.696(7)
	12	metal atoms (no close metalloid atoms)[a]	
4.8 O,N(c)	6	Ti	2.040(3)
	0.74	O,N(a) (2 × 0.37)	2.319(1)
3.0 O,N(a)	6	Ti	2.097(9)
	1.2	O,N(c) (4 × 0.30)	2.319(1)

[a]There are no Be–(O,N) distances less than 3.16 Å, *i.e.* no close Be–(O,N) neighbors.

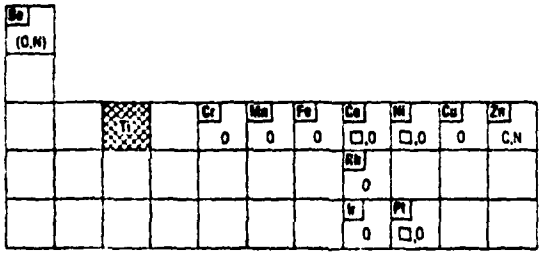

Fig. 1. Table of elements M forming η phase $T_tM_mX_x$ with T = Ti and X = C, N, O or vacancy (□) as indicated. (After ref. 3 including present result for M = Be.)

form even after extended heat treatments of Zr–Be [16], Hf–Be [17] or Zr–Hf–Be [17] glasses at elevated temperatures. For these systems $r_T/r_M \approx 1.42$ (T = Zr, Hf), making an η phase at the equiatomic composition unfavorable.

Partial substitution of zirconium and hafnium for titanium provides further information on the occurrence of the η phase. This phase was also observed to form quite readily upon heating of (Ti, Be)-rich Ti–Zr–Be [18] and Ti–Hf–Be [17] glasses. The maximum change in the lattice parameter ($a_0 \approx 10.77$ Å) and the MAV ($\bar{V}_{T,M} \approx 13.0$ Å^3) of η phase upon substitution of zirconium or hafnium for titanium is similar (on a fractional basis) to the maximum change in the corresponding quantities of m-TiBe upon substitution of zirconium [7] or hafnium [17] for titanium in that phase. Upon adjustment of r_T for the apparent limit of substitution [7] of zirconium or hafnium for titanium in the η phase we find $r_T/r_M \approx 1.31$; this is close to the value for $Ti_3Be_3(O,N)_x$ given above and may represent the critical radius ratio for the formation of this η phase. Size considerations also suggest that further η phases with M = Be may well form with T = V, Nb, Mo and other transition metals.

Some phases of the Ti_2Ni and W_3Fe_3C types have been found to be associated with binary metal–metal glasses and metal–metal glasses containing oxygen additions. Examples are Ti_2Ni, which occurs as an equilibrium phase in a Ti-rich composition range of the Ti–Ni system which readily forms glasses [19], and η phases found after crystallization of Nb–Ni–O and Zr–Cu–O glasses [20].

The formation of the η phase upon heat treating Ti–Be and (Ti, Be)-rich ternary glasses in the presence of an (O, N) atmosphere confirms the need for well-controlled atmospheric conditions in the thermal processing of impurity-sensitive materials such as these glasses.

ACKNOWLEDGMENTS

The work at Northeastern University was sponsored by ONR under Contract N14-76-C-820. Ms. E. Musso provided the technical assistance for all work carried out at the Materials Research Center of the Allied Chemical Corporation.

REFERENCES

1 W. B. Pearson, *A Handbook of Lattice Spacings and Structures of Metals and Alloys*, Vol. 2. Pergamon Press, New York, 1967.
2 W. B. Pearson, *The Crystal Chemistry and Physics of Metals and Alloys*, Interscience, New York, 1972.
3 H. H. Stadelmaier, in *Developments in the Structural Chemistry of Alloy Phases*, Plenum Press, New York, 1969, p. 141.
4 E. Parthé, W. Jeitschko and V. Sadagopan, *Acta Crystallogr., 19* (1965) 1031.
5 U.S. Patent No. 3,989,517 (1976), to L. E. Tanner, R. Ray and C. F. Cline.
6 L. E. Tanner and R. Ray, *Scr. Metall., 11* (1977) 783.
7 L. E. Tanner and B. C. Giessen, *Metall. Trans., 9A* (1978) 67.
8 M. Fischer, D. E. Polk and B. C. Giessen, in *Rapid Solidification Processing, Principles and Technologies*, Claitor's Publishing Division, Baton Rouge, La., 1978, p. 140.
9 C. T. Prewitt, *PRUIT, a FORTRAN Program for Least-squares Refinement on X-ray Diffraction Intensities*, State Univ. New York, Stony Brook, N.Y., 1965.
10 *International Tables for X-Ray Crystallography*, Vol. 1, Kynoch Press, Birmingham, 1969.
11 W. Jeitschko, H. Nowotny and F. Benesovsky, *Monatsh. Chem., 95* (1964) 156.
12 A. Westgren, *Jernkont. Ann., 117* (1933) 1.
13 M. H. Mueller and H. W. Knott, *Trans. Metall. Soc. AIME, 227* (1963) 674.
14 G. A. Yurko, J. W. Barton and J. G. Parr, *Acta Crystallogr., 12* (1959) 909.
15 H. H. Stadelmaier and R. A. Meussner, *Monatsh. Chem., 96* (1965) 228.
16 L. E. Tanner and R. Ray, *Acta Metall., 27* (1979) in the press.
17 L. E. Tanner, to be published; see also U.S. Patent 4,118,222 (1979 to L. E. Tanner, and *Scr. Metall., 12* (1978) 703.
18 L. E. Tanner and R. Ray, to be published; see also U.S. Patent 4,050,931 (1977) to L. E. Tanner, R. Ray and C. F. Clive.
19 D. E. Polk, A. Calka and B. C. Giessen, *Acta Metall., 26* (1978) 1097.
20 D. E. Polk, C. Dubé and B. C. Giessen, in B. Cantor (ed.), *Rapidly Quenched Metals III*, The Metals Society, London, 1978, p. 425.

Materials Science and Engineering, 38 (1979) 49 - 53

Thermal Behavior of Zr–Cu Metallic Glasses

A. J. KERNS*, D. E. POLK, R. RAY† and B. C. GIESSEN

Dept. of Chemistry and Institute of Chemical Analysis, Applications and Forensic Science, Northeastern University, Boston, Mass. 02115 (U.S.A.)

(Received May 1, 1978; in revised form September 11, 1978)

SUMMARY

Zr–Cu metallic glasses containing between 50 and 66.5 at.% copper were prepared in an arc furnace quenching unit. Scanning calorimetry was used to characterize the glass transition temperature T_g, the crystallization temperature T_c and the heat of crystallization ΔH_c. T_g and T_c were found to increase monotonically with increasing copper content over the composition range studied while ΔH_c decreased linearly with increasing copper content: $T_c - T_g$ remained approximately constant. An exothermic relaxation effect, qualitatively similar to that previously reported for metal–metalloid glasses, was observed over a temperature range of about 100 K immediately preceding T_g.

1. INTRODUCTION

Amorphous metals (A.M.s), especially those produced by splat cooling, are a topic of much current interest [1, 2]. On a chemical basis, one may group many of the already reported A.M.s into two categories: transition metal–metalloid A.M.s such as Pd–Si [3, 4] and the Fe–Ni–P–B–C family of metallic glasses [5, 6] (type T–X), and A.M.s such as Nb–Ni [7] and Zr–Cu [8] which combine an early and a late transition metal (type T–T). In the former group a glass is formed only in a rather narrow concentration range (typically at about 15 - 25 at.% X), while in the second group amorphous phases can be retained within a composition range of up to 40 at.% or more. However, it is noted that A.M.s containing no T metals, *e.g.* Mg–Zn [9], have been prepared and that A.M.s which can be considered to be mixtures of the T–X and T–T types, *e.g.* Ti–Ni–Si, have also been studied [10]; a more comprehensive classification has been given in ref. 11.

Because of its fundamental importance, the thermal behavior of A.M.s, especially as revealed by scanning calorimetry, has been studied extensively. The thermal properties which are catalogued are associated with the metastable nature of the A.M. These include the crystallization temperature T_c, the heat of crystallization ΔH_c and the thermal manifestation of the glass transition (a sudden increase ΔC_p in the specific heat to a liquid-like value which occurs at the glass transition temperature T_g), as well as exothermic effects which have been ascribed to relaxation effects [12]. Such thermal studies have concentrated primarily on T–X type amorphous metals, but limited data on T–T type metals, especially Zr–Cu alloys which appear to have become the canonical T–T type amorphous alloys, have also been reported for specific compositions [13 - 15]. Thus, structural [16, 17], electrical [18] and magnetic [19, 20] properties of Zr–Cu glasses have already been studied.

This paper presents calorimetric data on T_g, T_c, ΔH_c and the relaxation effects obtained from amorphous Zr–Cu alloys containing 50 - 66.5 at.% copper.

2. EXPERIMENTAL

Alloys were prepared by arc melting together 99.9% zirconium and 99.9% copper. Amorphous alloy samples were prepared in an arc furnace quenching unit [21, 22] in which

*Present address: Polaroid Corporation, New Bedford, Mass.

†Present address: Allied Chemical Corporation, Morristown, N.J.

a small molten droplet of the alloy is quenched to a foil shape between two flat copper surfaces. Amorphous alloys spanning the composition range 50 - 66.5 at.% copper were prepared; all samples which were characterized thermally were previously determined to be amorphous by X-ray diffraction. Calorimetric measurements were made either with a Dupont 900 calorimeter equipped with a differential scanning calorimetry (DSC) cell or with a Perkin–Elmer DSC-2. T_g and T_c were measured as the onset temperatures of their respective effects, defined as the temperature at which the extrapolated baseline and the steepest tangent to the peak intersect. Generally, thermograms were taken at a heating rate of 20 K min^{-1}; standard calorimetric procedures, *e.g.* for calibration, were followed. Further details are given in ref. 23.

3. RESULTS

All the thermograms for the different alloys exhibited qualitatively similar behavior; as an example Fig. 1 shows the output from the Dupont unit obtained from amorphous $Zr_{0.40}Cu_{0.60}$. The manner in which T_g and T_c are evaluated from the thermograms is illustrated in the figure. It is seen that an exothermic "relaxation" effect (A) precedes a well-defined glass transition (B) which is followed by one or more exothermic peaks due to crystallization (C); each of these effects will be discussed later.

3.1. Glass transition

The glass transition temperatures which were obtained using the Dupont unit for this series of alloys are shown in Fig. 2. T_g is seen to increase monotonically with increasing copper content. A similar compositional dependence of T_g was obtained from different samples prepared at a later time and measured with the Perkin–Elmer unit; comparison of the two data sets suggests that the small fluctuations of the observed T_g from a smooth curve are not real. Values of ΔC_p of about 4 - 5 cal mol^{-1} K^{-1} (beyond the negative deviation due to the relaxation effect) were observed; this value decreases somewhat at the high copper limit of the composition range studied, although this is

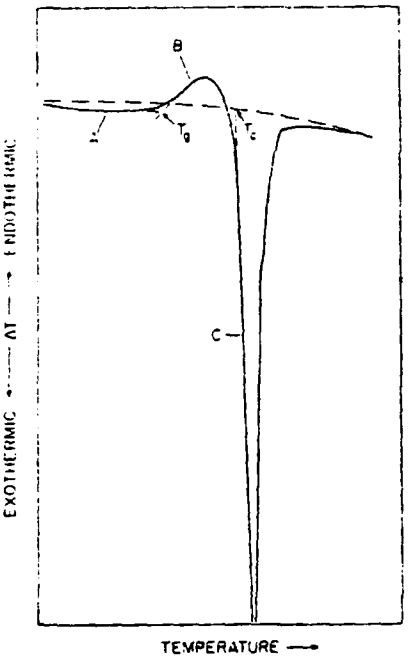

Fig. 1. Thermogram from Dupont unit for $Zr_{0.40}Cu_{0.60}$ scanned at 20 K min^{-1}. The signal which would be obtained from the extrapolated low temperature specific heat is shown by a broken curve; the observed slope and curvature reflect primarily the shape of the baseline. The thermogram exhibits an exothermic relaxation A, a glass transition B and a crystallization exotherm C. Also illustrated is the manner in which the glass transition temperature T_g and the crystallization temperature T_c are determined.

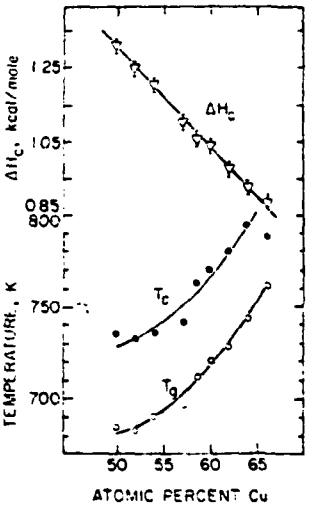

Fig. 2. Values of the glass transition temperature T_g, crystallization temperature T_c and heat of crystallization ΔH_c obtained from the Dupont unit with a scanning rate of 20 K min^{-1}.

presumably due to the onset of crystallization before the full ΔC_p was observed, *i.e.* a relatively lower $T_c - T_g$.

.2. Relaxation effect

The thermal manifestation identified as a relaxation effect is visible over a temperature range of about 100 K immediately preceding ıe glass transition for a scanning rate of _0 K min^{-1}. It was found that the magnitude of the relaxation effect could vary somewhat om sample to sample of the same composion, presumably owing to the different thermal histories (*i.e.* temperature–time relation during quenching) of the different mples. If the sample is heated past relaxtion to the glass transition and then cooled rapidly in the calorimeter before crystallizaon occurs, no exothermic relaxation effect observed in the second heating scan, *i.e.* the relaxation went to completion during the first can; this is consistent with the observed ariability of the relaxation effect for different as-quenched samples of the same composition.

Typically, the relaxation results in the eduction of the apparent C_p by 1 - 2 cal mol^{-1} K^{-1}; the energy associated with the elaxation, obtained by extrapolating the low emperature specific heat to the glass transition, ranged from about 50 to 100 cal mol^{-1}. Given the variability between amples, no systematic compositional dependence of the relaxation behavior on composition was apparent.

.3. Crystallization behavior

The crystallization temperatures T_c and heats of crystallization ΔH_c are also shown n Fig. 2.

Like T_g, T_c is seen to increase with increasing copper content. The difference between T_c and T_g, previously related to the quenchability of the glass [6], is seen to be approximately constant with composition. The line drawn through the T_c points has the ame shape as that through the T_g points; the omewhat greater fluctuations about this line for the T_c points than for the T_g points may eflect in part the different thermal histories of the samples which can affect the ease of crystallization.

The ΔH_c values range from 880 to 1300 cal mol^{-1} and exhibit a linear dependence on composition, although ΔH_c on the one hand and T_g and T_c on the other change with composition in opposite directions. For some alloys, a second much smaller exothermic peak was observed at somewhat higher temperatures; the reported ΔH_c values represent the total heat release.

4. DISCUSSION

It is believed that Zr–Cu is the only inter-transition metal binary glass forming system for which a well-defined ΔC_p associated with the glass transition has been reported; *e.g.* amorphous Nb–Ni [24, 25] and Ti–Ni [10] alloys do not exhibit this effect. The glass transition temperature is of major theoretical interest since it is an intrinsic property of the amorphous phase, *i.e.* it is not related to a first order transition between phases as is T_c. This characteristic of amorphous Zr–Cu alloys makes them ideal for a study of the changes of T_g with composition as various elements are added; such data have recently been obtained [26].

The data reported here are in good agreement with the observation of a T_g of about 450 °C for $Zr_{0.40}Cu_{0.60}$ [13]. However, our data are significantly different from the values of ref. 14; their value for T_g for $Zr_{0.50}Cu_{0.50}$ of about 740 K is about 60 K higher than our value of T_g for the same composition (although they presumably used the midpoint definition of T_g [6]; if so, the difference would be reduced to about 50 K). Recent observations [25] of substantial increases of T_g at small levels of metalloid additives such as oxygen may be relevant in this context. Most importantly, we see no evidence for a relative maximum or break in T_g at about 60 at.% copper as was indicated in ref. 14; our data are approximately linear over this region. However, an eventual downturn of T_g as the Cu content increases is not unexpected since extrapolation of the T_g data of Fig. 2 to pure Cu gives a number which is unreasonably high relative to the melting temperature of Cu.

It is noted that T_g for the Zr–Cu alloys does not scale with the liquidus temperature nor with the thermal properties of the elements (the heat of vaporization and melting point of elemental copper are lower

than those of zirconium). In contrast, copper has a higher Young's modulus E than zirconium. Previous studies have shown a correlation between E of the glass and E of related crystal phases [27, 28] and E of Zr–Cu glasses is indeed observed to increase as the copper content increases [14, 15], although more data would be desirable to determine whether or not the relative maximum in E at about 60 at.% copper shown in ref. 14 exists. A correlation between T_g and E of the glass has been suggested before [14], and a discussion of this correlation will be given elsewhere [29].

For the Zr–Cu alloys reported here T_c scales closely with T_g, suggesting that the micromechanisms of both processes may be controlled by similar interatomic forces in this composition range for this alloy system. However, this scaling cannot be generalized since T_c and T_g are often observed to have different dependences on temperature, *i.e.* temperature coefficients, for selected composition ranges; this is implicit in the observations that the value of $T_c - T_g$ can vary significantly for compositions for which all intermediate compositions are also glass forming [6] and that a glass transition may or may not be seen [6]. While $(T_c - T_g)/T_c$ is generally small, T_c and T_g are equivalent only in a first order approximation; they represent different processes which need not scale together. Thus care must be exercised in using them interchangeably.

The values of the heats of crystallization are in the range typically measured for T–X type glasses, *e.g.* 1.13 kcal mol^{-1} for $Pd_{0.80}Si$ [4] and 1.01 kcal mol^{-1} for $Fe_{0.40}Ni_{0.40}P_{0.14}B_{0.06}$ [6]. The value of ΔH_c = 1.26 kcal mol^{-1} reported in ref. 13 for $Zr_{0.40}Cu_{0.60}$ is higher than our measured ΔH_c = 1.04 kcal mol^{-1} for the same composition; we note, however, that the present value is consistent with the other ΔH values of this study.

The exothermic relaxation effect has previously been studied for $Pd_{0.775}Cu_{0.06}Si_{0.165}$ and $Pd_{0.48}Ni_{0.32}P_{0.20}$, where the heat of relaxation was found to be 190 and 250 cal mol^{-1} respectively for melt-spun ribbons [12]. Such ribbons are expected to have experienced a quench rate similar to that produced by the arc furnace quenching unit used to prepare our Zr–Cu samples which showed a significantly lower heat of relaxation, *i.e.* 50 - 100 cal mol^{-1}. Given the previous data on the T–X glasses and the present observations on T–T glasses, it is likely that such relaxation effects will generally be found for amorphous metals. While the overall relaxation behavior for Zr–Cu is similar to that found for Pd–Si glasses [12], we have found no indication of a substructure to this peak similar to that found in Pd–Si glasses and taken to indicate two different types of relaxation processes [12].

Finally, we note that additional details of the relaxation effect and the effect of low temperature annealing on the crystallization exotherms of $Zr_{0.40}Cu_{0.60}$ are given in ref. 23 and are available from the authors. Also, the glass forming region in the Zr–Cu system is larger than that studied here; in a previous study [30] using splat cooling the formation of the amorphous phase from 33.4 to 70 at.% copper was observed.

ACKNOWLEDGMENTS

We thank the Office of Naval Research for support of this work and Prof. D. Turnbull, Harvard University, for permission to use the DSC-2 unit.

REFERENCES

1 N. J. Grant and B. C. Giessen (eds.), Proc. 2nd Int. Conf. on Rapidly Quenched Metals, Section I, M.I T. Press, Cambridge, Mass., 1976; Section II, Mater. Sci. Eng., 23 (1976) 81 - 308.
2 Metallic Glasses, Am. Soc. Metals, Metals Park, Ohio, 1978.
3 P. Duwez, R. H. Willens and R. C. Crewdson, J. Appl. Phys., 36 (1965) 2267.
4 H. S. Chen and D. Turnbull, Acta Metall., 17 (1969) 1021.
5 P. Duwez and S. C. H. Lin, J. Appl. Phys., 38 (1967) 4096.
6 D. E. Polk and H. S. Chen, J. Non-Cryst. Solids, 15 (1974) 165.
7 R. C. Ruhl, B. C. Giessen, M. Cohen and N. J. Grant, Acta Metall., 15 (1967) 1693.
8 R. Ray, B. C. Giessen and N. J. Grant, Scr. Metall., 2 (1968) 357.
9 A. Calka, M. Madhava, D. E. Polk, B. C. Giessen, H. Matyja and J. Vander Sande, Scr. Metall., 11 (1977) 65.

10 D. E. Polk, A. Calka and B. C. Giessen, Acta Metall., in the press.
11 D. E. Polk and B. C. Giessen, in Metallic Glasses, Am. Soc. Metals, Metals Park, Ohio, 1978, p. 1.
12 H. S. Chen and E. Coleman, Appl. Phys. Lett., 28 (1976) 245.
13 J. M. Vitek, J. B. Vander Sande and N. J. Grant, Acta Metall., 23 (1975) 165.
14 H. S. Chen and J. T. Krause, Scr. Metall., 11 (1977) 761.
15 L. A. Davis, C.-P. Chou, L. E. Tanner and R. Ray, Scr. Metall., 10 (1976) 937.
16 Y. Waseda, T. Masumoto and S. Tamaki, Inst. Phys. Conf. Ser. No. 30, 1977, p. 268.
17 L. Jennings, D. Chipman and B. C. Giessen, to be published.
18 R. Oberle, H. U. Kuenzi, H. J. Guntherodt and B. C. Giessen, to be published.
19 F. R. Szofran, G. R. Gruzalski, J. W. Weymouth, D. J. Sellmyer and B. C. Giessen, Phys. Rev. B, 14 (1976) 2160.
20 G. R. Gruzalski, J. W. Weymouth, D. J. Sellmyer and B. C. Giessen, in R. A. Levy and R. Hasegawa (eds.), Proc. 2nd Int. Conf. on Amorphous Magnetism, Plenum Press, New York, 1977, p. 235.
21 M. Ohring and A. Haldipur, Rev. Sci. Instrum., 42 (1971) 530.
22 M. Fischer, D. E. Polk and B. C. Giessen, in Proc. Conf. on Rapid Solidification Processing, Reston, 1977, Claytor's Publ. Co., Baton Rouge, La., 1978.
23 A. J. Kerns, Ph.D. Thesis, Northeastern Univ., Boston, Mass., 1974.
24 B. C. Giessen, M. Madhava, D. E. Polk and J. Vander Sande, Mater. Sci. Eng., 23 (1976) 145.
25 D. E. Polk, C. Dube and B. C. Giessen, in B. Cantor (ed.), Proc. 3rd Int. Conf. on Rapidly Quenched Metals, Brighton, 1978, The Metals Society, London, 1978, p. 220.
26 R. V. Raman, Ph.D. Thesis, Northeastern Univ., Boston, Mass., 1977.
27 L. A. Davis, in Metallic Glasses, Am. Soc. Metals, Metals Park, Ohio, 1978, p. 190.
28 C.-P. Chou, L. A. Davis and M. C. Narasimhan, Scr. Metall., 11 (1977) 417.
29 B. C. Giessen and F. Spaepen, to be published.
30 R. Ray, D. Sc. Thesis, M.I.T., Cambridge, Mass., 1969.

Measurement of Young's Modulus on Small Samples of Amorphous Metals Using the Impulse Induced Resonance Technique

S. H. WHANG, L. T. KABACOFF, D. E. POLK, AND BILL C. GIESSEN

An impulse induced resonance technique capable of measuring the velocity of an ultrasonic extensional wave on a short (~1 cm long) ribbonlike sample has been applied for the first time to the study of glassy metals: the Young's modulus E was calculated from this velocity and the density. This technique is especially useful for measuring E on amorphous metal samples produced by the piston and anvil technique for rapid liquid quenching: standard techniques for measuring E are not readily applicable to such samples because of their small size. Details of the technique are given, and the dimensional limits necessary to avoid dispersion effects are discussed. The results agree well with those obtained by "pulse-echo" measurements on long ribbons. The Young's moduli of two metallic glasses most readily prepared with the piston and anvil quenching technique are reported.

RECENTLY, there has been increasing interest in the Young's modulus (E) of metallic glasses, in particular the relationship of E to other mechanical properties such as the yield strength and microhardness of the glass as well as to thermal properties such as the glass transition or crystallization temperature. Recent measurements of E for metallic glasses[1,2] have generally been made by the "pulse-echo" technique in which an extensional ultrasonic wave pulse is introduced into a ribbonlike sample (typically many centimeters long) produced by rapid quenching of the liquid using a melt spinning process.[3,4] The velocity V_E of the extensional wave is determined by measuring the time required for the pulse to travel down the ribbon and return after reflection from its end. E is then given by ρV_E^2 (Ref. 5), where ρ is the density of the sample.

The arc-melting piston and anvil technique[6] is another rapid liquid quenching technique which has been used to prepare samples of a wide variety of metallic glasses. Further, this method has been utilized to produce amorphous metal samples for compositions which cannot as readily be made amorphous by melt spinning because, *e.g.*, the quench rate achieved by melt spinning under standard conditions is too low to prevent crystallization (as for $Ti_{0.80}Ni_{0.015}Si_{0.185}$)[7] or the high melting point of the alloy (*e.g.* $Ta_{0.555}Ir_{0.445}$)[8] or its chemical reactivity produces a severe crucible problem for the melt spinning process. However, the circular foils produced with the piston and anvil technique are generally less than about 2 cm in diam., and application of the conventional pulse-echo method to the short strips cut from such foils is difficult because of echo overlap and resonance effects. An alternative approach is to use the pulse-echo technique with a much narrower pulse width and mHz frequencies, but this is not readily applicable to samples having the dimensions characteristic of our samples because of dispersion effects.

The "vibrating reed" technique has been used to determine E from short ribbons,[9,10] but this technique generally produces much less precise results, *e.g.* the uncertainty in the accuracy of a measurement of E by this method was estimated to be ±10 pct.[10] Further, the values produced by this technique are highly sensitive to variations in the sample thickness,[10] so that it is especially unsuited to piston and anvil quenched samples.

Thus, an accurate method for measuring V_E on samples having lengths of about one cm, typical of samples readily produced by the piston and anvil technique, would be very useful. The "impulse induced resonance" technique, developed by K. A. Fowler[11] and applied, *e.g.*, to the measurement of V_E of short silicon carbide whiskers,[12] is such a method, and we have applied it to the measurement of E of short, ribbonlike metallic samples, as previously reported in a letter.[13] In the present paper we describe this method and its application in detail. We have confirmed the accuracy of the impulse induced resonance technique by comparing V_E obtained by this method from small samples, cut from both piston and anvil quenched foils and melt spun ribbons, to V_E measured by the pulse-echo technique on a longer melt spun ribbon. As an example of the utility of the impulse induced resonance technique, we present V_E data obtained from piston and anvil quenched metallic glasses having the compositions mentioned above.

EXPERIMENTAL METHODS AND DATA EVALUATION

Velocity Measurements

A schematic of the experimental setup used for the velocity measurement in both the pulse-echo (PE) and impulse induced resonance (IIR) modes is shown in Fig. 1. The ribbonlike sample is glued to the end of a

S. H. WHANG is Staff Scientist, Materials Science Division, Institute of Chemical Analysis, Applications and Forensic Science, Northeastern University, Boston, MA 02115. L. T. KABACOFF, formerly Research Associate, Materials Science Division, Institute of Chemical Analysis, Applications and Forensic Science, Northeastern University, Boston, MA 02115, is now with Naval Surface Weapons Center, White Oak, MD 20910. D. E. POLK, formerly Senior Scientist, Materials Science Division, Institute of Chemical Analysis, Applications and Forensic Science, Northeastern University, Boston, MA 02115, is now President, MARKO Materials, Inc., Watertown, MA 02172, and BILL C. GIESSEN is Associate Director, Institute of Chemical Analysis, Applications and Forensic Science and Professor of Chemistry, Northeastern University, Boston, MA 02115.

Manuscript submitted March 19, 1979.

ISSN 0360-2133/79/1112-1789$00.75/0

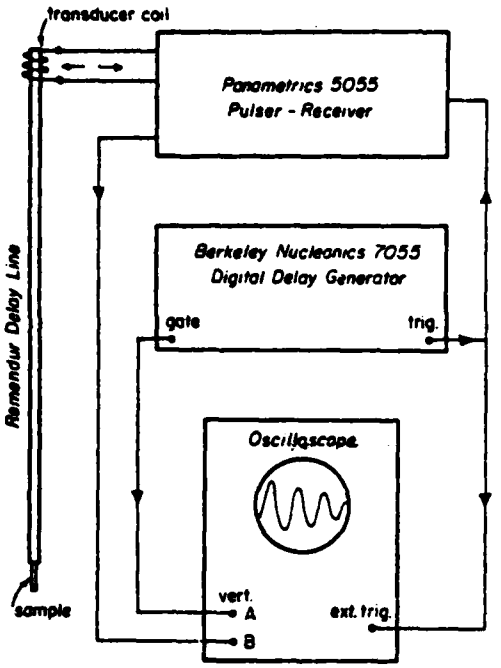

Fig. 1—Schematic of experimental setup used for velocity measurement.

magnetostrictive Remendur delay line with Duco cement. A broad-band sound pulse is introduced into the delay line by means of a Panametrics 5055 Pulser-receiver and a transducer. With a transducer coil length of 1.27 cm, most of the energy is concentrated in the range from 80 kHz to 160 kHz with a maximum intensity at about 100 kHz.[14]

The pulse travels down the delay line and, at the interface between the rod and the sample, part of the pulse is reflected back towards the transducer and part is transmitted into the sample. The reflection coefficient R at the interface is given by:

$$R \equiv \left(\frac{P_r}{P_i}\right)^{1/2} = \frac{(Z_2 - Z_1)}{(Z_2 + Z_1)}$$

where P_r and P_i are reflected and incident power respectively, $Z = \rho V_E A$ is the acoustical impedance. ρ is the density, V_E is the velocity of extensional waves and A is the cross-sectional area.[5] The subscripts refer to the media on either side of the interface, with medium 1 carrying incident and reflected pulses and medium 2 carrying the transmitted pulse. A negative value of R implies phase reversal. That portion of the pulse which enters the sample is reflected from the free end of the ribbon back towards the interface where part is reflected back into the sample and part is transmitted towards the transducer. Pulses returning to the transducer coil produce a voltage therein, this voltage being amplified by the pulser-receiver and displayed on the oscilloscope.

In the pulse-echo technique, one measures, at the transducer, the time interval t between the arrival of the pulse reflected from the interface and the arrival of the pulse reflected from the end of the sample. For our PE measurements, this is done with a Berkeley Nucleonics digital delay generator using a procedure described below. One then determines the velocity of sound in the sample from the relation $2L = V_E t$, where L is the length of the ribbon. (In practice, we measured the change in this time t related to a change (about 10 cm) in the sample length in order to eliminate the effects from the glued, nonideal rod-sample interface.) When the sample length becomes less than approximately twice the length of the transducer coil, the echoes overlap, making time measurements uncertain or impossible.

The impulse induced resonance technique[12] is based on the fact that, under certain circumstances, an extensional mode resonance can be initiated by the incoming sound pulse; the conditions controlling this resonance mode are discussed in the following. When the impedance of the delay line is greater than that of the sample (the condition used in our measurements), resonance occurs when V_E and L are such that the length of the sample corresponds to one quarter of the wavelength for one of the frequencies f_R contained in the pulse, *i.e.* when,

$$V_E = \lambda f_R = 4Lf_R = \frac{4L}{T} \quad (Z_{\text{delay line}} > Z_{\text{sample}})$$

where T is the period of the resonance. In this case, a wave traveling through the sample undergoes phase reversal upon reflection from the free end, but no phase reversal upon reflection from the interface with the delay line. On the other hand, if the impedance of the sample is greater than that of the delay line, phase reversal will occur upon reflection at both ends of the sample. Then, the velocity is given by:

$$V_E = \frac{2L}{T} \quad (Z_{\text{delay line}} < Z_{\text{sample}})$$

In either case, the resonating sample introduces back into the delay line a sinusoidal stress wave which is detected at the coil and displayed on the oscilloscope: the period T can then be measured from this damped sine wave.

As mentioned earlier, the frequency spectrum of the transducer coil which was utilized was concentrated between 80 and 160 kHz, so that this is the frequency range available for resonance. Since the amplitude of the sine wave due to resonance increases as the intensity at the exciting frequency increases, a sample length having a resonance for a frequency of about 100 kHz (the frequency of maximum intensity of the initial pulse) is desirable in order to increase the accuracy of the measurement. Further, the amplitude of the resonance also depends on the degree of impedance mismatch between the delay line and the sample. The optimal sample length L is ~10 mm (from $L = \lambda/4 = V_E/4f$ with $f = 100$ kHz and $V_E = 4 \times 10^5$ cm/s, as is typical for the samples of interest).

Figure 2 shows a resonance pattern typical of that obtained from the short samples. The two different step functions superimposed on the sine wave are used to measure the period of the resonance, as discussed in the following.

The Berkeley Nucleonics digital delay generator produces a voltage "step pulse" of known duration, adjustable to 10 ns, thus providing an accurate measure of time. The pulser-receiver simultaneously activates the transducer (introducing the sould pulse into the delay line), the delay generator and the oscilloscope. The delay generator then produces the step pulse, a constant output of ±4 V for a prese-

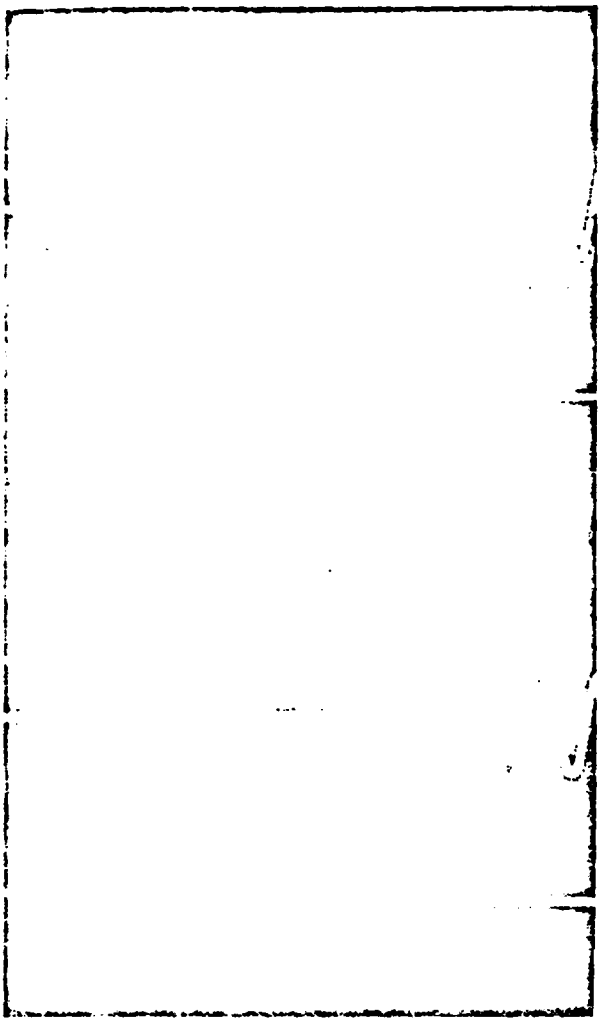

Fig. 2—A section of a typical resonance pattern shown with two different voltage steps, corresponding to the ends of two voltage pulses of different duration produced by the digital delay generator, superimposed thereon. As shown, the time difference of the duration of the two pulses is equal to four periods.

lected time interval, at the end of which the output voltage is reduced to 0. Using a dual input oscilloscope, one can superimpose the resonance signal and the "cutoff" voltage step from the delay generator, as shown in Fig. 2. The duration of the step pulse is varied until its cutoff point corresponds to a selected point on the resonance curve, most conveniently the cross-over point as shown in Fig. 2, and the corresponding time (*i.e.* step pulse duration) is recorded. The duration of the step pulse is then changed to make the cutoff step coincident with the equivalent point on the resonance curve for a different cycle, *i.e.* to a point separated from the first by an integer number of periods. The period is then the time difference between the step pulse durations divided by the number of cycles separating the equivalent points which were chosen. In Fig. 2, the step has been moved by four cycles; measurements over a large number of cycles (10 or more) were used to increase the accuracy of the determination of the period. (In the PE technique, step pulses of different duration were utilized in a similar way to measure the time difference between distinct echoes.)

As noted above, a typical resonance period is 10^{-7} s. If measurements are made over ten periods, the maximum error is $\pm 4 \times 10^{-9}$ s, or 0.04 pct. In practice, the major contribution to the error in our measurement of V_E is the uncertainty in our measurement of length. In the present study, the length of IIR samples (typically ~1 cm) was measured with a traveling microscope with a maximum error of ±0.002 cm, or 0.2 pct, for a single measurement.

Sample Preparation and Attachment

The Metglas 2826A sample ($Ni_{0.36}Fe_{0.32}Cr_{0.14}P_{0.12}B_{0.06}$) was obtained from Allied Chemical Corporation. Other alloys were produced from high purity elements in the arc-melting furnace and quenched using melt spinning and arc-melting piston and anvil processes.

Melt spun ribbons were generally about 2 mm wide and 25 to 50 μm thick. Foils prepared by the piston and anvil technique were typically ~2 cm in diam, and different samples ranged from 20 to 50 μm in thickness. Samples were judged to be amorphous when X-ray diffraction patterns, taken using Mo K_α radiation, exhibited only the broad peaks typical of amorphous metals. For the PE technique, the edges of the melt spun ribbon were generally sufficiently regular so that the ribbons could be used in their as-spun condition after being cut, perpendicular to their length, to the chosen length. For IIR measurements, both ribbons and foils were cut and polished to rectangular strips, typically ~10 mm long and ~0.5 mm wide.

The samples were attached to the end of the delay line using Duco cement. A rig was designed to hold the sample abutting firmly against the delay line while the cement was applied and dried. For the resonance technique, it was found necessary to have the sample held uniformly against the delay line (otherwise the regular, sine-like resonance pattern was not observed) and to use a minimal amount of cement (a shift in the period was observable when excessive cement was used).

It is necessary that the ribbon samples have a width sufficiently narrow to avoid dispersion effects (*i.e.* dependence of the velocity on λ). For example, the phase velocity V for an extensional wave in a circular bar is approximated by the Pochhammer-Chree relation:[5]

$$V = \{1 - 1/4\pi^2\sigma^2(d/\lambda)^2\}V_E \text{ (for } d/\lambda < 0.4)$$

where σ is Poisson's ratio, λ is the wavelenth, and d the diameter of the bar; *i.e.* the observed velocity is a function of frequency and sample dimensions. For a typical $\sigma = 0.35$, $d/\lambda = 0.1$ would produce a $V/V_E = 0.997$, *i.e.* a 0.3 pct reduction in velocity.

For our PE measurements, d/λ values of ~0.05 were typical, where d is now taken as the sample width. For such samples, no degradation of the sharpness of the pulse from dispersion effects could be seen and the measured velocity was independent of small changes in the sample width.

For IIR measurements, a somewhat smaller d/λ value, *i.e.* d/λ of the order of 0.01, was found necessary in order to make the measured period independent of the sample width. For some wider samples, the period of the sinusoidal pattern changed slightly as a function

of cycle number, and the average period measured from such a pattern did not correspond to the true V_E for that material; therefore, in addition to measuring the time for about ten cycles (preferably from about cycle 3 to cycle 13) to achieve high precision in the measurement of T, the period was also measured for each cycle in that interval to confirm that T was indeed constant for the pattern. It is noted that a smooth resonance pattern like that shown in Fig. 2 is required to obtain a valid V_E. In some cases, the "resonance" damped out much more quickly than in Fig. 2 or was superimposed on a longer period oscillation, or the amplitude of each peak did not decrease at a constant rate; such patterns did not produce a correct V_E. Other experimental difficulties, *e.g.* a sample which was improperly attached to the delay line, a sample wherein either end was not cut perpendicular to the ribbon direction or a sample which was internally nonuniform, could also lead to a very irregular "resonance" pattern. In practice, the validity of the V_E measured by the IIR technique was assured by making measurements on different samples, including samples of different widths.

Because samples made from piston and anvil foils were not always uniform in thickness, the effect of variations in the cross-sectional area was checked by deliberately tapering the width of a number of samples by up to 30 pct, a percentage variation greater than that encountered in the as quenched samples. It was found that, for samples where $d/\lambda \simeq 0.5$ mm/40 mm, such tapering produced no measurable change in the measured value of T, and hence V_E.

Density Measurements

Densities were measured using the Archimedian principle by weighing samples both in air and immersed in toluene. Measurements of the density of amorphous $Cu_{0.65}Zr_{0.35}$ were made directly on amorphous ribbons. For the $Ti_{0.80}Ni_{0.015}Si_{0.185}$ and $Ta_{0.555}Ir_{0.445}$ alloys, the densities of the amorphous alloys were assumed to be 1.0 pct lower than the values for the corresponding crystalline alloys, which were measured. This is a density difference typical of our measurements in the Zr-Cu system;[15] since an *accurate* measurement on the small samples obtained from piston and anvil foils is difficult, use of an amorphous density estimated in this manner was preferred. The density of Metglas 2826A ribbons was measured here and had also been previously reported.[16]

EXPERIMENTAL DATA AND DISCUSSION

Representative V_E values obtained with the IIR technique are given in Table I as well as, for comparison purposes, some V_E values obtained with the PE technique. Also given are the measured density values and the Young's moduli calculated from $E = \rho V_E^2$.

To confirm the validity of the IIR technique, V_E values were measured on melt spun ribbons both by the PE technique and, using small samples (about 1 cm long) cut from the same ribbon, by the IIR technique. This was done for both amorphous $Zr_{0.35}Cu_{0.65}$ (lines 1 and 2, Table I) and Metglas 2826A (lines 5 nad 6, Table I). It can be seen that the IIR technique produced the same value as the PE technique in both cases. Both sets of values are the average for several measurements, though in each case the scatter is small; *e.g.* repeated PE measurements on different samples from the Metglas ribbon gave a V_E range of $4.34 \pm 0.02 \times 10^5$ cm/s, while repeated IIR measurements gave a V_E range of $4.34 \pm 0.04 \times 10^5$ cm/s. In addition, the measured values of V_E for the Metglas samples agree well with the previously reported value (line 4) for this alloy, though this very good agreement may be fortuitous since it is not known whether or not our 2826A sample came from the same "batch" as that in Ref. 16, and, if not, what the variations from batch to batch typically might be.

Table I. Properties of Metallic Glasses

	Alloy	Method	V_E (10^3 m/s) (10^5 cm/s)	ρ (10^3 kg/m^3) (g/cm^3)	E (10^{10} N/m^2) (10^{11} dyne/cm^2)
1)	$Zr_{0.35}Cu_{0.65}$ (melt spun)	PE	3.47	7.76	9.34
2)	$Zr_{0.35}Cu_{0.65}$ (melt spun)	IIR	3.47	7.76	9.34*
3)	$Zr_{0.35}Cu_{0.65}$ (piston and anvil)	IIR	3.47	7.76*	9.34
4)	Metglas 2826A (Ref. 15)	PE	4.34	7.46	14.05
5)	Metglas 2826A	PE	4.34	7.49	14.11
6)	Metglas 2826A	IIR	4.35	7.49	14.17
7)	$Ta_{0.555}Ir_{0.445}$	IIR	2.98	19.04†	16.91
8)	$Ti_{0.80}Ni_{0.015}Si_{0.185}$	IIR	4.75	4.44†	10.02

* Assumed to be equal to the density of the amorphous melt spun ribbon of this composition.
† The indicated density for the glass was assumed to be 1.0 pct less than that of the crystalline alloy, which was measured.

To confirm the suitability of the IIR technique for the measurement of V_E on piston and anvil samples, it was applied to piston and anvil samples of $Zr_{0.35}Cu_{0.65}$ made from the same master alloy as the melt spun ribbon. It can be seen (Table I) that the V_E measured in this way is the same as that measured from the ribbon, though the *exact* agreement may again be fortuitous.

As examples of special utility of the IIR technique, V_E values from two additional amorphous metals are given in lines 7 and 8 in Table I. $Ta_{0.555}Ir_{0.445}$ has a liquidus temperature of ~1950°C;[17] thus, though this alloy is readily produced as a metallic glass by the arc-melting piston and anvil technique,[6] the rather high melting temperature makes standard melt spinning procedures difficult. For $Ti_{0.80}Ni_{0.015}Si_{0.185}$, the corrosiveness of the liquid and the high quench rate needed to produce the glass make the piston and anvil technique the method of choice for producing this glass from the liquid. For such piston and anvil samples, the IIR technique provides a useful capability.

As discussed earlier, good reproducibility was obtained in the measurement of V_E by both the IIR and PE techniques. Typically, V_E for a given sample can

be determined to ±0.2 pct, where the measurement of sample length produces the major part of this uncertainty. E values are somewhat more uncertain, because of uncertainties in the density values, but are considered to be accurate to somewhat better than ±1 pct.

In evaluating the accuracy of elastic constants obtained by such measurements, it should also be considered that the measured value of V_E for an amorphous alloy of a given composition can vary because of variations in the internal state of the system. It is known that a "*relaxation*" can occur in a metallic glass upon annealing,[18,19] wherein the structure remains fully amorphous but relaxes to a lower energy state. This is known to produce a small change in the elastic moduli of the glass, typically of the order of 1 or 2 pct.[20,21] Similarly, samples having different thermal histories from being quenched at very different cooling rates can also exhibit variation in the moduli.

Even more of a potential problem arises from the fact that the Young's modulus typically increases by about 30 pct upon crystallization.[20] Since the X-ray diffraction patterns may not readily indicate when up to ~5 pct of the sample exists in an ultrafine crystalline state, a modulus up to about $(0.05) \times (0.30) \simeq 1.5$ pct higher than that for the fully amorphous state could be measured on a sample that was mistakenly believed to be fully amorphous. This would be most likely to occur for a composition which was difficult to quench to a glass, *i.e.* one requiring a high quench rate, and in fact an unusually large variation in the value of V_E measured from different samples was observed in some such cases. This problem can be especially severe for the piston and anvil samples where different parts of the foil may have been quenched at different rates. To minimize this possibility, V_E values were measured on several samples cut from different piston and anvil foils, and the measured V_E value was considered valid when a variation of no more than ±1 pct was obtained.

ACKNOWLEDGMENTS

We thank L. C. Lynnworth and K. A. Fowler of Panametrics, Inc. for valuable discussions and suggestions. This research was sponsored by the U.S. Army Research Office: two of us (B.C.G. and L.T.K.) acknowledge further support by the Office of Naval Research. Contribution No. 59, Institute of Chemical Analysis, Applications and Forensic Science.

REFERENCES

1. L. A. Davis, C.-P. Chou, L. E. Tanner, and R. Ray: *Scr. Met.*, 1976, vol. 10, p. 937.
2. H. S. Chen and J. T. Krause: *Scr. Met.*, 1977, vol. 11, p. 761.
3. R. Pond, Jr. and R. Maddin: *Trans. TMS-AIME* 1969, vol. 245, p. 2475.
4. H. H. Liebermann: *Rapidly Quenched Metals III*, B. Cantor, ed., p. 34, The Metals Society, London, 1978.
5. W. P. Mason: *Physical Acoustics and Properties of Solids*, Van Nostrand, Princeton, N.J., 1958.
6. M. Fischer, D. E. Polk, and B. C. Giessen: *Rapid Solidification Processing: Principles and Technologies*, R. Mehrabian, B. H. Kear and M. Cohen, eds., p. 140, Claitor's Publishing Division, Baton Rouge, LA, 1978.
7. D. E. Polk, A. Calka, and B. C. Giessen: *Acta Met.*, 1978, vol. 26, p. 1097.
8. S. Davis, M. Fischer, B. C. Giessen, and D. E. Polk: *Rapidly Quenched Metals III*, B. Cantor, ed., vol. 2, p. 425, The Metals Society, London, 1978.
9. H. S. Chen, N. J. Leamy, and M. Barmatz: *J. Non-Cryst. Solids*, 1971, vol. 5, p. 444.
10. B. S. Berry and W. C. Pritchet: *J. Appl. Phys.*, 1973, vol. 44, p. 3122.
11. K. A. Fowler: U.S. Patent No. 3,595,069, July 27, 1971.
12. L. C. Lynnworth, E. P. Papadakis, and K. A. Fowler: *Int. Adv. Nondest. Test.*, 1977, vol. 5, p. 71.
13. S. H. Whang, L. T. Kabacoff, D. E. Polk, and B. C. Giessen: *J. Mater. Sci.*, in press.
14. L. C. Lynnworth: Technical Memorandum UR 141, Panametrics Inc., Waltham, Massachusetts 1975.
15. L. Kabacoff, D. E. Polk, R. Raman, S. H. Whang, and B. C. Giessen: unpublished research, Northeastern University, Boston, MA 02115, 1979.
16. L. A. Davis: *Metallic Glasses*, p. 190, ASM, Metals Park, OH, 1978.
17. *Constitution of Binary Alloys*, Second. Suppl., F. A. Shunk, ed., p. 463, McGraw-Hill, New York, 1969.
18. H. S. Chen and E. Coleman: *Appl. Phys. Lett.*, 1976, vol. 28, p. 245.
19. A. J. Kerns, D. E. Polk, R. Ray, and B. C. Giessen: *Mater. Sci. Eng.*, 1979, vol. 38, p. 49.
20. B. S. Berry: *Metallic Glasses* p. 161, ASM, Metals Park, OH, 1978.
21. C. A. Pampillo and D. E. Polk: *Mater. Sci. Eng.* 1978, vol. 33, p. 275.

Letters

A technique for the measurement of Young's modulus of small metallic glass samples

Metallic glasses are frequently prepared by the arc-melting piston-and-anvil quenching process [1]; for refractory or reactive metallic glasses [2, 3], where melt spinning is not readily applicable, this technique is presently the principal preparation method. It produces small alloy discs from which rectangular samples with typically ~ 1.5 cm length can be cut. These samples are too short to allow precise measurements of the sound velocity V_E (and thus the Young's modulus E from the relation $E = \rho V_E^2$, where ρ is the density) by the ultrasonic pulse echo (P.E.) technique now generally used for dynamic measurements on long melt spun metallic glass ribbons; accordingly, E values have not been reported for such alloys. It is obvious that short samples are also unsuitable for static determinations of E.

We have applied the impulse-induced resonance (I.I.R.) technique developed by Fowler and co-workers [4, 5] to such short glassy metal specimens. This technique uses the same experimental arrangement as that used by us for P.E. measurements of V_E, although our technique for measuring time for P.E. measurements differs from that typically used. An alloy sample is attached to a magnetostrictive Remendur delay line into which a broad-band sound pulse is introduced by a transducer connected to a Panametrics 5055 Pulser-receiver; the latter also activates a Berkeley Nucleonics digital delay generator and an oscilloscope. The physical measurement, however, differs in the two methods; instead of determining the time required for the pulse to traverse the sample, as in the P.E. method, in the I.I.R. technique one initiates an extensional mode resonance in the sample; from the (measured) period T of this resonance and the length of the sample, V_E and hence E can be derived for samples of ~ 10 mm length. With proper procedure (uniform and narrow samples and correct specimen attachment) reproducible well-shaped resonance patterns are obtained which lead to T values precise to ± 0.04%. The uncertainty in V_E is primarily due to the measurements of the sample length and is ± 0.2%, about equal to that for P.E. data, giving an uncertainty of ± 0.4% in E from V_E. An uncertainty in E of the same order of magnitude is due to the density measurement on the available small sample quantities. (It should be noted that the I.I.R. technique is distinct from the "vibrating reed" method [6]. The latter is also unsuitable for short piston-and-anvil glass samples, as a uniform sample thickness is required; the accuracy of E obtained with the vibrating reed technique is estimated to be ~ 10% [6].)

As shown in Table I for $Zr_{0.35}Cu_{0.65}$, V_Es measured by the I.I.R. method on a short, narrow strip from a piston-and-anvil sample and by the P.E. method on a melt spun ribbon are in close agreement, illustrating the validity of I.I.R. results. Also shown are results obtained from two other amorphous metals which are more readily prepared by the piston-and-anvil quenching process than by melt spinning. Melt spinning of amorphous $Ti_{0.60}Ni_{0.40}$ is not readily accomplished because of the reactivity of this alloy (i.e. the resultant

TABLE I Properties of metallic glasses

	Measurement method	V_E (10^5 cm sec^{-1})	ρ (g cm^{-3})	E (10^{11} dyn cm^{-2})
$Zr_{0.35}Cu_{0.65}$ (piston-and-anvil)	I.I.R.	3.47	7.76*	9.34
$Zr_{0.35}Cu_{0.65}$ (melt spun)	P.E.	3.47	7.76	9.34
$Ti_{0.60}Ni_{0.40}$	I.I.R.	4.03	5.90	9.58
$Nb_{0.55}Ir_{0.45}$	I.I.R.	3.27	14.09†	15.06

* Assumed equal to that measured from the melt-spun ribbon.
† Assumed to be 1% less than that of the corresponding crystalline alloy.

0022–2461/80/010247–02$02.20/0

interactions with the crucible) and the high quench rate necessary to achieve the fully amorphous state; melt spinning of $Nb_{0.55}Ir_{0.45}$ is difficult because of the high liquidus temperature of this alloy.

A comprehensive description of the I.I.R. method, its application and limitations, and further data obtained with it will be published subsequently [7]; in the meantime, experimental details can be obtained from the authors.

Acknowledgements

The authors thank L. C. Lynnworth and K. A. Fowler of Panametrics, Inc for valuable discussions and suggestions. This research was sponsored by the U.S. Army Research Office; two of us (B.C.G. and L.T.K.) acknowledge further support by the Office of Naval Research.

References

1. M. FISCHER, D. E. POLK and B. C. GIESSEN, in "Rapid Solidification Processing: Principles and Technologies", edited by R. Mehrabian, B. H. Kear and M. Cohen (Claitor's, Baton Rouge, Louisiana, 1978) p. 140.
2. S. DAVIS, M. FISCHER, B. C. GIESSEN and D. E. POLK, in "Rapidly Quenched Metals III", Vol. 1, edited by B. Cantor (The Metals Society, London, 1978) p.425.
3. D. E. POLK, A. CALKA and B. C. GIESSEN, *Acta Met.* 26 (1978) 1097.
4. K. A. FOWLER, U.S. Patent no. 3 595 069, 27 July (1971).
5. L. C. LYNNWORTH, E. P. PAPADAKIS and K. A. FOWLER, *Int. Adv. Nondest. Testing* 5 (1977) 71.
6. B. S. BERRY and W. C. PRITCHETT, *J. Appl. Phys.* 44 (1973) 3122.
7. S. H. WHANG, L. T. KABACOFF, D. E. POLK and B. C. GIESSEN, *Met. Trans.* (in press).

Received 22 March
and accepted 6 June 1979

S. H. WHANG
L. T. KABACOFF
D. E. POLK
B. C. GIESSEN
Materials Science Division, ICAAFS,
341 Mugar,
Northeastern University,
Boston, Massachusetts 02115, USA

Thermal expansion of gallium borate

Recently, Bither and Young [1] synthesized a number of borates under high pressure and high temperature conditions, and found that they belong to $R\bar{3}C$ space group and are isotypic with the calcite structure. A perusal of the literature shows that the thermal expansion of gallium borate which has the same structure as calcite, has not been so far studied. As the authors have determined the precision lattice parameters and the coefficients of thermal expansion of a number of carbonates [2–5], nitrates [6, 7] and borates [8, 9], it is thought worthwhile to include the borates synthesized by Bither in the general programme of X-ray investigation on calcite-type compounds.

The sample used in the present study was kindly supplied by Professor Bither, Central Research Department, E.I. du Pont de Nemours and Company, Experimental Station, Wilmington, Delaware, USA. It was found necessary to heat the sample to 600° C to obtain well-resolved sharp lines in the high-angle region. The sample for study was prepared by filling the powder in a thin walled quartz capillary. Using Cu*K* radiation, powder photographs at different temperatures were recorded in the temperature range 38 to 900° C. Temperature control was facilitated by the use of voltage stabilizer and a variac. The temperature could be held constant within about 2° C. Details of the experimental technique and the method of evaluating the precise lattice parameters and the coefficients ot thermal expansion has been described in an earlier paper [2].

Reflections from $(1.2.1\bar{4})_{\alpha_1}$, $(1.2.1\bar{4})_{\alpha_2}$, $(2.2.\bar{1}2)_{\alpha_1}$, $(2.2.\bar{1}2)_{\alpha_2}$, $(4\bar{1}6)_{\alpha_1}$, $(4\bar{1}6)_{\alpha_2}$, $(3\bar{2}9)_{\alpha_1}$ and $(3\bar{2}9)_{\alpha_2}$ in the Bragg angle region 65° to 80° were used to evaluate the lattice parameters at different temperatures. In evaluating the lattice parameters independent measurements and calculations were made on several films and the average of the deviations of the individual values from the mean was taken as the error in the lattice

0022–2461/80/010248–02$02.20/0

The Niobium (Columbium)-Palladium Constitution Diagram

B. C. GIESSEN, N. J. GRANT, D. P. PARKER, R. C. MANUSZEWSKI, AND R. M. WATERSTRAT

The Nb-Pd system was investigated over the entire composition range by metallography and X-ray diffraction analysis. The solubility limits of terminal and intermediate phases and solidus temperatures were determined. α-Nb dissolves ~36 at. pct Pd at. 1520°C and ~20 at. pct Pd at 800°C; α-Pd dissolves ~31 at. pct Nb at 1610°C and ~18 at. pct Nb at temperatures below 1500°C. The presence of three intermediate phases $NbPd_2$ ($MoPt_2$-type), α-$NbPd_3$ ($TiAl_3$-type), and β-$NbPd_3$ (β-$NbPd_3$-type) was confirmed: $NbPd_2$ melts at 1610°C and one of the $NbPd_3$ phases transforms at the same temperature into α-Pd solid solution which melts at 1625°C. In addition, an approximately equiatomic high-temperature phase α-NbPd with a homogeneity range of ~11 at. pct was found which melts at 1520 to 1565°C and probably is an extension of and isomorphous with the α-Pd solid solution. Five three-phase reactions are described, and crystal chemical relationships are discussed.

IN the course of an extended study of the phase diagrams of refractory metals, a number of T_5-T_{10} systems, *i.e.*, binary systems composed of one of the T_5 transition metals V, Nb, or Ta on the one side and one of the T_{10} metals, Pd or Pt, on the other, have been investigated in a collaborative effort. Of the six systems thus defined, studies of the V-Pt system,[1] the Ta-Pd system[2] and the Pt-rich portion of the Ta-Pt system[3] have already been presented; for V-Pd a phase diagram is given in the literature.[4] The present paper reports the Nb-Pd system; the remaining system, Nb-Pt, will be reported in a subsequent publication.

Early surveys of the Nb-Pd system are due to Greenfield and Beck[5] and Knapton;[6] crystal chemical surveys of intermediate phases were made independently by Giessen, Parker and Grant[7] (also reported in Ref. 8) and Maldonado and Schubert;[9] Pd(Nb) terminal solid solutions were studied by Kudielka-Artner and Argent[10] and Catterall and Barker;[11] individual intermediate phases were reported by Dwight[12] and Giessen and Grant:[13] phase diagrams were worked out by Savitskii *et al*,[14] Parker,[15] and Bowers[16] (only the first of these has been published): reviews were given *e.g.* by Shunk[17] and Pearson.[18]

The following alloy phases were reported: terminal solid solutions with extensive mutual solubilities;[6,14] a σ phase at ~ Nb_2Pd[5,7,14,15,16] or as a high-temperature phase at Nb_3Pd_2[9] (however, in contrast to this, *no* σ phase was observed by Knapton[6]); a low temperature phase Nb_3Pd_2 (NbRu structure type);[9] an unidentified high temperature phase α-NbPd[7] or Nb_2Pd_3:[10] $NbPd_2$[7,9,11,13,15] ($MoPt_2$[= $NbPt_2$] structure type[9,13]); $NbPd_3$[7,8,9,12,14,15,16] or α-$NbPd_3$[7] ($TiAl_3$ type[7,9,12]) and β-$NbPd_3$ (β-$NbPd_3$ type[8,19]).

The principal conflicts among these reports pertain to the existence of the σ phase and to the details of the phase diagram. It was the prime object of the present study to resolve conflicts in the data and to provide a more reliable constitution diagram.

EXPERIMENTAL METHODS

The starting materials were as follows:

Niobium rondelles, 99.6 pct pure, obtained from the Electro Metallurgical Co.,* with a typical major impurity analysis (wt pct): Ta (0.15); Ti, Fe, O (0.1 each); C, H (0.05 each); niobium powder (−325 mesh), 99.8 pct pure, obtained from Leico Industries, Inc., with typical major impurity analysis: O (0.4); Fe, Si (0.01 to 0.1 each); Al (0.003 to 0.03); high purity Nb rod 99.8 pct, obtained from Johnson-Matthey Chemicals Limited containing Ta < 50 ppm, Mg 1 ppm, Ag 1 ppm and no other metallic impurities detectable by spectrographic analysis. This material also contained C (53 ppm). No oxygen analysis was available. The latter material was used only to duplicate critical compositions in the range of 30 to 40 at. pct Pd.

Palladium wire, obtained from the International Nickel Co., and palladium powder (−325 mesh) obtained from Engelhard Industries Inc. These metals were not chemically analyzed but had a nominal purity of 99.95 pct.

Sample preparation, vacuum heat treatment, metallography, and X-ray diffraction studies followed closely the methods used in earlier, related studies by the authors and their collaborators for which details are given in Refs. 1 through 3, 20, and 21; procedures will therefore be described only where they differ from those described in the recently published,

*Certain commercial materials and equipment are identified in this paper in order to specify adequately the experimental procedure. In no case does such identification imply recommendation or endorsement by the National Bureau of Standards, nor does it imply that the material or equipment identified is necessarily the best available for this purpose.

B. C. GIESSEN is Professor of Chemistry and Mechanical Engineering, Northeastern University, Boston, MA 02115. N. J. GRANT is Professor of Materials Science and Engineering, Massachusetts Institute of Technology, Cambridge, MA 02139. D. P. PARKER, formerly with MIT is now President, Parker & Associates, Wellesley, MA 02181. R. C. MANUSZEWSKI, formerly with the ADAHF Research Unit at NBS, is now Production Engineer, Morganite Corporation, Dunn, NC 38334, and R. M. WATERSTRAT is Research Associate, ADAHF Research Unit, National Bureau of Standards, Washington, DC 20234.

Manuscript submitted August 21, 1978.

ISSN 0360-2133/80/0512-0709$00.75/0

prior study of the Ta-Pd system.[2] Alloy compositions are estimated to have an accuracy of ±1 at. pct, and the temperature measurements are accurate to ±10°C unless otherwise noted. The temperature measurements were based on the International Practical Temperature Scale of 1968 (IPTS 68).

Alloy preparation by arc-melting or, for powder constituents, sintering followed by arc-melting, composition analysis by weight balance to 1 at. pct, temperature measurement by thermocouples, heat treatments in quartz tubes (to 1100°C) and a high-temperature vacuum furnace (up to 1900°C) were as discussed in Refs. 1 and 2. Temperature measurement by optical pyrometry was carried out with a calibrated Leeds and Northrop instrument. To achieve homogenization, alloys with more than 30 at. pct Pd were annealed at 100 to 150°C below the solidus points or, at least 1400°C for about 12 h; alloys lower in Pd were annealed at 1700 or 1900°C for three or two h, respectively. Subsequent equilibration treatments were carried out at various temperatures following the typical schedule given in Table I. Metallographic and X-ray diffraction techniques (CuK_α radiation) and the determination of solidus and invariant reaction temperatures also followed exactly the techniques described in Ref. 1.

Quenching at rates of 30 to 100°C/s, as generally used in this work,[1,2] was not fast enough to allow retention of the high-temperature phase α-NbPd (see below); rapid quenching[22] using an arc furnace quenching unit[23] yielding cooling rates of about 10^{6}°C/s[22,23] was therefore employed as part of an ongoing study of rapidly-quenched transition metal phases.[23] This process yielded foils of ~30 μ thickness cooled at $\sim 10^{5}$°C/s.[22,23]

Table I. Typical Equilibration Treatments for Niobium-Palladium Alloys

Temperature, °C	Time, h
1900	2
1700	3
1520	4
1450	6
1400	12
1300	48 (2 days)
1200	168 (1 week)
1100	336 (2 weeks)
1000	504 (3 weeks)
900	744 (1 month)
800	1488 (2 months)

RESULTS AND DISCUSSION

The Constitution Diagram

The proposed constitution diagram for the niobium-palladium system is shown in Fig. 1. Crystallographic data,[8,12,13,24] composition limits and melting temperatures of the intermediate phases are summarized in Tables II and III. The phase diagram differs significantly from the only one previously published.[14,25] There are seven invariant reactions:

- a eutectic reaction, L = α-Nb solid solution + α-NbPd, at 1520°C;
- a peritectic reaction, $L + NbPd_2 = \alpha$-NbPd, at ~1565°C;
- a peritectic reaction, L + α-Pd solid solution = $NbPd_2$, at ~1610°C.
- congruent formation of $NbPd_3$ from α-Pd solid solution, at ~1610°C.
- congruent solidification of α-Pd solid solution, at ~1625°C;
- a eutectoid reaction, α-NbPd = α-Nb solid solution + $NbPd_2$, at 1255°C;
- a eutectoid reaction, α-Pd solid solution = $NbPd_2$ + $NbPd_3$, at ~1560°C.

In the following, the proposed phase diagram, Fig. 1, and some metallographic and X-ray diffraction evidence for it will be discussed, with prime attention to complex features of the diagram.

Palladium is soluble in the bcc α-Nb solid solution up to ~36 at. pct Pd at 1520°C, but there is a rapid decrease in solubility, beginning at the eutectoid temperature of 1255°C, and the solid solution range ex-

Table II. Crystallographic Data for Niobium-Palladium Intermediate Phases

Intermediate Phase	Crystal System	Space Group	Structure Type	Number of Atoms Per Unit Cell	Reference	Composition Limits, or Composition, At. Pct Pd	Melting Point, °C
α-NbPd*	(cubic)	(O_h^5-Fm3m)	(Cu)	(4)	24	49 to 58 1520°C	1565†
$NbPd_2$	Orthorhombic	D_{2h}^{25}-Immm	$MoPt_2$	6	13	~67 1400°C	1610
α-$NbPd_3$‡	Tetragonal	D_{4h}^{17}-I4/mmm	$TiAl_3$	8	12	~76 1300°C ~75 850°C	1610¶
β-$NbPd_3$	Orthorhombic	D_{4h}^{12}-Pmmn	β-$NbPd_3$	24	8	~75 1300°C	

*Data in parentheses were obtained from a metastable (rapidly-quenched) sample.
†Peritectic decomposition temperature.
‡α-$NbPd_3$ structure is present in (Nb, Pd) Pd_3 alloys and after annealing at 850°C.
¶Transformation to α-Pd solid solution; melting point of solid solution ~1625°C.

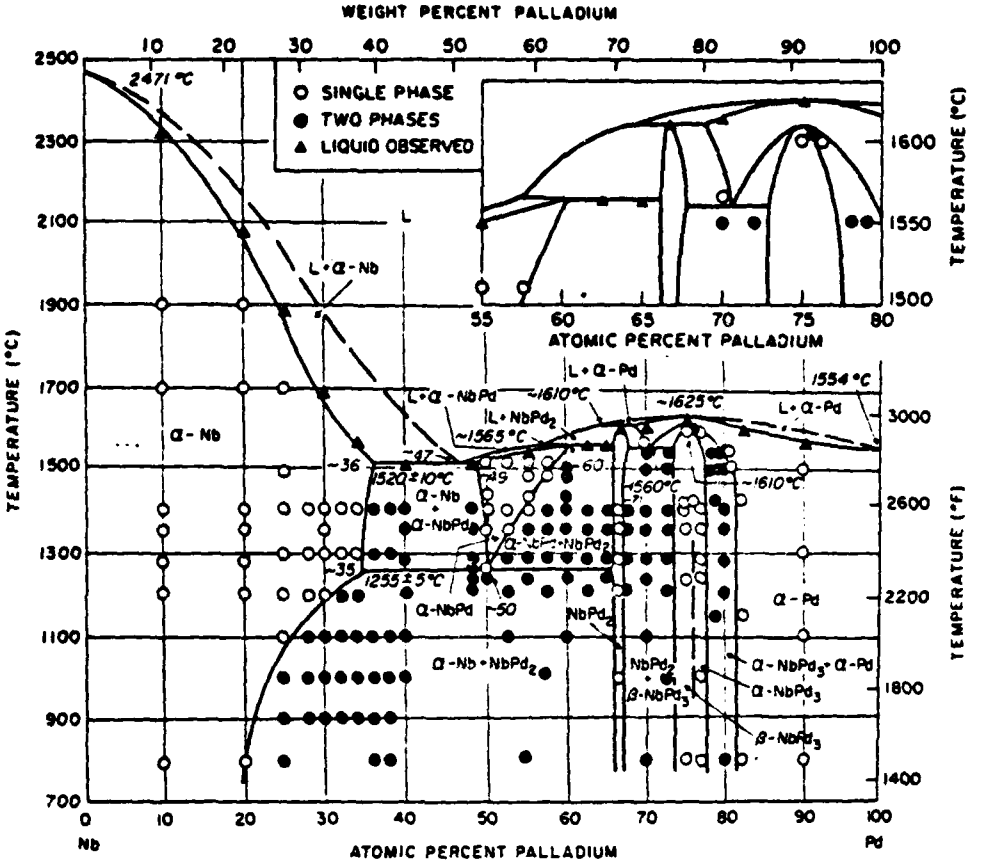

Fig. 1—The Nb-Pd constitution diagram.

Table III. Lattice Parameters of Intermediate Phases and Terminal Solid Solutions in the Niobium-Palladium System

At. Pct Pd	Phase	Lattice Parameters a_0	b_0	c_0	c_0/a_0	Reference
10	α-Nb	3.274				*
20	α-Nb	3.255				*
25	α-Nb	3.242				*
50†	α-NbPd	4.020				24
52†	α-NbPd	4.012				24
55†	α-NbPd	4.004				24
67	$NbPd_2$	2.839	8.376	3.886		13
75	α-$NbPd_3$	3.895		7.913	2.032	12
75	β-$NbPd_3$	5.486	4.845	13.602		8
82	α-Pd	3.905				*
90	α-Pd	3.901				*

*This study.
† Data were obtained from a metastable (rapidly-quenched) sample.

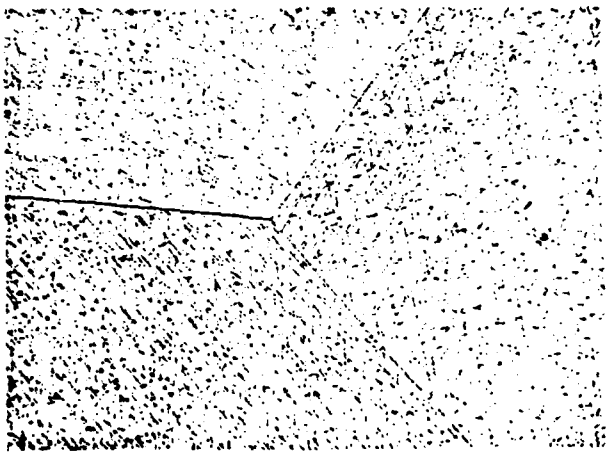

Fig. 2—25 at. pct Pd. Annealed at 1100°C for 2 weeks. Large α-Nb solid solution grains with a network of fine striations due to precipitation or martensitic transformation (see text). Magnification 116 times.

tends only to ~20 at. pct Pd at 800°C. The solvus boundary was located primarily by metallographic observations on equilibrated alloys with 20 to 40 at. pct Pd quenched from various temperatures. The α-Nb solid solution produced by quenching from the single-phase region contains a fine network of striations (Fig. 2) which could be very fine, plate-like precipitates of $NbPd_2$ but might also reflect a martensitic transformation of the α-Nb solid solution upon quenching. Some martensitic platelets could be seen under high magnification and these may be the "Nb_3Pd_2 (γ)" phase which was reported by Maldonado and Schubert.[9] X-ray patterns from such alloys, however, show no lines other than those for the α-Nb solid solution (indicating ≤ ~5 pct second phase): the nature of the striations is thus not understood. For the determination of the α-Nb solvus line, however, it is of importance only that two-phase microstructures containing the (striated) grains of α-Nb solid solution and globular, isothermal precipitates of $NbPd_2$ can be observed (Fig. 3), indicating that the alloy had been equilibrated in the α-Nb + $NbPd_2$ region. Figure 4 documents an interesting morpho-

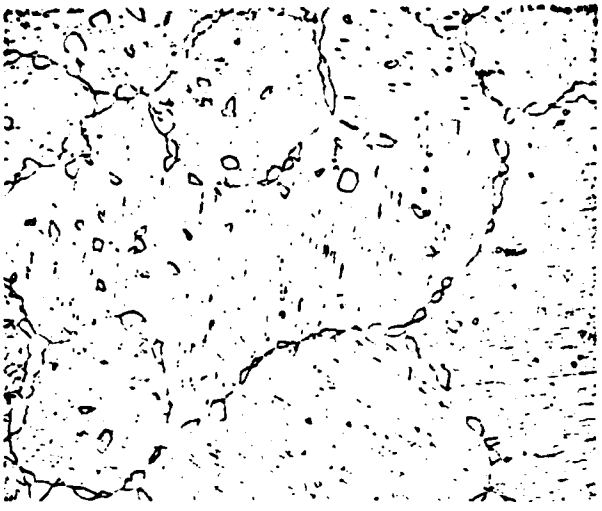

Fig. 3—30 at. pct Pd. Annealed at 1100°C for 2 weeks and quenched. Grains of α-Nb solid solution as in Fig. 2, with globular isothermal precipitates of $NbPd_2$, mainly on grain boundaries. Magnification 128 times.

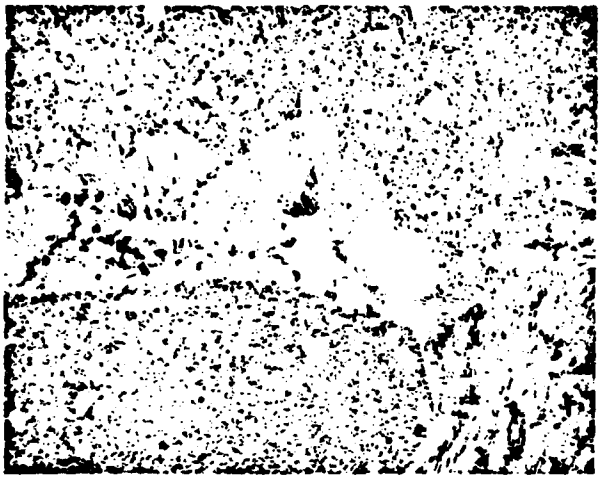

Fig. 4—32 at. pct Pd. Annealed at 900°C for 1 month. Cellular pearlitic microstructure of α-Nb solid solution and $NbPd_2$ consuming unresolved, fine precipitate of $NbPd_2$ in α-Nb solid solution. Magnification 312 times.

Fig. 5—48 at. pct Pd. As-cast. Primary dendrites of α-NbPd which have decomposed into unresolved, fine eutectoid of α-Nb solid solution + $NbPd_2$, surrounded by pearlitic eutectic of α-Nb solid solution + decomposed α-NbPd. Magnification 123 times.

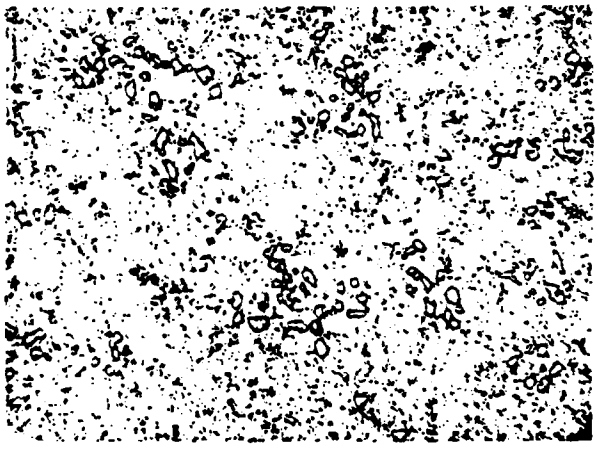

Fig. 6—52.5 at. pct Pd. Annealed at 1288°C for 10 h. Globular isothermal $NbPd_2$ precipitates (light) in matrix of α-NbPd eutectoidally decomposed into α-Nb solid solution and $NbPd_2$. Magnification 415 times.

logical change taking place in this two-phase field: a cellular pearlitic (α-Nb solid solution + $NbPd_2$) microstructure forms upon prolonged low-temperature annealing, consuming the material consisting of a fine precipitate of $NbPd_2$ in α-Nb solid solution.

The microstructure of an as-cast alloy located in the narrow composition range between the eutectic (α-Nb + α-NbPd) and the α-NbPd phase is shown in Fig. 5. It consists of α-NbPd primary dendrites which have decomposed into a fine (unresolved) eutectoid structure (α-Nb solid solution + $NbPd_2$) and the eutectic (α-Nb solid solution + decomposed α-NbPd). The fine (unresolved) eutectoid structure is also shown in Fig. 6 for an alloy annealed in the (α-NbPd + $NbPd_2$) field near the α-NbPd/(α-NbPd + $NbPd_2$) phase boundary. The fine eutectoid structure spheroidizes to form a coarser two-phase microstructure upon annealing below the eutectoid temperature (Fig. 7); the latter was located by comparison of micrographs such as those given in Figs. 6 and 7. Similar microstructures have been observed in the Ta-Pd system for an analogous high-temperature phase (β-TaPd).[2] The occurrence of the peritectically formed phase $NbPd_2$ was confirmed by some critical experiments which were designed to distinguish between a peritectic and a congruent transformation by improving the accuracy of the solidus data in the region from 60 to 70 at. pct Pd. In these experiments we placed pairs of samples close together in two separate crucibles and carefully measured the difference in their melting points by direct observation during heating. The relative positions of the four solidus points shown in this region are thereby established with a relative precision of ±5°C even though the absolute temperatures are less accurate. The relative positions of these solidus points (see insert in Fig. 1) rule out a congruent transformation and supports the peritectic construction. One or both of the two $NbPd_3$ phases form by transformation from

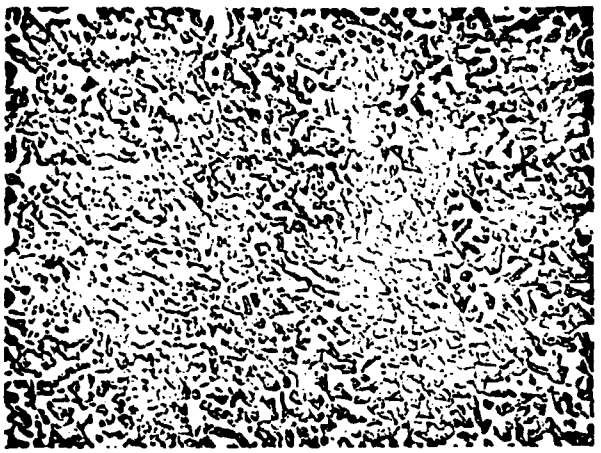

Fig. 7—52.5 at. pct Pd. Annealed at 1216°C for 12 h. Decomposed α-NbPd annealed below eutectoid temperature forming coarse, partly spheroidized microstructure of α-Nb solid solution and $NbPd_2$. Magnification 415 times.

α-Pd solid solution. The α-Pd solid solution dissolves up to ~31 at. pct Nb at ~1610°C, but only ~18 at. pct Nb at temperatures ≤ 1500°C; it has a congruent melting point maximum at 1625°C and 75 at. pct Pd (Fig. 1).

The temperature of the transformation from α-Pd to $NbPd_3$ of 1610°C (only ~15°C below the melting point of the α-Pd solid solution) was located by examining X-ray patterns of quenched alloys which either showed broadened lines of fcc α-Pd solid solution or sharp lines of ordered phase(s), depending on the annealing temperatures. The high-temperature region is further documented by micrographs of alloys in the region of the eutectoid α-Pd solid solution → $NbPd_2$ + $NbPd_3$; these alloys show decomposed lamellar or spheroidized two-phase structures depending on the annealing temperature; Fig. 8 shows the lamellar decomposition products of the eutectoid transformation in an alloy quenched from the α-Pd region. The quench was too slow to retain α-Pd, but the highly oriented lamella of $NbPd_2$ and $NbPd_3$ are evidence for the prior existence of large single grains of α-Pd. The lamellar structure is metastable and will transform to a spheroidized structure if the alloy is annealed for a sufficient time in the two-phase region *below* 1560°C. Figure 8 therefore constitutes evidence that the alloy was annealed *above* the transformation temperature where large single-phase grains existed and that these prior grains transformed by a eutectoid reaction during quenching. We have located the transformation temperature by annealing this structure at lower temperatures and observing whether or not a spheroidal decomposition occurs. The relative locations of the two $NbPd_3$ phases could not be deduced from metallographic observations (see below). The semicoherent precipitation of α-$NbPd_3$ from α-Pd solid solution is shown in Fig. 9.

The Nb-Pd phase diagram presented here resembles that given by Savitskii *et al*[14] in some features, including the large terminal solid solubilities, the presence of a eutectic near the equiatomic composition and a melting point maximum for Pd the solid solution; however, their diagram[14] and the present one differ in too many important features (*e.g.*, their diagram shows the σ phase, but the α-NbPd and $NbPd_2$ phases are absent, in their diagram, in contrast to the present one) for a comparison of details to be useful

Intermediate Alloy Phases

Our principal results center on the observed alloy phases: these will be reviewed in order of increasing Pd content.

σ Phase. A major finding is the absence of a σ phase in the Nb-Pd system, which confirms the negative result of Knapton[6] but conflicts with reports on the existence of this phase from several other prior investigators.[5,7,9,14-16] We have therefore performed additional experiments to explain this rather significant disagreement.

The σ phase was first reported by Greenfield and Beck[5] who used Nb metal with a significant amount

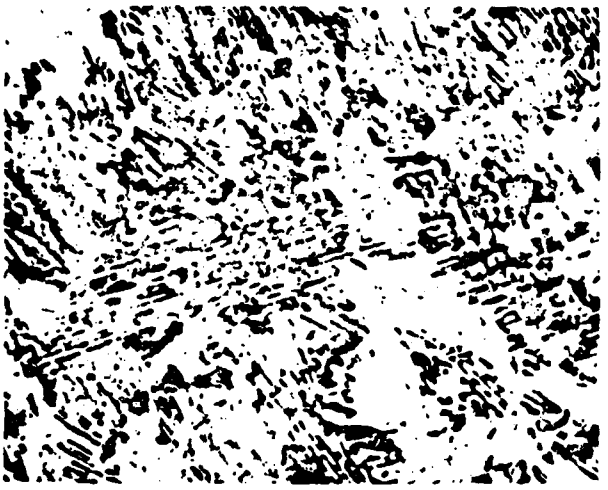

Fig. 8—70 at. pct Pd. Annealed at 1580°C (above the eutectoid temperature) for 2 h. Coarse lamellar eutectoid of $NbPd_2$ and $NbPd_3$ formed by decomposition of a prior α-Pd solid solution during quenching. Magnification 316 times.

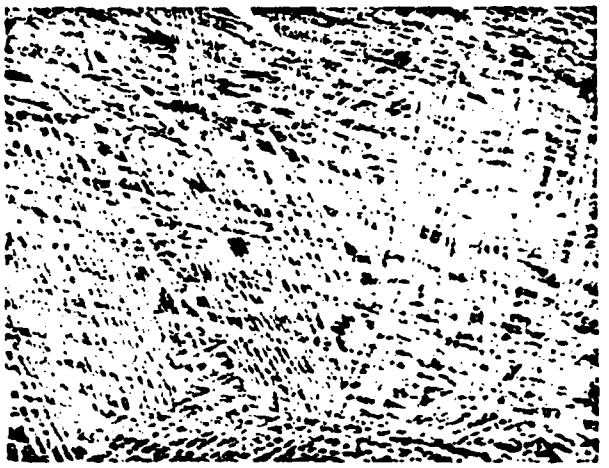

Fig. 9—80 at. pct Pd. Annealed at 1357°C for two days. Semicoherent precipitate of α-$NbPd_3$ from supersaturated α-Pd solid solution. Magnification 385 times.

of impurities (0.5 wt pct (6 at. pct) C and metallic impurities at a lower level). In the case of the other, subsequent studies which report σ, final alloy purity cannot be readily ascertained, or it is not certain whether σ was unambiguously defined by X-ray diffraction. Knapton,[6] using Nb from Johnson-Matthey Co., Ltd. (no data on purity are given), made a deliberate attempt to confirm the observation of σ phase and studied alloys in the appropriate composition range (30 to 50 at. pct Pd) annealed in the temperature range (1000 to 1200°C) of Ref. 5. However, there was no evidence of σ phase formation.

We have therefore made attempts to reproduce the compositions and temperatures reported in both studies[5,6] by preparing an alloy $Nb_{0.60}Pd_{0.40}$ using high purity Nb with analysis as described above. Both in the as-cast state and after an annealing treatment identical to that reported by Greenfield and Beck[5] (72 h at 1000°C) the alloy consisted of two phases (α-Nb + $NbPd_2$) without any evidence of σ phase. Also, as stated, σ did not form in any of our other alloys after annealing at temperatures between 1400 and 800°C. The question therefore arises whether the presence of impurities has contributed to the conflicting results by affecting alloy structure in the present or other studies. While the possibility cannot be excluded that the present negative findings are due to an undetermined type of contamination, this appears to be extremely unlikely in view of the materials and procedures used, especially as compared to the earlier studies (except that of Ref. 6, which yielded the same negative result). It is more likely that the presence of unidentified impurities was the cause of the reported instances of σ formation (where such was actually observed). To strengthen this hypothesis, we prepared an additional $Nb_{0.66}Pd_{0.34}$ alloy using high purity Nb (see above) and ternary $(Nb_{0.66}Pd_{0.34})_{1-x}M_x$ alloys with M = C, O, V, Ta, and other elements and x = 0.04 to 0.10. While the metalloid additives (C,O) were not found to promote σ formation in Nb-Pd, the T_5 metal additives (V,Ta) had this effect, strongly stabilizing new ternary σ phases: these results will be described in more detail elsewhere.[26] We conclude that the σ phase is not an equilibrium phase of the binary Nb-Pd system.

"Nb_3Pd_2 (r)". Maldonado and Schubert[9] have reported the existence of a phase with an orthorhombic structure (NbRu type) derived by a deformation of the bcc structure of α-Nb solid solution. The phase had been found after annealing $Nb_{0.75}Pd_{0.25}$ at 650°C for 500 h and $Nb_{0.66}Pd_{0.34}$ at 700°C for 48 h and was designated as Nb_3Pd_2 (r) to indicate a room-temperature phase.[9] We did not observe diffraction peaks due to this phase in alloys in this composition range which were annealed at ≥ 800°C. While this phase may indeed be an equilibrium low-temperature phase below 800°C, it is also possible that it is a metastable phase formed (in this intermediate composition range of structural instability[27]) by cold-working and then inadequately annealing the alloy powders used in the X-ray diffraction studies. The unidentified microstructural features observed in this composition range (see above) may be significant in this context.

α-NbPd. The structure of α-NbPd is not known from direct high-temperature measurements at this time, but the results of the rapid quenching experiments, yielding a Cu-type phase, and the crystal chemical considerations given in the following strongly suggest that this phase is a disordered solid solution with an fcc Cu-type structure, as given in Tables II and III. α-NbPd is thus, in effect, an extension of the isostructural α-Pd solid solution: the two portions of this solid solution field are separated over a narrow range of ~9 at. pct by the compound $NbPd_2$. Relevant crystal chemical considerations are the extended shape of the α-NbPd phase field which is not suggestive of an ordered phase, comparison with the related systems V-Pd[4] and V-Pt,[1] where continuous α-Pd or α-Pt terminal solid solutions exist up to and beyond the equiatomic compositions, and consideration of the close structural relation of $NbPd_2$ and α-$NbPd_3$ to the fcc Cu-type, as discussed previously in detail for the analogous high-temperature phase β-TaPd.[2] However, it should be pointed out that ordering, *e.g.* into the AuCu type with $c/a \cong 1.0$ would not be detected by the present X-ray measurements and thus cannot be specifically ruled out for α-NbPd.

$NbPd_2$ and $NbPd_3$. The structures of the intermediate phases $NbPd_2$, α-$NbPd_3$, and β-$NbPd_3$ have been reported previously,[7,8,9,12,13] and the present study confirms these results (Table II). The lattice parameters presented in Table III are from Ref. 8, 12, and 13; they were not refined further here. The homogeneity range of $NbPd_2$ is quite narrow (< ±1 at. pct), whereas the homogeneity range of $NbPd_3$ is broader (~74 to 77 at. pct Pd). α $NbPd_3$ and β-$NbPd_3$ are structurally closely related:[8,18] they differ only in the stacking sequence of the rectangular $NbPd_3$ layers comprising either phase, with a three-layer sequence for α-$NbPd_3$ (as in the parent Cu type) and a six-layer sequence for β-$NbPd_3$.[18]

The two $NbPd_3$ modifications apparently occupy adjacent phase fields, with the tetragonal α-modification forming at slightly higher Pd contents. On the basis of the observed transformation of a β-$NbPd_3$ alloy to α-$NbPd_3$ after annealing at 850°C, it is also possible that one of these phases is a high-temperature modification: matters are further complicated by the possibility that even small amounts of impurities may affect the stacking sequence and structure.[3] A close study of this aspect of the constitution diagram has not been made and, in the absence of further information, the two phases are shown in Fig. 1 separated by a dashed line.

Frank-Kasper Phases. The other two T_5Pd systems contain Frank-Kasper (tetrahedrally close packed) phases:[18,28] in the V-Pd system there is a stable A15-type phase V_3Pd[4] and in the Ta-Pd system a σ phase is found which is stable up to approximately 2550°C.[2] However, no corresponding phases of either type occur in the Nb-Pd system. Thus the Nb-Pd system is unique among these three systems in not forming Frank-Kasper phases or, in fact, any T_5-rich intermediate phases. Instead it appears that there is a greater solubility of Pd in the bcc α-Nb solid solution than in either the α-V(Pd) or α-Ta(Pd) solution. This observation may be of some practical importance in developing useful Nb alloys by suppressing the formation of brittle A15 or σ phase type compounds.

Mean Atomic Volumes. The mean atomic volumes $\bar{V}$ of all phases listed in Tables II and III are plotted in Fig. 10; all $\bar{V}$ values show a negative deviation

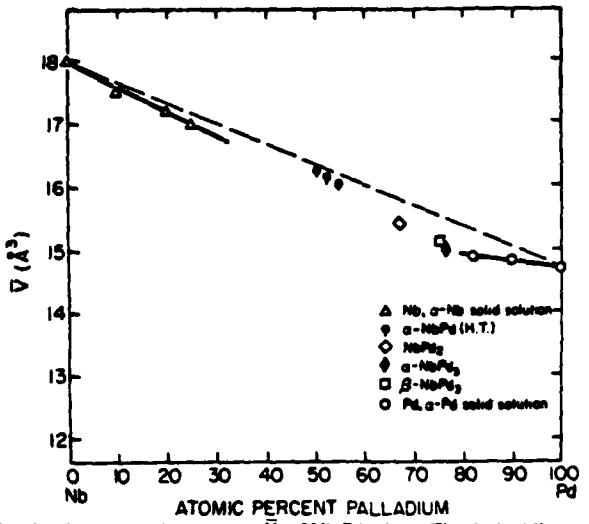

Fig. 10—Mean atomic volumes, $\bar{V}$, of Nb-Pd alloys. The dashed line represents a linear interpolation between pure Nb and pure Pd.

from a linear interpolation line, with the maximum negative deviation of $\bar{V}$ from this line at the composition $NbPd_3$, as observed previously for $TaPd_3$ (Ref. 2) and $TaPt_3$.[3] The $\bar{V}$ values for the α-NbPd solid solution lie only slightly below the linear interpolation line and suggest a change of the partial molar volume of Nb from $\bar{V}_{Nb} \sim 16Å^3$ in the terminal α-Pd solid solution to $\bar{V}_{Nb} \sim 18$ to $19Å^3$ in α-NbPd, $NbPd_2$ and $NbPd_3$.

CONCLUDING REMARKS

As to desirable further experimental work on the constitution of this system, there are two principal areas: First, detailed studies of intermediate transformation products, if any, in the α-Nb solid solution, and second, the composition and temperature range of α-$NbPd_3$ and β-$NbPd_3$.

The present paper completes the series on the T_5-Pd constitution diagrams,[1,2] with T_5 = V, Nb, Ta. They share certain general characteristics, such as the presence of AB_2 and AB_3 phases and extensive mutual terminal solid solubilities; there are also significant differences, such as which phases are present in the T_5-rich region. A further comparative study of the alloy chemical data for all T_5-T_{10} systems, including metastable phases, will be given later.[24]

ACKNOWLEDGMENTS

We wish to thank Dr. J. H. Brophy and the International Nickel Corporation for a gift of Pd metal and to acknowledge assistance in the rapid quenching work by Mr. M. Utterback.

This investigation was supported at the Massachusetts Institute of Technology by the Advanced Research Project Administration under ARPA Contract SD-90, at Northeastern University by the Office of Naval Research under Contract N14-76-C-820, and at the National Bureau of Standards by Research Grant DE05031 to the American Dental Association Health Foundation from the National Institute of Dental Research and is part of the dental research program conducted by the National Bureau of Standards in cooperation with the American Dental Association Health Foundation. It is also part of the materials research program conducted by the Massachusetts Institute of Technology and the materials research program conducted by Northeastern University.

REFERENCES

1. R. M. Waterstrat: *Met. Trans.* 1973, vol. 4, pp. 455-66.
2. R. M. Waterstrat, B. C. Giessen, R. Koch, and R. C. Manuszewski: *Met. Trans. A*, 1978, vol. 9*A*, pp. 643-48.
3. B. C. Giessen, R. H. Kane and N. J. Grant: *Trans. TMS-AIME*, 1965, vol. 223, pp. 855-63.
4. W. Koester and W. D. Haehl: *Z Metallk.*, 1958, vol. 49, pp. 647-49.
5. P. Greenfield and P. A. Beck: *Trans. AIME*, 1956, vol. 206, pp. 265-76.
6. A. G. Knapton: *J. Less-Common Metals*, 1960, vol. 2, pp. 113-24.
7. B. C. Giessen, D. Parker, and N. J. Grant: *J. Met.* (abstract), January 1964, vol. 16, pp. 92-93.
8. B. C. Giessen and N. J. Grant: *Acta Crystallgr.*, 1964, vol. 17, pp. 615-16.
9. A. Maldonado and K. Schubert: *Z. Metallk.*, 1964, vol. 55, pp. 619-26.
10. E. Kudielka-Artner and B. B. Argent: *Proc. Phys. Soc. London.*, 1962, vol. 80, pp. 1143-48.
11. J. A. Catterall and S. M. Barker: *Plansee Proc.*, 1964, pp. 577-87.
12. A. E. Dwight: "Columbium Metallurgy," *AIME Met. Soc. Conf.*, 1961, vol. 10, pp. 383-406, Interscience Publishers, NY.
13. B. C. Giessen and N. J. Grant: *J. Less-Common Metals.*, 1965, vol. 8, pp. 114-19.
14. E. M. Savitskii, V. V. Baron, and A. N. Khotinskaya: *Russ. J. Inorg. Chem.*, 1961, vol. 6, pp. 1316-17.
15. D. P. Parker: B.Sc. Thesis, Massachusetts Institute of Technology, Cambridge, MA, 1963.
16. I. Bowers: Personal Communication to B. C. Giessen, Oxford University, England, 1968.
17. F. A. Shunk: *Constitution of Binary Alloys, 2nd suppl.*, pp. 195-96, McGraw-Hill, New York, NY, 1969.
18. W. B. Pearson: *The Crystal Chemistry and Physics of Metals* and Alloys, pp. 330-31, Wiley-Interscience, New York, NY, 1972.
19. W. B. Pearson: *Handbook of Lattice Spacings and Structures of Metals and Alloys*, vol. 2, p. 1111, Pergamon Press, NY, 1967.
20. R. M. Waterstrat: *Met. Trans.*, 1973, vol. 4, pp. 1585-92.
21. B. C. Giessen, H. Ibach and N. J. Grant: *Trans. TMS-AIME*, 1964, vol. 230, pp. 113-22.
22. A. K. Sinha, B. C. Giessen and D. E. Polk: *Treatise on Solid State Chemistry*, vol. III, pp. 1-88, Plenum Press, NY, 1976.
23. M. Fischer, D. E. Polk, and B. C. Giessen: *Rapid Solidification Processing—Principles and Technologies*, R. Mehrabian, B. H. Kear, and M. Cohen, eds., pp. 140-48, Claitor's Publ. Div., Baton Rouge, LA, 1978.
24. B. C. Giessen, Northeastern University, Boston, MA, and R. M. Waterstrat, National Bureau of Standards, Washington, D. C.: Unpublished research, 1978.
25. R. P. Elliott: *Constitution of Binary Alloys, 1st suppl.*, pp. 265-66, McGraw-Hill, New York, NY, 1965.
26. R. M. Waterstrat, National Bureau of Standards, Washington, D. C., and B. C. Giessen, Northeastern University, Boston, MA: Unpublished research, 1978.
27. D. L. Ritter, B. C. Giessen, and N. J. Grant: *Trans. TMS-AIME*, 1964, vol. 230, pp. 1259-67.
28. D. P. Shoemaker and C. B. Shoemaker: *Developments in the Structural Chemistry of Alloy Phases*, pp. 107-39, Plenum Press, NY, 1969.

MAGNETIC PROPERTIES OF AMORPHOUS $RE_{65}Al_{35}$ ALLOYS

Bill C. Giessen, William A. Hines and
Lawrence T. Kabacoff

Abstract - Ribbons of amorphous $RE_{65}Al_{35}$ alloys (where RE = Ce, Pr and Dy) were prepared by melt spinning under vacuum. Magnetization measurements, carried out on a vibrating sample magnetometer with magnetic fields $H \leq 20$ kOe and over a temperature range 2.8 °K $\leq T \leq$ 300 °K, are reported here. $Dy_{65}Al_{35}$ and $Pr_{65}Al_{35}$ demonstrated a ferromagnetic-like ordering which was characterized by the appearence of a cusp at 30 °K and 7 °K, respectively. In both cases, hysteresis and relaxation effects occurred below the ordering temperature. Amorphous $Ce_{65}Al_{35}$ exhibited a negative paramagnetic Curie temperature of -40 °K, but did not order for temperatures down to 2.8 °K. The results are discussed in terms of the random atomic arrangement and its influence on the exchange and anisotropy interactions.

INTRODUCTION

In recent years, both basic and applied researchers have devoted considerable effort to the study of disordered materials such as magnetic glasses, amorphous semiconductors and amorphous metallic alloys[1]. Because of the existence of highly localized moments, the magnetic properties of rare earth amorphous alloys are of particular interest. Fundamental questions concerning magnetic moment formation and magnetic interactions (applied field, exchange and anisotropy), in situations where the atomic arrangements are random, remain unanswered. In order to shed light on the above questions, we are systematically studying the magnetic properties of the amorphous RE_xAl_{1-x} alloys, where RE represents a 4f rare earth element. This paper presents measurements of the bulk magnetization on three amorphous alloys which span the rare earth series: $Ce_{65}Al_{35}$, $Pr_{65}Al_{35}$ and $Dy_{65}Al_{35}$. Direct comparisons can be made with the corresponding crystalline alloys[2]. The RE_2Al crystalline phase represents an isostructural series of compounds with the orthorhombic Co_2Si-type (oP12) crystal structure. This structure has 12 atoms in a unit cell (8 RE and 4 Al) with 2 inequivalent RE sites. The RE coordination number is 13 (8 RE and 5 Al) while that for Al is 10 (all RE).

EXPERIMENTAL APPARATUS AND PROCEDURE

The amorphous alloys were prepared by melt spinning under vacuum resulting in ribbons 2 mm wide and 25 μm thick. The magnetic measurements were carried out on a P.A.R. model 155 vibrating sample magnetometer with magnetic fields $H \leq 20$ kOe and over a temperature range 2.8 °K $\leq T \leq$ 300 °K. The magnetometer was calibrated against the known room temperature saturation magnetization for Ni (55.01 emu/g) while the temperature calibration was based on the ideal Curie-Weiss behavior of the paramagnetic salt $Gd_2(SO_4)_3 \cdot 8H_2O$.

Manuscript received March 8, 1980.
This work is supported by the CNR under grant no. N14-76-C-820, the AFOSR under grant no. 80-0030 and the NSWC under grant no. IR-102. The authors are with Northeastern University, Boston, MA 02115, University of Connecticut, Storrs, CT 06268 and Naval Surface Weapons Center, Silver Spring, MD 20910, respectively.

X-ray diffraction patterns confirmed that the alloys were amorphous.

EXPERIMENTAL RESULTS AND ANALYSIS

For the three amorphous alloys, measurements of the bulk magnetization were made as a function of temperature for various magnetic fields. $Dy_{65}Al_{35}$ and $Pr_{65}Al_{35}$ exhibited magnetic ordering at $T_o = 30$ °K and 7 °K, respectively. In both cases, the magnetic ordering is characterized by a cusp-like behavior for low fields; the cusp broadens and disappears for $H > 4$ kOe. This is illustrated for $Dy_{65}Al_{35}$ in Fig. 1. Figure 2 shows the magnetization obtained at H = 18 kOe versus temperature throughout the entire range for $Dy_{65}Al_{35}$. A similar ferromagnetic-like magnetization versus temperature curve is obtained for $Pr_{65}Al_{35}$. For both $Dy_{65}Al_{35}$ and $Pr_{65}Al_{35}$ at fixed temperature below T_o, the magnetization rises

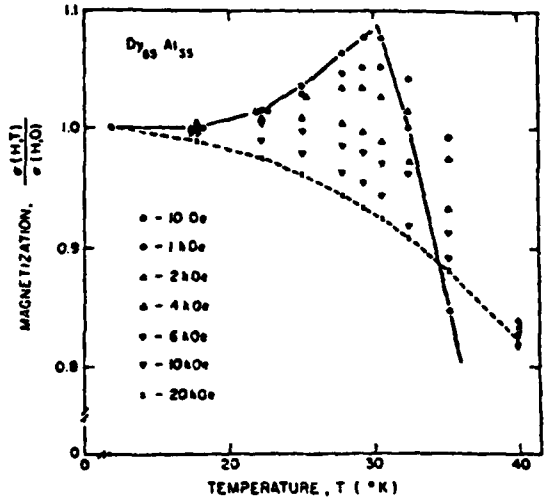

Fig. 1. $Dy_{65}Al_{35}$ magnetization normalized to value extrapolated for 0 °K, $\sigma(H,T)/\sigma(H,0)$, versus temperature, T, for various magnetic fields. Measurements were taken by starting from the virgin magnetic state above the ordering temperature.

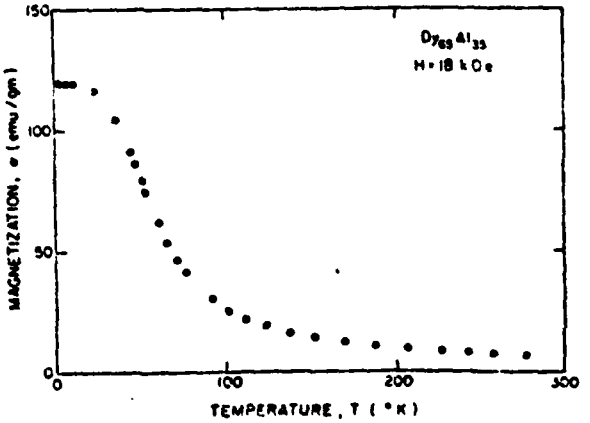

Fig. 2. $Dy_{65}Al_{35}$ magnetization at 18 kOe, $\sigma(18\text{-kOe},T)$, versus temperature, T.

0018-9464/80/0900-1203$00.75 © 1980 IEEE

sharply as the field is increased and then tapers off. However, saturation is not obtained for either alloy with the highest field available (20 kOe). Also, below the respective ordering temperatures, the magnetic behavior is characterized by hysteresis and relaxation effects. This is illustrated for $Pr_{65}Al_{35}$ in Fig. 3. If the sample is cooled below the ordering temperature in the presence of a large magnetic field (~ 18 kOe), a significant residual magnetization component exists when the field is then reduced to small values (~ 20 Oe). As shown in Fig. 3, this large residual magnetization (open circles) decreases sharply as the temperature is increased through the ordering temperature, becoming consistent with the previously described (reversable) magnetization versus temperature behavior (closed circles). Measurements of the coercive field, H_c, were made for both alloys as a function of temperature below T_o. Defining the transition temperature, T_c, as the temperature at which H_c extrapolates to zero, it was determined that T_c = 30 °K and 6 °K for $Dy_{65}Al_{35}$ and $Pr_{65}Al_{35}$, respectively. Amorphous $Ce_{65}Al_{35}$ did not order for temperatures down to 2.8 °K, and there was no evidence of hysteresis or relaxation effects.

For the three amorphous alloys, measurements of the bulk magnetization were made as a function of magnetic field for various temperatures. Figure 4 shows two of the many isotherms measured for $Dy_{65}Al_{35}$. For temperatures above the ordering temperature, the isotherms were straight lines through the origin. (As indicated before, below the ordering temperature, the magnetization does not saturate for H = 20 kOe.) Similar behavior was observed for $Pr_{65}Al_{35}$. Using the linear isotherms for all three alloys, values of the magnetic susceptibility, χ, were calculated from the slopes. In general, for the temperature range 50 °K ≤ T ≤ 300 °K, the susceptibility values provided excellent fits to the Curie-Weiss law

$$\chi = N p^2 \mu_B^2 [3k_B(T - \theta)]^{-1}, \qquad (1)$$

where p is the moment per RE atom and N is the number of RE atoms per gram. Figures 5 and 6 show the reciprocal susceptibility versus temperature for $Dy_{65}Al_{35}$ and $Ce_{65}Al_{35}$, respectively. From the fits to (1), values for θ and p were obtained for all three alloys. For $Dy_{65}Al_{35}$, $Pr_{65}Al_{35}$ and $Ce_{65}Al_{35}$, we find that θ = 41 °K, 8 °K and -40 °K, while p = 11.0, 3.47 and 2.31, respectively. Table I provides a summary of magnetization data for the three alloys (listed in row one). We note that the θ-values (row two) for $Dy_{65}Al_{35}$ and $Pr_{65}Al_{35}$ are positive and close to the corresponding ordering temperatures, T_o (row three), and transition temperatures, T_c (row four); while the θ-value for $Ce_{65}Al_{35}$ is negative. Also the experimental p-values (row five) are very close to the values calculated for the respective RE^{3+} ions by the Hund rules (row six). Finally, magnetization values obtained at the highest field (20 kOe) for $Dy_{65}Al_{35}$ and $Pr_{65}Al_{35}$ (row seven), are three to four times smaller than the saturation values calculated by assuming complete alignment of the above moments (row eight). For comparison, values for the "$Gd_{65}Al_{35}$" composition have been included in Table I. These values were obtained by interpolation from earlier work on Gd_xAl_{1-x} amorphous alloys[3].

DISCUSSION AND CONCLUSIONS

For both the amorphous $Dy_{65}Al_{35}$ and $Pr_{65}Al_{35}$ alloys, the Curie-Weiss susceptibility curves for temperatures above the respective ordering temperatures were typical of ferromagnetic behavior (i.e.

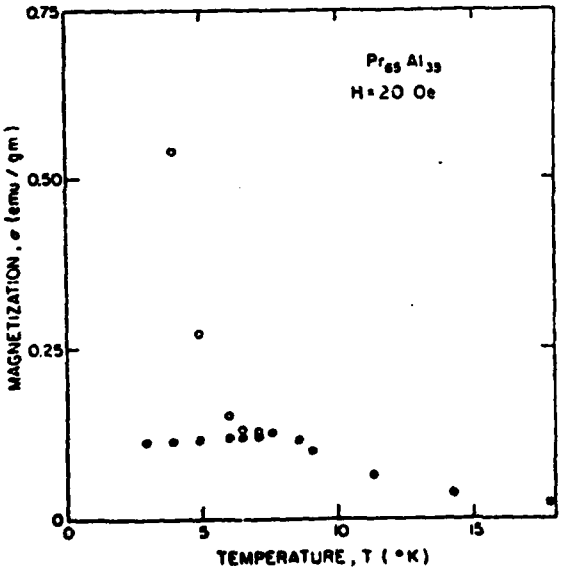

Fig. 3. $Pr_{65}Al_{35}$ magnetization at 20 Oe, σ(20-Oe,T), versus temperature, T. Open circles - sample cooled below the ordering temperature in a field of 18 kOe; closed circles - sample cooled below the ordering temperature in zero magnetic field.

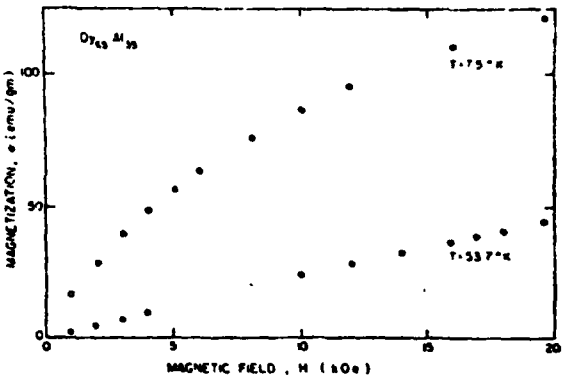

Fig. 4. $Dy_{65}Al_{35}$ magnetization at 7.5 °K and 53.7 °K, σ(H,T), versus magnetic field, H.

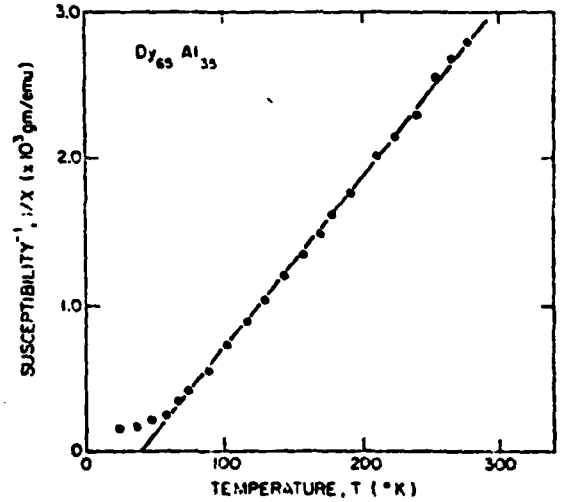

Fig. 5. $Dy_{65}Al_{35}$ reciprocal susceptibility, $1/\chi(T)$, versus temperature, T. A similar plot was obtained for $Pr_{65}Al_{35}$.

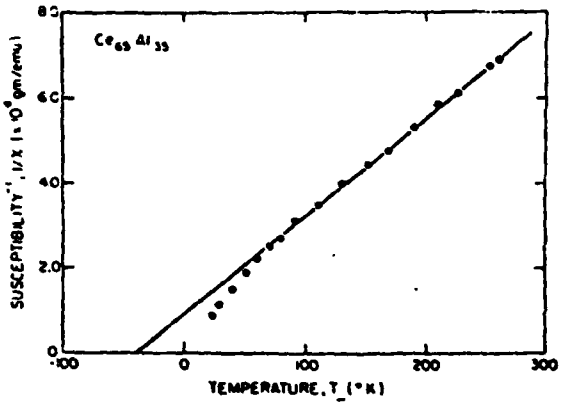

Fig. 6. $Ce_{65}Al_{35}$ reciprocal susceptibility, $1/\chi(T)$, versus temperature, T.

TABLE I: Magnetic data for the amorphous $RE_{65}Al_{35}$ alloys.

$RE_{65}Al_{35}$	$Ce_{65}Al_{35}$	$Pr_{65}Al_{35}$	$Gd_{65}Al_{35}$*	$Dy_{85}Al_{35}$
θ (°K)	-40	8.0	114	40.5
T_o(°K)	-	7.2	51	30.0
T_c(°K)	-	6.2	81	30.3
p_{exp}	2.31	3.47	**	11.0
$p_{calc.}$	2.54	3.58	7.94	10.6
σ(emu/g)	-	29.8	***	121
σ_o(emu/g)	-	111	228	326

*see ref. [3], values obtained by interpolation
**"consistent with Gd^{3+} ion"[3]
***"saturates easy, little or no anisotropy"[3]

positive values for θ). Also, the existence of a spontaneous magnetization was apparent in both cases. We attribute a ferromagnetic-type of ordering to $Dy_{65}Al_{35}$ and $Pr_{65}Al_{35}$, without the implication of a strictly parallel alignment of moments. The onset of hysteresis and relaxation effects below the respective ordering temperatures, as well as the lack of saturation, provides evidence for strong local anisotropy. This is expected for these systems since $L \neq 0$. We note that similar work on amorphous Gd_xAl_{1-x} alloys (where $L = 0$) showed little or no such anisotropy effects[4]. As in crystalline rare earth metals and alloys, the exchange appears to arise from the RKKY-type indirect interaction between the RE moments. However, because of atomic disorder, both positive (ferromagnetic) and negative (anti-ferromagnetic) interactions are possible. It should be noted that the RKKY interaction is normally long range in pure metals, compounds and dilute alloys. However, it is strongly dependent on the conduction electron mean free path which is of the order of the interatomic distances in amorphous metals and alloys. Consequently, the range of the RKKY coupling is considerably reduced and, hence, a nearest neighbor model might be more appropriate. The local anisotropy at a RE site arises from the electrostatic fields due to neighboring atoms. Because of atomic disorder, random orientations occur in the local easy axis. The combined effect of the exchange and anisotropy interactions described above can lead to significant fluctuations in the magnetic moment directions and would account for the cusp behavior and "spin-flop" transition around the ordering temperature. Such behavior has been described by Ferrer and Zuckermann[5] using a random magnetic anisotropy model.

Evidence for the RKKY-type exchange interaction also comes from the negative θ-value for $Ce_{65}Al_{35}$. However, in the case of $Ce_{65}Al_{35}$, the disordered atomic structure inhibits any tendency for anti-ferromagnetic ordering. The results reported here appear to contradict the work of Buschow[6] on amorphous Gd-alloys in which it was concluded that the RKKY interaction was of minor importance. Buschow suggests an exchange mechanism that proceeds via the RE 5d-electrons and, consequently, is always positive. Finally, we note that the corresponding crystalline Gd_2Al and Dy_2Al alloys exhibit anti-ferromagnetic ordering while crystalline Pr_2Al does not order.

ACKNOWLEDGMENTS

The authors are grateful to Dr. J. R. Cullen for many helpful discussions and to Ms. C. Modzelewski for assisting with the magnetometer measurements.

REFERENCES

[1] Amorphous Magnetism II, edited by R. A. Levy and R. Hasegawa (Plenum Press, New York, 1977).
[2] L. R. Sill and R. R. Biggers, J. Appl. Phys. 49, 1500 (1978).
[3] T. R. McGuire, T. Mizoguchi, R. J. Gambino and S. Kirkpatrick, J. Appl. Phys. 49, 1689 (1978).
[4] N. Heiman and N. Kazama, J. Appl. Phys. 49, 1685 (1978).
[5] R. Ferrer and M. J. Zuckermann, Can. J. Phys. 56, 1093 (1978).
[6] K. H. J. Buschow, Solid State Commun. 27, 275 (1978).

Thermoelectric power of magnetic and nonmagnetic amorphous metals

Soumen Basak and S. R. Nagel
The James Franck Institute and The Department of Physics, University of Chicago, Chicago, Illinois 60637

B. C. Giessen
Department of Chemistry, Northeastern University, Boston, Massachusetts 02115

(Received 26 December 1979)

The thermoelectric power of a number of magnetic and nonmagnetic amorphous metallic alloys has been measured as a function of temperature between 15 and 580 K. The temperature dependence of the thermopower for the magnetic alloys is qualitatively different from that for the nonmagnetic alloys. The data for the nonmagnetic alloys are consistent with the extended Ziman theory for transport in liquid and amorphous metals. It is argued that the data for the magnetic alloys are consistent with a model, based on the Kondo scattering of conduction electrons by spins situated in low internal fields, which was recently proposed to explain the resistivity minima observed in these materials.

Recent studies of electronic transport in metallic glasses have revealed two distinctly different types of anomalous resistivity behavior. Some of these glasses show a small but monotonic decrease of resistivity with increasing temperature, over as wide a range as 4 to 600 K in some cases.[1-5] The amorphous alloys Cu-Zr (Refs. 3 and 4) and Be-Ti-Zr (Ref. 5) are examples in this group, which consists of many glasses having no magnetic constituents. The other type of anomalous resistivity is found in amorphous alloys containing some ferromagnetic or antiferromagnetic elements, such as Fe-B, Fe-Ni-P-B, or Fe-Ni-Cr-P-B. In these, the resistivity shows a minimum in the temperature range 10 to 300 K and an approximate logarithmic increase of the resistivity with decreasing temperature below the minimum.[6,7] Such resistivity behavior could have been associated with the Kondo effect normally observed in crystalline alloys containing small amounts of magnetic atoms, except for the fact that these glasses are strongly ferromagnetic. As is well known, the large internal field experienced by the magnetic atoms in a ferromagnet precludes the possibility of their giving rise to Kondo scattering of the conduction electrons.

Several theories have been proposed to explain the negative temperature coefficient of resistivity, $\alpha \equiv (1/\rho)\, d\rho/dT$, observed in metallic glasses. One of these is the generalized Ziman theory of electronic transport in liquid metals.[1,8,9] It deals with the normal potential scattering contribution to the electrical resistivity as modified by the absence of periodic order in a glass, and can lead to a positive or negative value of α depending on the relative positions of $2k_F$ and k_p, where k_F is the Fermi wave vector of the conduction electrons and k_p denotes the position of the first peak in the x-ray structure factor of the glass. An alternative theory[6,10] proposes the existence of quantum-mechanical two-level tunneling states for some of the atoms in a disordered solid. The Hamiltonian for electrons scattering from the localized excitations arising from these tunneling states is assumed to be identical with the Kondo Hamiltonian, which can give rise to both a resistivity minimum and a negative value of α over a wide temperature range. However a recent calculation of this effect by Black *et al.*,[11] using parameters for the tunneling model deduced from ultrasonic experiments, indicates that this model would give a resistivity anomaly three orders of magnitude too small to fit the data.

A recent work[12] has resurrected the idea of a real Kondo effect in explaining the resistivity minima observed in the magnetic glasses. Instead of proposing a structural modification to the Kondo theory, it considers the spin-flip scattering of electrons from magnetic atoms sitting in regions of zero effective field.[13] That a small fraction of the magnetic atoms may actually exist in such field-free regions in a concentrated ferromagnet such as $Fe_{0.80}B_{0.20}$ has been demonstrated by Grest and Nagel[12] on the basis of Monte Carlo calculations of the effective-field distribution $P(H)$ in such materials, and follows essentially from the large disorder inherent in the glasses. This result therefore reconciles the coexistence of Kondo-type resistivity anomaly and ferromagnetism in these amorphous alloys and implicitly predicts a difference in the thermoelectric power behavior between magnetic and nonmagnetic glasses. Such a prediction would not, however, follow from the tunneling-level model which views both magnetic and nonmagnetic glasses identically as regards the effects of structure on their transport properties. Besides these three, other theories proposed to explain the negative α include the Mott s-d scattering model,[4] and those that study the interference between phonon and im-

purity scattering.[14]

In order to identify the scattering mechanism which most accurately describes the transport in the glass it is necessary to study some transport property, other than the resistivity, whose predicted behavior in the various models will be substantially different. In a previous communication[5] a study of the resistivity α and the thermoelectric power Q in a Be-Ti-Zr glass over an extended range of temperature was reported. It was shown there that both the negative temperature coefficient of resistivity and the positive thermoelectric power varying linearly with temperature observed over the entire range from 10 to 600 K could be explained on the basis of the extended Ziman theory if the condition $2k_F \cong k_\rho$ was satisfied for the alloy. However, this behavior of Q was not consistent with the predictions of either the tunneling-level model or the *s-d* scattering model. In this paper we present a more extensive study of the thermoelectric power of both magnetic and nonmagnetic glasses.[15]

The samples were in the form of ribbons of width 1–2 mm and thickness 30–60 μm. The thermoelectric power of each sample was measured relative to that of a 99.999+% pure lead wire using the integral method.[5] The absolute thermopowers were calculated using the new standard scale for lead obtained by Roberts[16] for temperatures up to 350 K. At higher temperatures the standard values used were those of Cook, Laubitz, and Van der Meer,[17] which were adjusted to join smoothly with the scale of Roberts. The uncertainty in the data was estimated to be 0.1 μV/K.

Figure 1 shows the data for amorphous $Cu_{0.50}Zr_{0.50}$ together with that reported previously[5] on the metallic glass $Be_{0.40}Ti_{0.50}Zr_{0.10}$ (Metglas 2204; Metglas is a registered trademark of Allied Chemical Corp.). The thermopower of Cu-Zr is *positive* and *linear in T* over the *entire* temperature range 10 to 580 K, as it is for the Be-Ti-Zr glass. The magnitude of Q is small in both these samples and is more similar to that of a noble metal than of a transition metal. We have also measured the resistivities of both samples and found them to decrease monotonically with increasing temperature over the *entire* range 10 to 580 K. For Be-Ti-Zr and Cu-Zr, the decrease in resistivity over this temperature range is about 9% and 6%, respectively. Sinha[1] has measured the resistivity and thermoelectric power of $(Ni_xPt_{1-x})_{0.75}P_{0.25}$ glasses as a function of temperature, though over much more limited ranges than is reported here. His resistivity measurements showed that α was negative for the glasses for which $0.20 \leq x \leq 0.50$, and positive for the glass with $x = 0.60$. The thermoelectric power for all the samples was small (varying between 1 and 2.5 μV/K), positive and linear in T in the range 80 to 300 K.

The abovementioned results are incompatible with a Kondo-type theory[6,10] based on tunneling levels for transport in these glasses. For if such tunneling levels were truly an intrinsic feature of the glassy structure contributing to electronic transport then the anomaly associated with Kondo-like behavior should have appeared in the thermopower data. Within the detecting capacity of our experiment (0.1 μV/K in a total of 4.5 μV/K) no such structure has been observed. This is consistent with the work of Black *et al.*[11] who predict that the tunneling-level anomalies, if present, will be too small to be detected in an experiment of such a degree of sensitivity. The thermopower results are also incompatible with the predictions of the *s-d* scattering model.[4,13] According to the Mott formula $Q \propto [\partial \ln \rho(E)/\partial E]_{E=E_F}$, the thermopower of elements with less than half-filled *d* bands should be opposite in sign to the thermopower of elements having more than half-filled *d* bands. A recent photoemission experiment[18] on Cu-Zr glasses concludes that the electronic structure of Cu-Zr in the vicinity of the Fermi level is mainly determined by the Zr *d* band, which is less than half-filled. The electronic structure of the Be-Ti-Zr glass can also be expected to be similar to that of the Ti or Zr *d* band, whereas that for Ni-Pt-P should be close to the nearly full *d* band structure of Ni and Pt. The positive thermoelectric power observed in all three glasses then

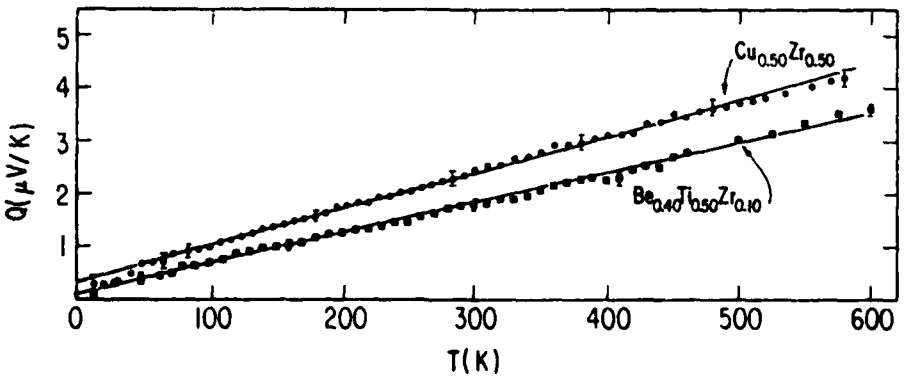

FIG. 1 Thermoelectric power of the nonmagnetic amorphous alloys $Be_{0.40}Ti_{0.50}Zr_{0.10}$ (Ref. 5) and $Cu_{0.50}Zr_{0.50}$.

directly contradicts the prediction of the *s-d* scattering model.

The generalized Ziman theory, on the other hand, is consistent with the temperature-dependent behavior of the transport coefficients reported above. The negative α of these glasses can be explained using the Ziman theory by assuming that the criterion $2k_F \cong k_p$ is satisfied for each alloy.[2,5,9] (Here k_p is not necessarily the first maximum of the total interference function but may be the maximum of one of the *partial* structure factors.) The same criterion also leads to a thermopower which is small, positive and linear in T, as was pointed out before.[5] The following expression for the thermoelectric power is obtained from the Ziman theory[19]:

$$Q = -\frac{\pi^2 k_B^2 T}{3|e|E_F}(3 - 2q - \tfrac{1}{2}r) \quad , \tag{1}$$

where

$$q = S(2k_F)|t(2k_F)|^2 \Big/ \int_0^{2k_F} |t(k)|^2 S(k) 4(2k_F)^{-4} k^3 \, dk \quad .$$

$S(k)$ denotes the structure factor, k_B is the Boltzmann constant, and r depends on the energy dependence of the t matrix, $t(k)$. From x-ray diffraction studies we find $k_p = 2.75$ Å^{-1} for Be-Ti-Zr (Ref. 5) and 2.73 Å^{-1} for Cu-Zr which, if $k_p \cong 2k_F$ (where we emphasize that a strict equality is not necessary and deviations of $\pm 15\%$ can be tolerated), give $E_F = 7.2$ and 7.1 eV, respectively. The measured slopes of the Q vs T curves for Be-Ti-Zr and Cu-Zr are 5.7×10^{-3} and 7×10^{-3} μV K^{-2}, respectively. Neglecting the term r in Eq. (1) above, these results imply $q = 2.3$ and 2.5 for the two glasses. These seem to be reasonable numbers if they are compared with a crude estimate of q from the definition in Eq. (1) with again $2k_F$ taken to be close to k_p.

Figures 2 and 3 show the absolute thermopower of five ferromagnetic Metglas alloys as a function of temperature between 15 and 580 K. In the low-temperature range up to 300 K our thermopower results for the Metglas alloys 2826, 2826A, and 2605A agree very well with those of Baibich *et al.*,[20] who have recently published data up to 300 K from measurements carried out independently in three different laboratories on three separately obtained batches of Metglas alloys. For the Metglas 2605 alloy our data agree well with that of Elzinga and Schroeder in that work,[20] but differs from the data of the other two measurements by almost 1 μV/k at 300 K. Between 300 and 580 K our results for the same alloy differ by the same amount from that of Teoh *et al.*,[21] whose high-temperature data on Metglas 2605 alloy join smoothly with the low-temperature data of Baibich and Muir (from Ref. 20) at 300 K. It is at once seen that the behavior of Q for these samples is *qualitatively different* from that for the nonmagnetic glasses shown in Fig. 1. For all magnetic samples the thermopower is negative, and has a negative slope at low temperatures, i.e., below 100 K. Most importantly, Q is *not linear* in T over any large range of temperature and shows structure similar to that observed in crystalline Kondo systems, i.e., nonmagnetic hosts containing dilute amounts of magnetic impurities. The resistivities of all these alloys also show minima similar to that observed in crystalline Kondo systems. However, the glasses all contain large concentrations of magnetic elements and it is not immediately clear why they should exhibit a Kondo-like behavior. Table I shows the compositions and some characteristics of the transport properties of the samples studied here.

The transport behavior of the magnetic samples cannot obviously be explained by the use of the Ziman theory. The tunneling-level model may lead to Kondo-like anomalies in the transport properties of the magnetic glasses, but it fails to explain why simi-

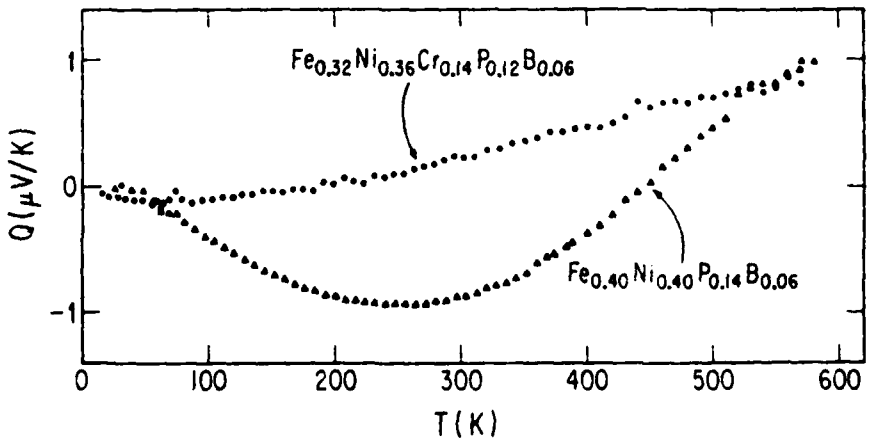

FIG. 2. Thermoelectric power of the amorphous magnetic alloys $Fe_{0.40}Ni_{0.40}P_{0.14}B_{0.06}$ and $Fe_{0.32}Ni_{0.36}Cr_{0.14}P_{0.12}B_{0.06}$

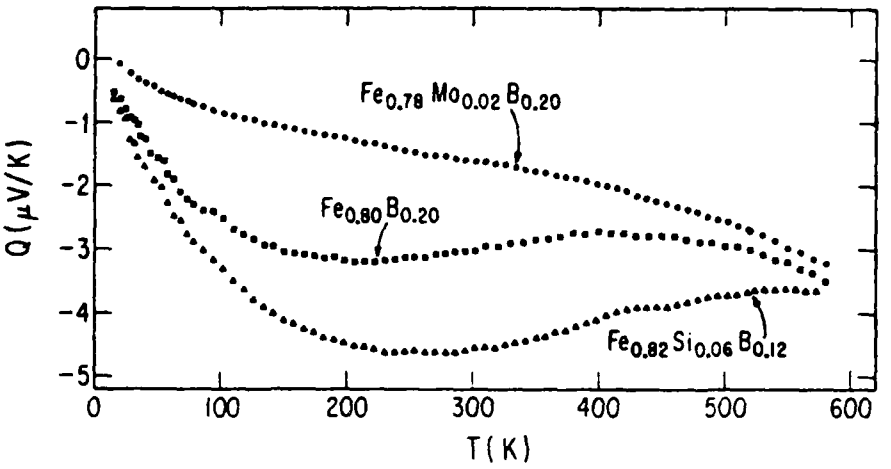

FIG. 3. Thermoelectric power of the amorphous magnetic alloys $Fe_{0.80}B_{0.20}$, $Fe_{0.78}Mo_{0.02}B_{0.20}$, and $Fe_{0.82}Si_{0.06}B_{0.12}$.

lar anomalies are not observed in the thermopower of the nonmagnetic glasses as well. However, the work of Grest and Nagel leads naturally to such anomalous transport behavior in magnetic glasses only and not in the nonmagnetic ones, whose positive and linear thermopower result therefore does not conflict with the central idea of this model.

In crystalline alloys the Kondo effect gives rise to anomalously large structures in the Q vs T curves, the magnitude of which can be ten times as much as that observed in the present case. It is argued in the following that this relative lack of structure in the thermopower does not rule out the possibility of a Kondo effect in the glasses. One reason for this is to be found in the Nordheim-Gorter rule,[19] according to which the thermopower contribution from a given electron scattering mechanism will be weighted by the relative contribution to the resistivity arising from that process. This relative contribution is given by ρ_K/ρ_T, where ρ_K is the Kondo contribution to the total resistivity, ρ_T. For the magnetic glasses Baibich *et al.*[20] have estimated this ratio to be $\sim 10^{-3}$ from the depth of the low-temperature minima observed in their ρ vs T curves. This means that even the unusually large Kondo contribution of 100 μV/K will produce a structure in the thermopower only on the order of 0.1 μV/K. Since this is below the detecting capacity of the present experiments, they conclude that the thermopower data do not exhibit any effect of the Kondo scattering. However, for reasons presented below, we believe that the above estimate of the size of ρ_K/ρ_T is incorrect since ρ_K is much larger than that suggested by the apparent low-temperature anomaly in the resistivity of these alloys. This can be understood in the light of the work of Grest and Nagel,[12] whose calculations yield an effective-field distribution $P(H)$ in such glasses that has a long tail extending through zero field to negative values of H. The Kondo contribution to a transport coefficient J ($J \equiv \rho$ or Q) arising from this distri-

TABLE I. Transport data for amorphous alloys.

Metglas alloy	Composition	$\rho_{300\,K}$ ($\mu\Omega$ cm)	$\rho_{4.2\,K}/\rho_{300\,K}$ [a]	T_{min} [a] (K)	$Q_{300\,K}$ μV/K	Ferromagnetic T_c [a]
2826	$Fe_{0.40}Ni_{0.40}P_{0.14}B_{0.06}$	145 ± 15	0.962	26	−0.90	537
2826A	$Fe_{0.32}Ni_{0.36}Cr_{0.14}P_{0.12}B_{0.06}$	155 ± 15	1.020	270	+0.25	250
2605	$Fe_{0.80}B_{0.20}$	130 ± 15	0.960	14	−3.00	647
2605A	$Fe_{0.78}Mo_{0.02}B_{0.20}$	120 ± 15	0.992	7 & 80	−1.60	595
2605S	$Fe_{0.82}Si_{0.06}B_{0.12}$	140 ± 15	0.966	16	−4.60	
2204	$Be_{0.40}Ti_{0.50}Zr_{0.10}$	300 ± 30	1.060	None	+1.85	Nonmagnetic
	$Cu_{0.50}Zr_{0.50}$	210 ± 20	1.043	None	+2.45	Nonmagnetic

[a]The entries in the columns $\rho_{4.2\,K}/\rho_{300\,K}$, T_{min}, and T_c are from Ref. 7 except for Fe-Si-B and Cu-Zr, for which the data are from the present work. The data for 2204 are from Ref. 5.

bution should approximately be of the form

$$J(T) = \int_{-\Delta}^{\Delta} J(T,H) P(H)\, dH \quad . \tag{2}$$

where $J(T,H)$ is the transport contribution due to Kondo scattering from a single spin in field H. The cutoff, Δ, in this integral is not known, but should not extend to such high fields that the concept of Kondo scattering from independent spins breaks down. The temperature dependence of the resistivity due to Kondo scattering from spins in low fields may be approximated by the Hamann formula[22] with T replaced by $(T^2+H^2)^{1/2}$. Thus the divergent term $\ln T$ in the resistivity is replaced by $\ln(T^2+H^2)$. In convoluting over $P(H)$ in Eq. (2) this H-dependent term smears out the low-T divergence, which might be the reason why the observed anomaly in the resistivity of the magnetic glasses is small compared to that in crystalline alloys. However the behavior of the thermoelectric power does not change drastically due to a small applied magnetic field.[23] Therefore, unlike in the resistivity, the convolution over $P(H)$ does not smear out the structure in the thermoelectric power. What may happen, in large applied fields, is that the peak in $Q(T)$ will shift to higher temperatures.[23] This would account for why the peaks we observe in $Q(T)$ seem to be at somewhat higher temperatures than is usually observed in crystalline materials. Although it is still important to use the Nordheim-Gorter rule, it is difficult to estimate the size of ρ_K/ρ_T since ρ_K may be much larger than simply the apparent divergence seen in the low-temperature resistivity of these alloys.

It is possible to make some qualitative remarks about the effects of Cr and Mo on the thermopower anomalies observed. It is known that in crystalline Kondo systems Cr produces a very small anomaly in Q, unlike the large negative anomalies produced by Fe, Co, etc. It appears from the data of Fig. 2 that even the small structure in Q observed in the Fe-Ni-P-B glass is substantially washed out by the addition of Cr, as is observed for the Fe-Ni-Cr-P-B glass. This could be the result of an algebraic addition of the Kondo anomalies separately produced by the magnetic species in these samples. Similarly the addition of Mo, which has a d-band structure resembling that of Cr, is seen to reduce the structure in Q of the Fe-B glass, as shown in Fig. 3. By contrast, the addition of Si is seen to further depress the thermopower curves for Fe-B and Fe-Ni-P-B,[20] although such behavior is not readily explained by the position of Si in the Periodic Table. However, since the presence of even minute amounts of magnetic impurities may produce substantial effects on the thermopower in crystalline materials, there remains a fair degree of uncertainty in the predictions of thermopower behavior based only on the nominal compositions of these glasses. For example, an analysis of the Metglas alloys 2605 and 2605S showed that the former contained ~ 150 ppm Cr and ~ 1000 ppm Mn, while the latter had ~ 750 ppm Cr and ~ 200 ppm Mn in it. Such magnetic impurities might have made significant contributions to the thermopower data.

In conclusion, our experiments appear to point out a qualitative difference in the transport behaviors of magnetic and nonmagnetic glasses. In the former the resistivity shows a minimum and the thermopower a Kondo-like structure, both of which are expected results from the work of Grest and Nagel. In the nonmagnetic glasses, the resistivity decreases with increasing temperature and the thermoelectric power is positive and linear in T over the entire temperature range studied. Both these observations can be explained by the extended Ziman theory with suitable assumptions about the relationship between the Fermi wave vector and the partial structure factors. These assumptions are also consistent with a model[24] for the stability of these glasses. The tunneling-level model and the s-d scattering model appear to be incompatible with these two groups of thermopower data.

S.R.N. acknowledges support from an Alfred P. Sloan Foundation Fellowship. This work was supported in part by NSF DMR77-09931 at the University of Chicago and by the Office of Naval Research at Northeastern University.

[1] A. K. Sinha, Phys. Rev. B 1, 4541 (1970).
[2] S. R. Nagel, J. Vassiliou, P. M. Horn, and B. C. Giessen, Phys. Rev. B 17, 462 (1978).
[3] T. Mizoguchi, S. von Molnar, G. S. Cargill III, T. Kudo, N. Shiotani, and H. Sekizawa, in *Amorphous Magnetism II*, edited by R. A. Levy and R. Hasegawa (Plenum, New York, 1977), p. 513.
[4] F. R. Szofran, G. R. Gruzalski, J. W. Weymouth, D. J. Sellmyer, and B. C. Giessen, Phys. Rev. B 14, 2160 (1976).
[5] S. R. Nagel, Phys. Rev. Lett. 41, 990 (1978).
[6] R. W. Cochrane, R. Harris, J. O. Strom-Olson, and M. J. Zuckermann, Phys. Rev. Lett. 35, 676 (1975); R. W. Cochrane and J. O. Strom-Olson, J. Phys. F 7, 1799 (1977).
[7] J. A. Rayne and R. A. Levy, Ref. 3, p. 319.
[8] R. Evans, D. A. Greenwood, and P. Lloyd, Phys. Lett. A 35, 57 (1971).
[9] S. R. Nagel, Phys. Rev. B 16, 1694 (1977); P. J. Cote and L. V. Meisel, Phys. Rev. Lett. 39, 102 (1977); K. Fröhöse and J. Jäckle, J. Phys. F 7, 2331 (1977).
[10] C. C. Tsuei, Solid State Commun. 27, 691 (1978).

[11]J. L. Black, B. L. Gyorffy, and J. Jäckle, Philos. Mag. B 40, 331 (1979).
[12]G. S. Grest and S. R. Nagel, Phys. Rev. B 19, 3571 (1979).
[13]T. E. Sharon and C. C. Tsuei, Phys. Rev. B 5, 1047 (1972).
[14]An-Ban Chen, Gideon Weisz, and Arden Sher, Phys. Rev. B 5, 2897 (1972).
[15]Soumen Basak and S. R. Nagel, Bull. Am. Phys. Soc. 24, 332 (1979).
[16]R. B. Roberts, Philos. Mag. 36, 91 (1977).
[17]J. G. Cook, M. L. Laubitz, and M. P. Van der Meer, J. Appl. Phys. 45, 510 (1973).
[18]P. Oelhafen, E. Hauser, H.-J. Güntherodt, and K. H. Bennemann, Phys. Rev. Lett. 43, 1134 (1979).
[19]R. D. Barnard, *Thermoelectricity in Metals and Alloys* (Taylor and Francis, London, 1972).
[20]M. N. Baibich, W. B. Muir, G. Bélanger, J. Destry, H. S. Elzinga, and P. A. Schroeder, Phys. Lett. A 73, 328 (1979).
[21]N. Teoh, W. Teoh, Sigurds Arajs, and C. A. Moyer, Phys. Rev. B 18, 2666 (1978).
[22]See J. Kondo, in *Solid State Physics*, edited by H. Ehrenreich, F. Seitz, and D. Turnbull (Academic, New York, 1969), Vol. 23, p. 183.
[23]See K. H. Fischer, in *Thermoelectricity in Metallic Conductors*, edited by F. J. Blatt and P. A. Schroeder (Plenum, New York, 1978), p. 295.
[24]S. R. Nagel and J. Tauc, Phys. Rev. Lett. 35, 380 (1975).

Rapid Solidification Processing, Vol. II, R. Mehrabian, B.H. Kear and M. Cohen, Eds., Claitor's Publ. Div., Baton Rouge, LA, p. 237 (March 1980)

PREPARATION OF METALLIC GLASS IN THICK RIBBONS BY A MULTI-LAYER MELT SPINNING PROCESS

B. C. Giessen, S. Davis and S. Whang
Materials Science Division
Institute of Chemical Analysis
Northeastern University
Boston, MA
and
B. H. Kear
United Technologies Research Center
East Hartford, CT

ABSTRACT

It is an inherent feature of rapidly solidified alloys that they have at least one thin dimension in the as-quenched state; subsequent consolidation is therefore required to produce a dense, solid body. As a first step towards circumvention of this limitation, thick ribbons of a metallic glass have been prepared by a multi-layer self-substrate quenching technique.

Thick ribbons (75-125 μm) of $Cu_{60}Zr_{40}$ metallic glass were prepared by the superposition of thin quenched layers on the inside of the rotating drum of a vacuum melt spinning unit. The multi-layer ribbons were ductile, strong, did not delaminate upon bending and showed no, or only narrow, zones of crystallization at the layer interfaces.

Possible further developments based on this technique are discussed.

Introduction

Due to its relative simplicity, cheapness and efficiency, compared to other rapid solidification processing methods, melt spinning or variations of this process, appears to be preferred for the preparation of metallic glasses in industrial quantities[1,2]. The parameters governing the melt spinning process have been reviewed[3].

One of the drawbacks of the technique is its apparent limitation to thin ribbons or sheets with a thickness of ~50μm, due to the necessity of maintaining at least one small dimension for rapid heat removal. Consequently, it has not yet been possible to prepare conventional metallic glasses directly from the melt in the form of bar stock or as thick sheet, although more recently, the two-step preparation of glassy metals as solid bodies from powders or thin sheet material by direct cold consolidation has been reported[4-6].

Development of a method for the direct preparation of thick sheet material (0.1-1mm thick) was therefore desirable. The building up of successive thin layers into a thick sheet appeared to be an attractive possibility and was therefore attempted.

Experimental

Melt Spinning: An "inside-of-drum" melt spinning unit, enclosed in a vacuum chamber, was used, Fig. 1. In normal operation of this unit, a small quantity of the alloy is induction melted in the crucible and is then ejected as a thin alloy jet against the inside of the rotating drum, where it is quenched and solidified as a narrow ribbon. Successive layers are prevented from overlapping by a pneumatically driven, axial movement of the crucible; spiral-shaped ribbons of 30 μm thickness, 1-2 mm width and 3 m length are normally obtained.

For the present work the operation was modified such that after melt spinning had been initiated and the jet had stabilized, translation of the crucible was halted to permit building up of multiple layers.

Choice of Alloy: The $Cu_{60}Zr_{40}$ alloy was selected for the present, preliminary experiments. This alloy readily forms a glass at critical cooling rates $R_c \sim 10^6$K/sec (using the relationship between R_c and T_{rg} given in reference (7)) due to its high reduced glass transition temperature $T_{rg} = 0.63$[8,9]. Further, this glass does not (or only slightly) embrittle upon heating. The suitability of $Cu_{60}Zr_{40}$ for self-substrate quenching as a glass had been established experimentally earlier by the demonstration that amorphous $Cu_{60}Zr_{40}$ sheets of 0.75 mm thickness can be produced by plasma spraying in inert gas against a rotating cooled disk[9].

Examination: The multiple-layer ribbons produced were studied by X-ray diffraction (XRD), optical metallography and SEM. Ribbons were also examined for possible delamination in both bend and tensile tests.

Results

Ribbons of 75-125 μm thickness consisting of 3-5 layers, respectively, were produced reproducibly in several runs. The multiple ribbons were fully ductile and did not delaminate in bend or tensile tests, Fig 2. XRD examination showed both the ribbon top and bottom surface to be amorphous. Cross-sectional optical micrographs are shown in Fig. 3. In Fig. 3(a), three layers of ~25μm thickness

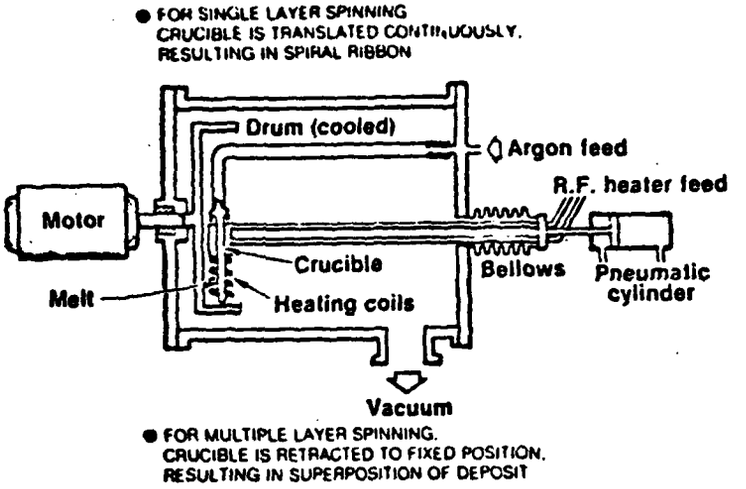

Fig. 1 - Schematic of inside-of-drum melt spinning apparatus

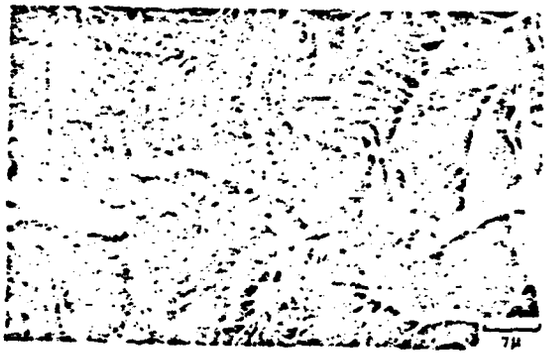

150X

Fig. 2 - Typical tensile fracture surface in a multi-layer $Cu_{60}Zr_{40}$ glassy ribbon, showing no evidence for delamination between layers.

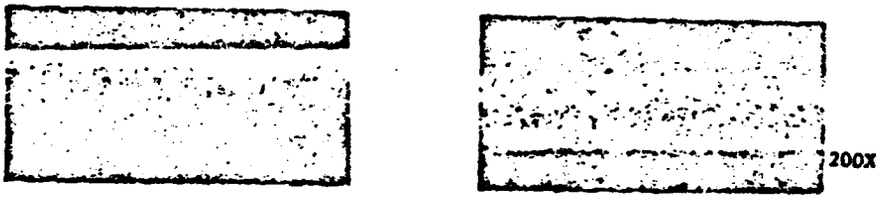

(a) (b)

Fig. 3 - Transverse section of triple-layer $Cu_{60}Zr_{40}$ glassy ribbon showing (a) visible and (b) invisible interfaces between layers (heavily etched.

each can be recognized, delineated by two interfaces which possibly is an indication of a minute amount of crystallinity (undetectable by XRD). In the cross-section shown in Fig. 3(b), interfaces could not be detected even after heavy etching. Tensile tests showed a rupture strength ~100,000 psi. Hardness values ranged from VHN = 650-700 kg/mm^2, indicating that the full strength of the ribbon had not been achieved in the tensile tests, due to the presence of surface imperfections.

From these results it is concluded that integral glass ribbons of intermediate thickness can be obtained by the present method, at least for the alloy composition selected.

Conclusion

The present, preliminary results suggest that multiple layer melt spinning may be a practical method for making thick ribbons of metallic glasses and other alloys requiring rapid solidification processing for their preparation.

Additional experiments are in progress to improve the multiple layer deposition process, to apply it to wider ribbons and to other glass forming alloys, especially those prone to embrittlement upon being reheated. Application to other types of processable alloys, e.g., those forming extended solid solutions, microcrystalline structures and metastable crystalline phases, are being studied, as well as modifications of the process to produce novel shapes.

Acknowledgement

This work was partially supported at Northeastern University by the Office of Naval Research.

References

1. R. B. Pond, U.S. Patent 2,825,108, March 4, 1958; U.S. Patent 2,976,590, March 28, 1961.

2. Metallic Glasses, J. Gilman and H. J. Leamy, Eds., ASM, 1976.

3. S. Kavesh, Rapid Solidification Processing: Principles and Technologies, R. Mehrabian, B. H. Kear and M. Cohen, Eds., Claitor's Publishing Division, Baton Rouge, LA, p. 165, 1977.

4. C. F. Cline, J. Mahler, M. Finger, W. Kuhl and R. Hopper, Ref. 3, p. 380, 1977.

5. H. H. Liebermann, these Proceedings.

6. D. G. Morris, these Proceedings.

7. H. A. Davies, Rapidly Quenched Metals III, Vol. 1, p. 1, 1978.

8. A. J. Kerns, D. E. Polk, R. Ray and B. C. Giessen, Materials Science and Engineering, Vol. 38, p. 49, 1979.

9. B. C. Giessen, N. M. Madhava, R. J. Murphy, R. Ray and J. Surette, Met. Trans., Vol. 8A, p. 364, 1977.

Scripta METALLURGICA Vol. 14, pp. 1061-1065, 1980
Printed in the U.S.A.

ON THE CHARACTERISTICS OF AMORPHOUS U-Fe ALLOYS FORMED BY LIQUID QUENCHING VS. IRRADIATION TECHNIQUES*

R. O. Elliott and D. A. Koss**
University of California
Los Alamos Scientific Laboratory
Los Alamos, New Mexico 87544

and

B. C. Giessen***
Department of Chemistry
Northeastern University
Boston, Massachusetts 02115

(Received June 5, 1980)
(Revised August 5, 1980)

Introduction

Metallic glasses are generally formed by procedures involving either liquid quenching or atomic deposition. However, it is also known that neutron irradiation of certain crystalline alloys will result in a transformation to the amorphous state. The first such report by Bloch was based on the intermetallic compound U_6Fe which became amorphous after an integrated exposure of 2.3×10^{17} fissions/cm^3 (1). In a separate study, Elliott and Giessen have shown that U-Fe alloys can also be melt quenched to form glasses (2). To our knowledge, there have been only two other observations of the formation of amorphous metals by neutron irradiation techniques (3,4), and there is no study which relates an amorphous metal produced by irradiation to that formed by liquid quenching. The purpose of this communication is to report differences in structural and thermal characteristics of amorphous metals based on U_6Fe but which are produced by either irradiation or liquid quenching techniques. For reasons discussed below, only liquid-quenched amorphous metals are referred to as glasses in the following.

Experimental

The U-14.3 at.% Fe master alloy was prepared by arc-melting components 99.9% pure. The uranium used in this study was 93% enriched U^{235}. The liquid quench technique involves a hammer-and-anvil, arc-furnace quenching unit (5) which is capable of quenching rates in the vicinity of 10^5 - 10^6 K/sec. Irradiation was performed in the thermal column at the Omega West Reactor in Los Alamos at flux rates of 3.7 and 1.0×10^{11} n/cm^2/sec to an integrated dose of 4.4×10^{17} fissions/cm^3. In all cases, the specimens consisted of foils ~ .03 mm thick x 3 mm diameter with 2-4 foils being tested at one time. The foils were examined by x-ray diffraction (XRD) with Cu Kα radiation and by differential scanning calorimetry (DSC) in a Perkin-Elmer DSC-2 calorimeter.

*Work performed under auspices of the U. S. Department of Energy

**On sabbatical leave from Michigan Technological University; present address is: Dept. of Metallurgical Engineering, Michigan Technological University, Houghton, MI 49931

***Research supported by the Office of Naval Research and the Army Research Office

0036-9748/80/101061-05$2.00/0

Results

Typical XRD patterns for amorphous U-Fe alloys in terms of interference functions I(K) [$K = 4\pi \sin\theta/\lambda$] are shown in Fig. 1. All of the samples exhibit three rather broad, asymmetric peaks in the range of K values investigated, and all of the samples exhibited peaks at roughly the same value of K, as shown in Table I. However, there are significant differences in the detailed nature of these peaks. The liquid quenched glass consistently exhibits a much more intense first peak which has a significantly smaller half-width than that of the amorphous alloy produced by irradiation (see Table I). A quenched-and-irradiated glass was also investigated; it yields diffraction patterns with peaks of intensity and width which are intermediate between those of the liquid quenched glass and the irradiated amorphous alloys. The irradiated amorphous alloys show more diffracted intensity between the first and second peaks as well as between the second and third peaks than does the liquid quenched glass as can be seen by careful examination of Fig. 1. Thus the interference functions in Fig. 1 indicate that while there is a great deal of similarity in the structure of these amorphous alloys, there are also significant differences in certain aspects of the structure of the U-Fe glass formed by liquid quenching when compared to an amorphous alloy formed by irradiation.

That a difference in structure between irradiated and liquid quenched amorphous metals exists is substantiated by the differential scanning calorimetry (DSC) data obtained upon heating the glasses. Such data is shown in Fig. 2 and indicates several features. Crystallization of the liquid quenched U-Fe glass involved two exothermic effects and thus occurs over a range of temperatures. In contrast, the crystallization process of the irradiated and the quenched/irradiated amorphous glasses is characterized by a single, sharp exotherm occurring at a temperature about 15K higher than the first exotherm of the non-irradiated glasses. The other distinct difference among the glasses involves the total heat of crystallization. For most glasses, this is about 40% of the heat of fusion of the alloy, which would correspond to $\sim$ 18.8 J/gm for the compound U_6Fe.* This value is comparable to 19.7 J/gm observed for the liquid quenched glass in Fig. 2 but is distinctly lower than the 31.8 J/gm observed for the amorphous alloy formed by irradiation. Many tests have reproduced the enhancement of the heat of crystallization of irradiated U-14.3 at.% Fe amorphous alloys. Typically the heat released is in the range of 31.8 to 32.6 J/gm compared to 17.6 to 20.5 J/gm for that of the liquid quenched glass of the same alloys. In all cases the crystallization process resulted in the same XRD patterns which are characteristic of the U_6Fe compound.

Discussion

A detailed accounting of the structural differences resulting in the behavior in Figs. 1 and 2 is beyond the scope of the information presently available. However, certain inferences can be made. In the absence of a study of the radial distribution function of these amorphous metals, the interference functions in Fig. 1 may be used to give an indication of their structural characteristics. Using the position of the first peak K_1, the approximate mean interatomic distances of the first nearest neighbor shell of atoms d_1 can be obtained by use of the Ehrenfest formula (9,10): $d_1 \times K_1 = \kappa$, where $\kappa = 7.90 \pm 0.10$ (10). The values of d_1 for the different glasses are listed in Table I along with the atomic diameter of uranium corrected for a coordination number of twelve (11).

Table I shows that the values of d_1 do not differ greatly among the amorphous alloys and, within the uncertainty of the value of κ, d_1 agrees well with the U - U distances based on the Goldschmidt diameter. The relative positions

*The estimated heat of fusion of the compound U_6Fe (46.9 J/gm) is based on a weighted average of the heats of fusion of pure U (6) and Fe (7) and the entropy of mixing due to the formation of the compound (8).

of the first and second maxima (K_1 and K_2) of the interference function are similar to numbers for amorphous alloys prepared by several different techniques; $K_2/K_1 = 1.68$ in this study vs. $(K_2/K_1)_{Avg.} = 1.75$ for ten different amorphous alloys (see Table 1 of Ref. 11). These calculations confirm the conclusion based qualitatively on Fig. 1 that there is much similarity in the structure of these amorphous alloys as well as others based on significantly different alloys and preparation techniques.

The differences in the amorphous metal structure brought about by fission fragment bombardment are strongly reflected in the resulting loss of intensity and broadening in the first XRD peak in Fig. 1 (see Table 1). Such behavior indicates an increase in structural disorder in the irradiated alloys, which is consistent with the increased energy released on crystallization of the irradiated alloys (Fig. 2). Previous studies have suggested that many amorphous alloys may have very similar structures regardless of preparation (10,12-14). In the present study, the very large differences between the amorphisation processes of liquid quenching versus irradiation results in less short range order in the irradiation-produced glasses.

Irradiation can cause amorphisation of an alloy by the rapid cooling of the thermal spike induced by atomic collisions with fission fragments and the resulting displacement cascades (4,15). We, therefore, conclude that such a combined thermal/atomic displacement process results in an amorphous solid with a structure characterized by a reduced degree of short range order in the irradiation produced amorphous alloy. The resulting "loss of local structure" would account for the decrease in intensity and broadening of the diffraction peaks. It would also be consistent with the increased and well-defined exothermic peak in the DSC data if, as appears quite possible, the resulting structure of the irradiated amorphous alloy requires a greater amount of atomic rearrangement upon crystallization to U_6Fe, where this rearrangement proceeds only at a higher temperature than in the irradiated glass, but in a one-step, coordinated manner. It should be noted that this does not imply that the irradiated amorphous alloy is more like a liquid than the liquid-quenched glass. On the contrary, the irradiated amorphous alloy is quite probably not a glass in the sense of the definition that the internal structure of a glass is closely related to that of a corresponding supercooled liquid which precedes it in its formation; instead, it is a different amorphous solid requiring further structural characterization for a description.

Modeling the atomic displacement cascade caused by the neutron irradiation as a thermal spike, Kramer, Johnson, and Cline calculate the "effective quench rate" of the cascade region in a metallic glass irradiated by fast neutrons to be $\sim 10^{14} - 10^{15}$ K/sec (15). Although the present experimental conditions differ somewhat, it is certain that the "effective quench rate" induced by neutron irradiation was much greater than $10^5 - 10^6$ K/sec which was used to produce the liquid quenched glass. The differences in short range order which are observed between the irradiated amorphous solid and the liquid quenched glass thus are not surprising; the "structural relaxation" or "atomic regrouping" which takes place in liquid quenched metallic glasses upon aging short times at temperatures somewhat lower than the crystallization or glass transition temperature (16,17) could not occur at the rapid quench rates.

The work by Bloch (1), Bethune (3), Lesuer (4) and this study raise the question as to which particular crystalline alloys, especially intermetallics, are susceptible to amorphisation by fission fragment irradiation. At this time the evidence is insufficient to classify the intermetallics accordingly; however, it is likely that the intermetallics which form glasses readily by liquid quenching (18) are also prone to forming amorphous solids by fission fragment bombardment. The present compound U_6Fe belongs to a group of actinide phases which readily form glasses upon liquid quenching (18); f-electron bonding may be responsible for its ready amorphisation (19).

This study also raises the question of irradiation "damage" to a glassy

alloy. There is some evidence to suggest that structured changes of amorphous alloys can occur upon irradiation (15,20-22) although the opposite conclusion has also been drawn (4). The results on the U-Fe alloys show that if a fissionable glassy alloy is exposed to irradiation, then there will be identifiable changes in the resulting atomic structures and thermal properties. Whether such structural differences result in significant changes of other properties remains to be demonstrated.

Summary

Amorphous alloys based on a U-14.3 at.% Fe alloy have been prepared by a liquid quenching and/or irradiation technique. The resulting amorphous alloys, as characterized by x-ray diffraction and differential scanning calorimetry data, are similar but not identical. When compared to the liquid-quenched glass, the irradiated material shows a less intense, broader first peak in the interference function data and a larger, narrower exothermic peak upon crystallization. We conclude that the much higher "effective quench rates" inherent in fission fragment bombardment can produce an amorphous metal with a structure characterized by a reduced degree of short range order when compared to a liquid-quenched glass. The irradiated amorphous alloy is probably not a glass in the sense that the structure of a glass is closely related to that of the supercooled liquid which preceded it in its formation; it is more like a different amorphous solid requiring further structural characterization for a description. These results also indicate that the structure of liquid quenched glasses will be affected by subsequent fission fragment irradiation.

Acknowledgements

The authors would like to thank R. N. R. Mulford, D. E. Peterson, and M. E. Bunker for their technical assistance and stimulating discussions. One of the authors, D. A. Koss, would like to acknowledge the support of the National Science Foundation through a Science Faculty Professional Development Grant in support of his sabbatical leave activities at Los Alamos Scientific Laboratory.

References

1. J. Bloch, J. Nucl. Mat'l. 6, 203 (1962).
2. B. C. Giessen and R. O. Elliott, in "Rapidly Quenched Metals III," Vol. 1, p. 406, The Institute of Metals, London (1978).
3. B. Bethune, J. Nucl. Mat'l. 30, 197 (1969).
4. D. Lesuer, Fizika 2 Suppl. 2, 13.1 (1970).
5. M. Fischer, D. E. Polk, and B. C. Giessen in Proc. Conf. Rapid Solidification Processing, Claitor's Publ. Div., Baton Rouge, LA, p. 140 (1978).
6. H. P. Stevens, High Temp. Sci. 6, 156 (1974).
7. L. S. Darken and R. P. Smith, Ind. Eng. Chem. 43, 1815 (1951).
8. O. Kubaschewski, E. L. Evans, and C. B. Alcock, "Metallurgical Thermochemistry," p. 212, Pergamon Press, New York (1967).
9. A. K. Sinha and P. Duwez, J. Phys. Chem. Solids 32, 267 (1971).
10. B. C. Giessen and C. N. J. Wagner, in Physics and Chemistry of Liquid Metals, p. 666, Marcel Dekker, New York (1972).
11. W. B. Pearson, "The Crystal Chemistry and Physics of Metals and Alloys," Wiley-Interscience, New York, NY, p. 151 (1972).
12. C. N. J. Wagner, Vac. Sci. Technol. 6, 650 (1969).
13. G. S. Cargill, J. Appl. Phys. 41, 12 (1970).
14. D. G. Walker, J. Nucl. Mat'l. 37, 48 (1970).
15. E. A. Kramer, W. L. Johnson and C. Cline, Appl. Phys. Lett. 35, 817 (1979).
16. H. S. Chen and E. Coleman, Appl. Phys. Lett. 28, 245 (1976).
17. R. L. Freed and J. B. Vander Sande, J. Non-Cryst. Solids 27, 9 (1978).
18. B. C. Giessen and D. E. Polk, in "Theory of Alloy Formation," L. H. Bennett, Ed., The Met. Soc. - AIME (1980), in print.
19. R. O. Elliott and B. C. Giessen, to be published.
20. B. T. Chang and J. C. M. Li, Scripta Met. 11, 933 (1977).
21. K. Doi, H. Kayano and T. Masumoto, Appl. Phys. Lett. 31, 421 (1977).
22. R. Yamamoto, H. Shibuta and M. Doyama, J. Nucl. Mat'l. 85, 603 (1979).

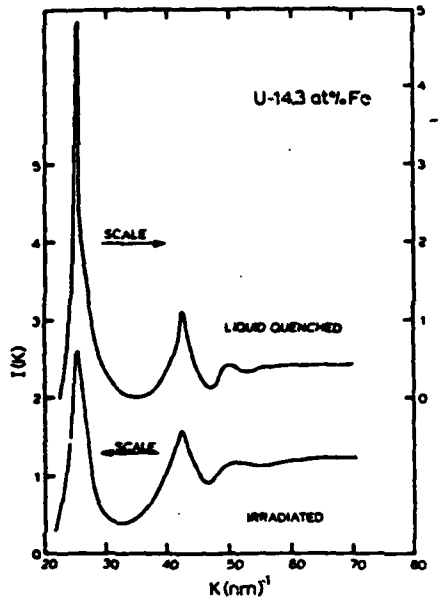

Fig. 1. Diffraction patterns [in terms of interference functions I (K)] of an amorphous U-14.3 at.% as formed by liquid quench and/or irradiation techniques.

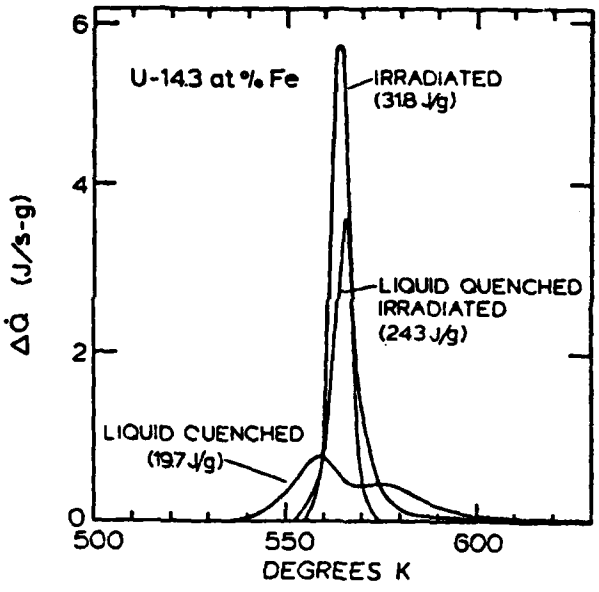

Fig. 2. Rate of energy release as a function of temperature for U-14.3 at.% Fe metallic glasses formed by liquid quench and/or irradiation techniques. Heating rate is 80 K/min.

TABLE I

Data on Peak Position of I(K) and Interatomic Distance on the U-14.3 Fe-Amorphous Alloy

Condition	Peak height† Width $(nm)^{-1}$	Positions of K_1 in nm^{-1} of peak maxima of I(K) K_1	K_2	K_2/K_1	Nearest neighbor distance* d_1 in nm	Goldschmidt Diameter nm for U
Liquid Quenched	48/1.0	25.1	42.5	1.69	0.315	0.310
Irradiated	26/2.5	25.4	42.7	1.68	0.311	0.310

†Peak height is relative unites as measured from I(K) = 0 in Fig. 1; peak width is at half height.

*Calculated using the Ehrenfest formula; see text.

JOURNAL DE PHYSIQUE Colloque C8, supplément au n°8, Tome 41, août 1980, page C8-95

ELABORATION OF AMORPHOUS METALS AND GLASS TRANSITION.

FORMATION AND CHARACTERIZATION OF AMORPHOUS METALS

B.C. Giessen and S. Whang

Materials Science Division, Institute of Chemical Analysis, Northeastern University, Boston, Massachusetts 02115, U.S.A.

ABSTRACT

This review deals with the definition of amorphous and glassy metals; the principal methods for their preparation by atom-by-atom deposition, rapid liquid quenching and particle bombardment; criteria for their formation, especially ready glass formation (RGF) and its alloy chemical foundations; and their classification. This is followed by a discussion of their elastic and plastic properties (Young's modulus and microhardness) and thermal stability (glass transition and crystallization temperatures), with emphasis on the correlation and composition dependence of these properties and without special reference to technically important glassy alloys.

INTRODUCTION

Glassy metals[1] are presently the subject of intense fundamental and applied studies. The former now cover virtually all physical phenomena displayed by crystalline solids, including their structure, electronic properties, strength, etc., as well as properties specific to the glassy state, such as glass formation, glass-liquid transition, structure modelling, and thermal stability. Application-oriented work has been stimulated primarily by technically interesting properties such as their magnetic softness combined with high permeability, their outstanding corrosion resistance properties and their high specific mechanical strength.

DEFINITION OF AMORPHOUS AND GLASSY METALS

To define the glassy state, we turn to Fig. 1 (after Ref. 2) which shows the change of a property such as the volume or heat content with temperature. When a liquid is supercooled (in constrained equilibrium) below the equilibrium melting point T_m, the viscosity η and with it the relaxation time τ increases until at a certain temperature, designated the (fictive) glass transition temperature T_g, the time available at temperature T_g becomes smaller than the relaxation time τ (T_g) and the alloy leaves internal equilibrium, changing at this temperature from a *supercooled liquid* to a *glass*. Upon subsequent reheating of the glass beyond T_g the regime of the supercooled liquid state is entered again, (unless crystallization intervenes before T_g is reached). In addition, relaxation processes generally occur before T_g which alter the glass and lower its glass transition temperature; T_g is thus a function of the quenching and heating history of the glass.

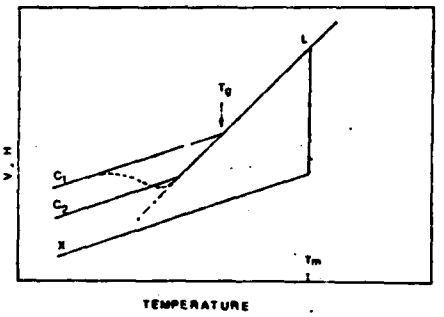

Figure 1

Metallic glasses are amorphous solids;[2,3] however, the latter term has wider meaning and includes also noncrystalline materials whose internal configurations do not correspond to those of any supercooled liquid. As an example we mention amorphous alloys produced by irradiation methods[4] (either from the crystalline state or a liquid quenched glass); they lack the high degree of short-range order typically present in liquid quenched glassy metals. Such amorphous solids should not be designated as glassy according to the present usage of this term. It should be apparent from the above discussion that formation of an amorphous material requires either bypassing of the crystallization process (e.g. by atomic deposition or rapid liquid quenching) or,

alternately, destruction of the crystallinity of a solid (by methods such as particle bombardment). Experimental approaches designed to accomplish this are reviewed in the next section.

PREPARATION METHODS

Amorphous metals can be prepared by a variety of methods[5,6] which can be divided into three main categories according to their main principle: atom-by-atom deposition; rapid liquid quenching; particle bombardment methods. (Probably some of the techniques based on the third principle actually also involve rapid liquid quenching as the active mechanism.) Operationally, the preparation methods based on these principles can be classified further as shown in Table 1. Due to space limitations, these methods cannot be described here in detail; instead, some salient aspects of their operation are reviewed briefly.

Table I

PREPARATION METHODS FOR AMORPHOUS METALS

I. Atom-by-Atom Deposition:
- A. From the Gas Phase:
  - 1) Vapor Deposition;
  - 2) Sputtering.
- B. From Liquid Solutions:
  - 1) Electrodeposition;
  - 2) Electroless Deposition.

II. Rapid Liquid Quenching:
- A. Continuous Flow Methods:
  - 1) Melt Spinning,
  - 2) Melt Drag, Melt Extraction,
  - 3) Dual Roller Quenching.
- B. Melt Droplet Methods:
  - 1) Powder Spraying,
  - 2) Electrohydrodynamic Droplet Extraction;
  - 3) Glazing:
    - a) "LASER GLAZING" by Laser Beam;
    - b) Layer Quenching by Electron Beam.

III. Particle Bombardment Methods:
- A. Neutron and Ion Bombardment Irradiation:
  - 1) Neutron Irradiation Leading to ~ Particle Self-Bombardment;
  - 2) Neutron Irradiation Leading to Fission Fragment Self-Bombardment,
  - 3) Fission Fragment Bombardment.
- B. Ion Implantation:
  - 1) Implantation of Glass Forming Elements;
  - 2) Melt Mixing (Short Ion Beam Bombardment).

Atom-by-atom methods are probably the most powerful ones for producing amorphous metals. By techniques such as vapor deposition or sputtering, alloys with which do not form glasses by any other method have been obtained in the amorphous state, such as alloys with compositions corresponding to high melting intermetallic phases. Further, thick samples usable for bulk processes can be obtained, e.g., by sputtering. On the other hand, the process is expensive and alloys produced by it are generally not ductile. Some liquid quenching methods, especially continuous melt flow methods such as melt spinning, have been engineered to industrial maturity[7,8] and are capable of producing technologically important alloys as rapidly quenched glasses relatively cheaply and in large amounts; with the product having the thin sheet shape desirable for some applications such as magnetic sheets for use in transformers[9] or as brazing foils.[5]

Other liquid quenching methods such as those based on surface heating (glazing) and ion bombardment or implantation offer promise for the production of glassy metal surfaces showing desirable corrosion or wear resistance; ion implantation[10] is presently much studied as a means of producing surface property improvements and it was found recently that the alloys formed from a base material by this technique become amorphous when certain critical alloying compositions are reached.

GLASS FORMATION

The following discussion is directed primarily at glass formation from a liquid.

Fundamental Parameters Determining Ready Glass Formation (RGF): Upon supercooling a liquid below its liquidus temperature T_m, a glass will form at the glass transition temperature T_g if crystallization of the melt into one or more crystalline phases is avoided in the interval from T_m to T_g.[3,11] Operationally, the important parameter is thus $(T_m - T_g)/T_m$, i.e. the temperature interval $T_m - T_g$, normalized by the melting temperature T_m. This parameter is a function of the reduced glass temperature $T_{gr} = T_g/T_m$ which thus plays a fundamental role in characterizing the glass forming ability of an alloy which scales with T_{gr}.

Assuming that homogeneous nucleation is the mode of crystallization of the liquid and using pertinent expressions for the rates of nucleation and growth as functions of supercooling, the critical cooling rate leading to crystallization of, e.g., <5% of the liquid can be calculated and T-T-T curves such as those shown e.g. in Fig. 2 of Ref. 2 can be obtained, with T_{gr} as the sole parameter. To retain a glass, the cooling process must be conducted such that the "nose" of the pertinent T-T-T curve is avoided. Calculations[12] using such diagrams show that the critical cooling rate R_c increases with decreasing T_{gr}, as shown in Fig. 3 of Ref. 13. One often defines as "readily glass forming" such alloys for which $R_c \lesssim 10^5$ K/sec corresponding to $T_{gr} \gtrsim 0.60$. In binary alloys, T_g varies monotonically and slowly with composition x over wide ranges of

X; in its variation with X, T_{gr} therefore depends more strongly on T_m (which shows much larger changes with composition) than on T_g; the RGF composition ranges are therefore primarily defined by T_m. Zr-Cu is shown in Fig. 2 as a typical binary system with a wide RGF composition range.[15]

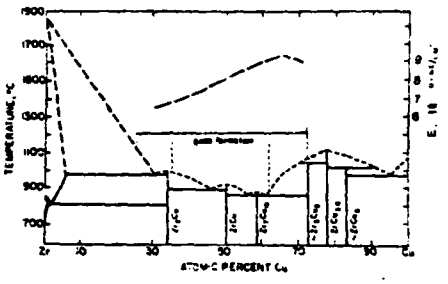

Figure 2

Ab Initio Calculations of Glass Forming Ability: Knowledge of the liquidus lines (i.e. features of the equilibrium phase diagram) and the glass transition temperatures thus suffice to determine the RGF properties of an alloy; generally these quantities must be obtained experimentally and are not easy to predict. However, recently considerable progress has been made[16] in obtaining the energetics of liquid alloys of simple metals from first principles; in connection with calculations of the energies of the crystalline phases involved, this allows construction of the phase diagram, and hence derivation of T_m, the principal quantity controlling the variation of T_{gr} with X. Theoretical calculations of T_g do not yet exist; however, T_g could be derived e.g. from claculations of the viscosity η as a function of temperature[17] (using the fact that T_g can be defined at the temperature at which $\eta \sim 10^{13}$P), yielding T_{gr} and hence R_c. It is therefore likely that in the near future theoretical ab initio calculations of R_c for binary alloys will be made and that the degree of glass forming ability of known glass forming alloys can then be confirmed and subsequently predicted for other, new compositions.

Operational Parameters Relating RGF Ability: As such calculations are not yet available, a number of operational parameters or alloy properties have been used for the prediction of RGF ability.[3] The more important known parameters determining RGF ability are listed in Table 2 of Ref. 3. Some of these characteristics (such as the melting point and the type of intermetallics present) are phase diagram features requiring knowledge of the phase diagram or its ab initio calculation by a hypothetical, systematic program involving the calculation and comparison of the structural energies of all possible intermetallic phases for all compositions.

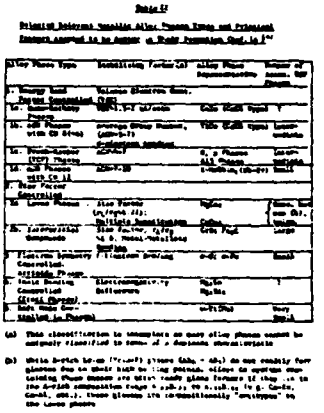

Pertinent characteristics not requiring knowledge or claculation of the phase diagram include (a) the size ratio r/R of the components, which is <0.85 for most RGF alloys and (b) the heat of formation ΔH_M of the liquids, which is $\lesssim$-10 Kcal/mole for most RGF alloys and can be obtained experimentally or theoretically by semiempirical approaches such as that of Miedema who utilizes the electronegativities and electron concentrations of the constituent elements to obtain ΔH_M.

RGF Maps: Used singly, neither r/R nor ΔH_M suffices to predict RGF ability. Together, however, they have been found to provide a useful criterium. Ready-glass-formation plots (RGF maps) can be constructed[18] which show that binary elemental combinations with size ratios r/R $\lesssim$0.85 and $\Delta H_M \lesssim$-10Kcal/mole generally possess RGF ability. As an example, a partial RGF map for Ni is given in Fig. 3; it shows good division between elements readily forming glasses with Ni and those that do not. It should be noted that these maps do not indicate the position and extent of the RGF composition range which is determined by the phase diagram features such as low liquidus temperatures and competing stable intermetallic phases.

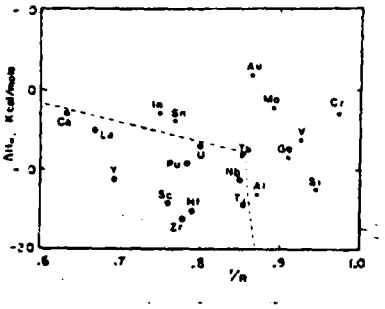

Figure 3

Structural Alloy Chemcial Approach: A different, alloy chemical approach to the prediction of RGF for binary alloys is based on the type of intermetallics occurring in the system.[14,16] In this approach the glass is considered somewhat like a (noncrystalline) alloy phase; in the same way in which the equilibrium alloy phase in homologous systems are often identical or structurally related Hume-Rothery phases, Laves phases, or related tetrahedrally-close-packed phases, interstitial phases, etc. the glass may be correlated with crystalline alloy phases by structure (based e.g. on similar short-range order or coordination number) or electronic considerations. Table 2 gives a listing of alloy phases that have been found to be connected with RGF in binary systems.[14] Generally these phases have compositions lying in or near the RGF composition range; however, if Laves-Friauf phases of composition AB_2 or related phases exist in an RGF system the glass tends to occur in the "opposite" region of the diagram where the larger element A is the majority component.[14,16,19] Presnece of both an RGF glass and a Laves phase in the same system is so frequent that one migh designate these glasses in view of their composition as "anti" -Laves phases.[19]

In the context of considering the glass as an alloy phase, Turnbull's concept[11] is of interest according to which there may be a number of alloy compositions for which the glass (formed by infinitely slow cooling) is the single phase with the lowest free energy compared to all possible isostoichiometric crystalline single phases; it is thus the single phase ground state for this composition. (Among organic glasses, there is at least one documented instance for which $T_g > T_m$, i.e., where the glass forms upon cooling at a temperature above T_m and where the glass transition thus is an equilibrium reaction rather than a constrained equilibrium reaction.)[20] It is not known whether this glass can also be prepared from the terminal crystalline phases as the product of a solid-state reaction between them.

CLASSIFICATION

Glassy metals can be classified on the basis of their constituents. In the light of the preceding discussion of formation, especially the RGF maps, it is clear that ready glass formation is not possible if the constituent elements are alloy chemically too similar; for RGF to occur they must differ in size by $\gtrsim$15% combined with a negative heat of mixing of $\gtrsim$-10 Kcal/mole (due to electron concentration and electronegativity difference).[21] On the other hand, there are probably also upper limits to the size difference and negative heat of mixing which are consonant with RGF; this point has not yet been established.

A brief listing of major and minor families of readily glass forming alloy combinations is given in Table 3 (after Ref. 3).

Table III. Readily Glass Forming Alloy Systems Based on Chemical Classification of Constituents (Ref. 3)

Group	Representative Systems
Major Systems	
T^2 (or noble) metal + metalloid (A)	Pd-Si, Co-P, Fe-P-C, Ni-P-B
T^1 metal + T^2 metal (or Cu)	Zr-Cu, Ti-Ni, Nb-Ni
A metal + B metal	Ca-Al, Mg-Zn
Lanthanide + T^2 or B metal	La-Ni, Ce-Al
Actinide + T^2 metal	U-Fe, Pu-Ni
Miscellaneous Systems	
T^1 metal + A metal	(Ti-Zr)-Be
Actinide + T^1 metal	U-Cr
A metal + T^2 metal	Ca-Ni, Ca-Pd

A metal = Li, Mg groups; T^1 metal = early transition metal (Sc, Ti, Y groups); T^2 metal = late transition metal (Mn, Fe, Co, Ni groups); B metal = Cu, Zn, Al groups; metalloid = B, C, Si, Ge, P

AD-A138 296 METASTABLE TRANSITION METAL ALLOYS PRODUCED BY RAPID QUENCHING: STRUCTURE..(U) NORTHEASTERN UNIV BOSTON MA BARNETT INST OF CHEMICAL ANALYSIS.. B C GIESSEN JAN 84 2/2

UNCLASSIFIED N00014-76-C-0820 F/G 11/2 NL

END
DATE FILMED
3 84
DTIC

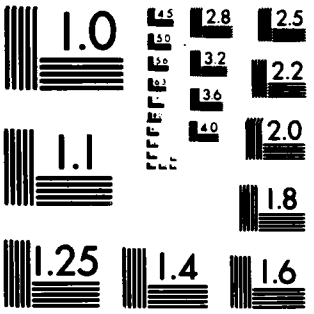

MECHANICAL PROPERTIES

In this survey, we have space only to discuss two sets of properties: elasticity, represented by the Young's modulus E, and plasticity, represented by the Vicker's microhardness H_v. We survey the correlation of these properties with each other and their variation with composition for some representative glassy alloy systems.

Elasticity: The Young's moduli E of many metallic glasses have been accurately determined using dynamic methods such as the pulse echo technique which is suitable for melt-spun ribbons of >10 cm length or the impulse-induced resonance technique appropriate for short samples of ~1 cm length such as those typically obtained by arc-furnace hammer-and-anvil quenching.[22] Typically, the compositional variations of E across metal-metal and metal-metalloid binaries A-B show approximately linear increases of E with increasing alloying element content X_B over a broad range of X_B. As an example, E for Zr-Cu glasses is shown schematically in Fig. 2.[15] In metal-metal glass systems with a sufficiently broad glassy composition range, a maximum of E is often found,[23] generally at a composition rich in the smaller component B, as seen also in the plot of Zr-Cu. The occurrence of a sharp maximum of E and its near-linear change with composition over a wide range of X_B are features not expected from simple quasichemical theories of elastic property variation. Correlations of the position of E_{max} with alloy chemical features of the equilibrium phase diagram have been noted.[23]

The Young's moduli of elemental metallic glasses have been predicted to be 20-30% lower than the values of the corresponding crystalline elements by calculations of the corresponding Debye frequencies;[24,25] however, at present few experimental data are available for comparisons of glasses and crystals. For elements the "crystalline" E values are known but elemental glasses are hard to prepare and measure; for alloys where E has been measured for the glasses, the values for the corresponding crystalline phases are not yet known. Preliminary data[26] show that the changes of E for the crystalline phases across the Zr-Cu diagram roughly follow those for the corresponding glasses.

Plasticity: Due to the absence of work hardening in glassy metals, they fail shortly after the onset of plastic deformation in tension; accordingly, tension stress-strain measurements cannot be used as an indicator of plastic strength. In compression, however, high strength values as measured, e.g., by the Vicker's microhardness H_v can be realized; this strength measure is therefore widely used. H_v has been shown to have a remarkably consistent correlation with the elasticity as measured by the Young's modulus E. For many metalloid-free metal-metal glasses varying over a wide range of strength values from soft glasses such as Ca-Zn[27] to high strength glasses such as Ta-Ir[22] there is a linear correlation between H_v and E,[28] implying that for all of these glasses, regardless of the nature of their interatomic interactions, size ratio, etc., the yield strain ε_y is approximately constant, according to the relation

$$\varepsilon_y = \sigma_y/E \propto H_v/E.$$

This result differs drastically from the situation for crystalline alloys, for which the theoretical yield strain is rarely reached due to dislocation movements; it implies that metallic glasses, due to the apparent absence of analogous defects promoting plastic deformation, "live up to" their full elastic strength potential more than crystalline materials.

It may be noted that for metalloid containing glassy metals a somewhat different H_v vs. E curve exists, with a narrow band of values corresponding to somewhat differing ε_y values; Chen[29,30] has suggested that ε_y depends on the differing Poisson ratios ν of these glasses.

Thermal Stability: Thermal effects of interest include, with increasing temperature, relaxation processes, the glass transition temperature (where observable), the crystallization temperature(s) and further transformation temperature(s). We do not address the relaxation effects here.

Glass Transition Temperature T_g: T_g is generally regarded as the most fundamental measure of thermal glass stability since the two structural entities involved in the glass transition,

i.e., the glass and the super-cooled liquid, are very similar in their atomic arrangements and many electronic properties (unlike the phases involved in a glass → crystal transition), differing drastically in viscosity, specific heat, and associated properties. A model for the glass transition can be given in terms of the free volume theory in which the glass transition involves a cooperative rearrangeability of the free volume V_f.[11]

For an elemental glass of atomic mass M is is therefore reasonable to model the glass transition process in analogy to the model for the melting process used in the derivation of the Lindemann expression [31] for the melting point T_m

$$kT_m \propto MV^{2/3}\theta_{D,cr}^2 \propto MV^{2/3}E_{cr}$$

where $\theta_{D,cr}$ is the Debye temperature of the crystal and E_{cr} is its Young's modulus and V is the atomic volumes. This leads to [32]

$$kT_g \propto MV^{2/3}\theta_{D,g}^2 \propto MV^{2/3}E_g$$

One expects that this relationship between T_g and E should be followed even more closely than the corresponding Lindemann relation for the melting point because of the much closer similarity between glass and liquid than between liquid and crystal.[32] Assuming the Lindemann relation to be valid, one would expect

$$T_g = \frac{E_g}{E_{cr}} \cdot T_m$$

Unfortunately, these relationships for T_g cannot be tested directly because elemental glasses always crystallize far below their glass transition. Measured T_g values for glassy metal all refer to alloys rather than elements; unfortunately, as discussed above, for these compositions the relevant property values of the crystalline phases such as E_{cr} or $\theta_{D,cr}$ are not yet available. In any case the Lindemann formula cannot be expected to hold for ordered intermetallics because the implified model for melting assumed for it may not agree with the melting mechanism for an ordered phase. Rather than attempting to make comparisons of the thermal properties of glasses with those of the crystalline phases at this time, we examine the relation between the thermal and elastic properties for glassy alloys. For the Zr-Cu system,[15] e.g., T_g and E_g are proportional to composition over a wide composition range, with the relationship

$$T_g = a \cdot E_g + b$$

over the linear range of values.[15] While a formula of this type can be understood readily in terms of the viscosity at T_g and its temperature dependence,[33] this expression obviously cannot hold for small values of E_g.

Crystallization Temperatures: The exothermic processes associated with equilibration may involve phase separation of a glass into two glasses, phase separation into a glass and a crystalline phase or crystallization into one or more phases; ordering reactions and recrystallization also occur. These complicated processes involving nucleation, growth and other phenomena cannot be readily and solely associated with the elastic properties of the glassy alloys and any observed empirical correlations of the crystallization temperature with E_g, etc. could therefore be considered as coincidental; nonetheless, correlations involving T_c are frequently made[34,35] in the absence of observable glass transitions. Probably the most important precaution necessary in evaluating T_c as a measure of thermal stability is to exclude "easy" crystallization processes from consideration such as those frequently taking place at the end of the glass forming range at low alloying element contents. An example of this situation is shown in Fig. 4 for the Ca-Al system,[19] where elemental Ca crystallizes "easily" at low Al contents of 15-20 at.pct. Al, while above ~30 at.pct. Al the "intrinsic" stability of the glass with respect to crystallization dominates the process. In comparing glass stability as measured by T_c for different systems, only glasses with high alloying content should therefore be considered and, secondly, only similar compositions can be compared meaningfully. If such precautions are taken, and identical, high-alloy-composition glasses are compared for chemically related systems, remarkably consistent correlations between T_c and E, as well as between T_c and the equilibrium melting points T_m of the crystalline phases are sometimes observed, as demonstrated for a series of T_5-T_9 glasses [34] (T_5 = Nb, Ta, T_9 = Rh, Ir) as shown in Fig. 5. Wang[36] has attempted to correlate glass stability with the structural complexity of the corresponding

alloy phases.

On the basis of these observations it is apparent that, at least in first order ealstic, plastic, and thermal stabilities of glasses scale together; in some cases, in addition, they are related to the corresponding properties of the crystalline equilibrium alloys.

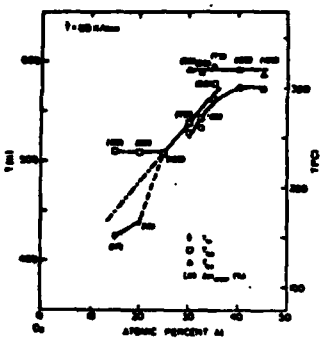

Fig. 4: Thermal effects observed on heating Co-Al glasses at 80 K/min.

Figure 4

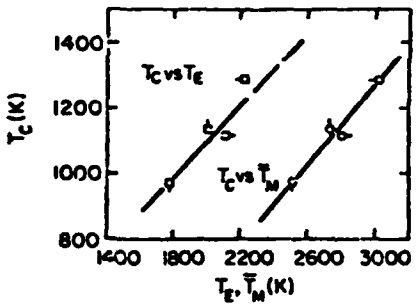

Figure 5

ACKNOWLEDGEMENT

Research at Northeastern University reviewed in this paper was funded by the U.S. National Science Foundation, Office of Naval Research and Army Research Office; we thank these agencies for their support.

REFERENCES

1. J.J. Gilman and J.H. Leamy, Eds., Metallic Glasses, American Society for Metals, Metals Park, (1978).
2. H.S. Chen, K.A. Jackson, in Metallic Glasses, ASM (1978).
3. D.E. Polk and B.C. Giessen, in Metallic Glasses, ASM (1978).
4. R.O. Elliott, D.A. Koss and B.C. Giessen, Formation of U-Fe Alloy Glasses: Liquid Quenching vs. Irradiation Techniques, Met. Trans., to be submitted.
5. R. Mehrabian, B.H. Kear and M. Cohen, Eds., Proceedings of a Conference on Rapid Solidification Processing (1977).
6. S. Kavesh, in Metallic Glasses, ASM (1978).
7. M. Cohen, B.H. Kear and R. Mehrabian, Eds., Proceedings of the Second International Conference on Rapid Solidification Processing, Reston, VA, (1980) in print.
8. D. Narasimhari, U.S. Patent 4,142,571 (1979).
9. C.D. Graham, Jr. and T. Egami, in Annual Review of Materials Science, 8, 423 (1978).
10. Abstract in Materials Research Society Meeting, Boston, MA, Nov. 1979.
11. D. Turnbull, Liquid Metals and Solidification, ASM, (1957).
12. H.A. Davies, in Proceedings of the Third International Conference on Rapidly Quenched Metals,B. Cantor Ed., 1, 1 (1978).
13. R.W. Cahn, Contemp. Phys., 21, 43 (1980).
14. B.C. Giessen and D.E. Polk, in Theory of Alloy Formation; Proc. of Symposium, New Orleans, LA AIME Meeting, Feb. 1979 , L.H. Bennett, Ed., The Met. Soc. AIME (1980), in print.
15. L.T. Kabacoff, R.Raman, S.H. Whang, D.E. Polk and B.C. Giessen, Thermal and Mechanical Behavior of Zr-Cu Metallic Glasses, to be published.
16. J. Hafner, Phys. Rev., B21, 406 (1980).
17. F. Spaepen and D. Turnbull, in Second International Conference on Rapidly Quenched Metals, N.J. Grant and B.C. Giessen, Ed. 205 (1976).
18. B.C. Giessen, to be published.
19. R. St. Amand and B.C. Giessen, Scripta Met., 12, 1021 (1978).
20. K.M. Ralls, T.H. Courtney and J. Wulff, in An Introduction to Materials Science and Engineering, 398, (1976).
21. A.R. Miedema, F.R. DeBoer and R. Boom, CALPHAD., 1, 341 (1977).
22. S.H. Whang, L.T. Kabacoff, D.E. Polk and B.C. Giessen, Met. Trans. A, 10A, 1789 (1979).
23. S.H. Whang and B.C .Giessen, Maximum Values of the Thermal Stability and Mechanical Properties of Binary Alloy Glasses as Functions of Composition Met. Trans., to be submitted.

24. D. Weaire, M.F. Ashby, J. Logan and M.J. Weins, Acta Met, 19, 779 (1979).
25. F. Cyrot-Lackmann, in Fourth International Conference on Liquid and Amorphous Metals, Grenoble, France (1980).
26. E. Wang, S. Whang and B.C. Giessen, Elastic and Plastic Properties of Intermetallic Compounds in Zr-Cu and Zr-Ni Systems, Met Trans A, to be submitted.
27. J.S. Hong, Ph.D. Thesis, Northeastern University, Boston, MA, (1979).
28. S. Whang, D.E. Polk and B.C. Giessen, A Correlation of Young's Modulus and Microhardness in Metallic Glasses, J. Appl. Phys. to be submitted.
29. H.S. Chen, J. Appl. Phys., 49. 462 (1978).
30. H.S. Chen, Rep. Prog. Phys., 43, 353 (1980).
31. F.A. Lindemann, Physik. Z., 11, 609 (1910).
32. B.C. Giessen, J. Hong, L. Kabacoff, D.E. Polk, R. Raman and R. St. Amand, Rapidly Quenched Metals III, B. Cantor, ed., The Metals Society, London, 1, 249 (1978).
33. B.C. Giessen and F. Spaepen, to be published.
34. S. Davis, M. Fischer, B.C. Giessen and D.E. Polk, R.Q.M. III, B. Cantor, ed, The Metals Society, London, 2, 425 (1978).
35. K.H.J. Buschow, Fourth International Conference on Liquid and Amorphous Metals, Grenoble, France (1980).
36. R. Wang, Proc. of Symposium, New Orleans, LA AIME Meeting, Feb. 1979, L.H. Bennett, ed., in print.

THE THERMOELECTRIC POWER OF THE METALLIC GLASS $Ca_{0.8}Al_{0.2}$

J.P. CARINI, Soumen BASAK and S.R. NAGEL
The James Franck Institute and The Department of Physics, The University of Chicago, Chicago, IL 60637, USA

B.C. GIESSEN and Ching-Long TSAI
Department of Chemistry, Northeastern University, Boston, MA 02115, USA

Received 14 November 1980

We report the first measurement of the thermoelectric power Q, of a metallic glass that contains only normal metals. The thermoelectric power of amorphous $Ca_{0.8}Al_{0.2}$ has been measured as a function of temperature from 10 K to 420 K. It is found that Q is positive, varies linearly with temperature and has a small slope. This is similar to the thermoelectric power found for other metallic glasses containing large concentrations of transition metal atoms.

In order to understand the unusual electronic transport behavior that appears in metallic glasses, a number of investigators have focused their attention on the thermoelectric power, Q, in these materials [1–8]. The thermoelectric power in metals is very sensitive to the mechanism for the scattering of conduction electrons so that a knowledge of this quantity can help to decide which scattering processes are relevant in the metals. In the nonmagnetic metallic glasses the measurements of Q have shown very simple behavior: over a large range of temperature (up to the crystallization temperature) Q varies approximately linearly with temperature. There also seems to be a correlation in these nonmagnetic alloys indicating that when the temperature coefficient of resistivity, $\alpha \equiv (1/\rho)\,\partial\rho/\partial T$ (where ρ is the resistivity), is negative the thermoelectric power tends to be positive. This behavior can be explained most simply in terms of the extended Ziman theory [9] for the resistivity of amorphous metals. It has been shown [4] that for the Ziman theory the thermoelectric power is

$$\frac{\pi^2 k_B^2}{3|e|E_F}\,T\left[3-2P-\tfrac{1}{2}r\right],$$

where E_F is the Fermi energy, e is the charge of the electron, r contains the energy dependence of the potential and

$$P \equiv \frac{S(2k_F)\,|v(2k_F)|^2}{\int_0^{2k_F} S(k)\,|v(k)|^2\,4(2k_F)^{-4}\,k^3\,dk}.$$

Here $S(k)$ is the structure factor and $v(k)$ is the pseudopotential. If $2k_F$ lies near k_p (which is the position of the first large peak in the structure factor) then P can become much larger than 1 and Q can change sign and become positive. The condition that $2k_F \approx k_p$ is also the criterion in the Ziman theory for a negative value of α. If $2k_F$ is far from k_p then Q should be negative as is expected for a normal metal. In a binary alloy these expressions become more complicated and one must rewrite them in terms of the partial structure factors. In this case one would expect to find a positive Q and negative α when $2k_F$ lies near the peak of any one of the partial structure factors.

One problem with the measurements that have been performed until now is that the glasses studied all contain a high concentration of transition metal elements. The pseudopotential that appears in eq. (2) must be replaced [10] by the appropriate t-matrix since one is definitely in the strong scattering regime. In this case there is some question whether the Ziman theory should still be applicable [11].

In this paper we report the first measurement of

Proc. 4th Int. Conf. on Rapidly Quenched Metals (Sendai, 1981)

HARDNESS vs. YOUNG'S MODULUS OF METALLIC GLASSES

S.H. Whang, D.E. Polk* and B.C. Giessen

Materials Science Division, Institute of Chemical Analysis, Northeastern University, Boston, MA 0211

INTRODUCTION

It had previously been demonstrated that there is an approximate correlation between the Young's modulus E and the Vickers microhardness H of metallic glasses (1). Further, it was noted (1) that in a plot of H vs. E, the metal-metal (M-M) glasses of intermediate hardness appeared to fall onto a curve distinct from that defined by the metal-metalloid (M-X) glasses; for a given hardness the M-M glass had a lower E. The yield stress σ_y of metallic glasses (and, since they are essentially elastic-plastic, the tensile strength) has been found to scale with the hardness, i.e. σ_y=H/3.1 (2), so that the maximum tensile elastic strain is given by ε_y=H/3.1 E. Because the curve relating H to E for the M-X glasses in Ref. 1 is not a straight line passing through the origin, ε_y for these glasses varies from 1.50 to 2.20%, while ε_y for the four M-M glasses studied in Ref. 1 was found to be about 2.10%.

Subsequently, a direct proportionality was demonstrated between H and the shear modulus G for the limited number of M-X glasses where this quantity was measured (3). In tension, non-brittle metallic glasses fail on a localized shear band (4); the observed correlation of H and G indicates that the M-X glasses which were studied (3) fail at a constant shear strain, within experimental uncertainty.

The data reported below were gathered in order to further explore the relationship between the strength and the elastic behavior of M-M glasses over a wide range of H and E and to compare this behavior to that of the M-X glasses.

EXPERIMENTAL METHODS

E data were calculated from the relation $E = \rho V_E^2$; here V_E is the velocity of an extensional wave. Where well-spun ribbons could be obtained, V_E was measured by the ultrasonic pulse-echo technique (5) on such ribbons; alternatively, the impulse induce resonance technique (6) was used on samples cut from foils which had been prepared by the arc-melting piston and anvil technique. For magnetic materials, the pulse-echo measurements were made on samples which were magnetically saturated by the application of a magnetic field sufficient to eliminate magnetostriction effects. The density ρ was either measured directly by an immersion technique or, in some cases, assumed to be 1% less than that of the corresponding crystalline alloy. H values were measured using a Shimadzu microhardness tester with loads ranging from 25 to 100 g; in each case indentation depths were chosen to be less than 1/6 of the thickness of the sample. We estimate that E is accurate to $\pm$ 1.5% and H is accurate (other than for a possible calibration error which would be present in all samples) to $\pm$ 3% (maximum estimated errors).

RESULTS AND DISCUSSION

Our results from measurements of H and E on glasses of the indicated compositions are given in Table 1 and are plotted in Figure 1.

Metal-Metal Glasses: Fig. 1 shows that for the wide range of M-M glasses studied (for which the E and H values cover almost an order of magnitude) H is directly proportional to E.

*CURRENT ADDRESS: Office of Naval Research, 800 North Quincy Street, Arlington, VA 22217

TABLE 1. Vickers Microhardness H and Young's Modulus E of Glassy Alloys

Alloy	H (10^9N/M^2)	E (10^{10}N/M^2)	Reference
1. $Ta_{.555}Ir_{.445}$	11.23	16.91	(6)
2. $Nb_{.55}Ir_{.45}$	10.02	15.06	(7)
3. $Ta_{.55}Rh_{.45}$	9.022	14.85	this study
4. $Nb_{.40}Ni_{.60}$	8.99	13.61	(8)
5. $Ta_{40}Ni_{.60}$	9.36	15.05	(8)
6. $Fe_{.75}B_{.25}$	10.94	18.62	this study
7. $Fe_{.80}B_{.20}$	10.00	16.66	"
8. $Fe_{.85}B_{.15}$	8.58	15.07	"
9. $Fe_{.78}Si_{.10}B_{12}$	9.28	15.67	(9)
10. $Fe_{.84}B_{.08}Zr_{.08}$	8.85	15.03	this study
11. $Ni_{.78}Si_{.10}B_{.12}$	8.00	13.65	(9)
12. $Co_{.78}Si_{.10}B_{.12}$	8.62	14.89	(9)
13. $Ni_{.36}Fe_{.32}Cr_{.14}P_{.12}B_{.06}$	8.07	14.05	this study
14. $Ti_{.50}Ni_{.40}Si_{.10}$	8.33	12.30	(10)
15. $Ti_{.65}Ni_{.25}Si_{.10}$	6.52	9.59	(10)
16. $Ti_{.60}Ni_{.40}$	6.71	9.58	(10)
17. $Zr_{.35}Cu_{.65}$	6.32	9.34	(11)
18. $Zr_{.70}Cu_{.30}$	4.08	6.52	(11)
19. $Zr_{.75}Cu_{.25}$	3.76	6.27	(11)
20. $(Zr_{.5}Cu_{.5})_{.90}B_{.10}$	6.30	9.31	this study
21. $Pt_{.48}Ni_{.36}P_{.16}$	5.38	9.76	"
22. $Pd_{.775}Cu_{.06}Si_{.165}$	4.99	8.77	"
23. $Pd_{.40}Ni_{.40}P_{.15}B_{.05}$	5.40	9.66	"
24. $Ca_{.65}Al_{.35}$	2.61	3.96	(12)
25. $Ca_{.65}Cu_{.35}$	1.77	2.89	(12)
26. $Ca_{.65}Zn_{.35}$	1.51	2.49	(12)
27. $Ca_{.65}Ag_{.35}$	1.28	2.68	this study
28. $Ca_{.65}(Al_{.5}Pd_{.5})_{.35}$	2.07	3.20	"

Where deviations from this relation occur, they are small ($\lesssim$ 5%); even for the Ta-Rh glass which deviated from the straight line for M-M glasses by the greatest amount, the deviation is only approximately twice the experminental uncertainty given above.

The near-universality of this linear relationship for M-M glasses is remarkable and is in striking contrast to the behavior of E vs. H for crystalline metals and alloys. However, it should be pointed out that for some binary alloy glass systems for which study of E and H was possible over a wide composition range, subtle deviations from the "master curve" occur; e.g., the values for Zr-Cu glasses, indicated by a dashed line in Fig. 1, lie on a somewhat different straight line which does not pass through the orgin; the same is true for some other alloy series not represented here (8).

The "master curve" for M-M glasses is characterized by a constant yield strain ε_y=H/3.1·E=0.022; this yield strain appears to be almost independent of the composition and properties of the glasses such as their cohesive energy or the atomic size ratio of constituents. Indeed, the constant value of ε_y for the M-M glasses suggests that these glasses possess inherently similar structures, atomic bonding character and, in particular, plastic flow mechanisms.

As mentioned, the observed universal linear relationship of H and E is in especially marked contrast to the behavior of crystalline alloys;

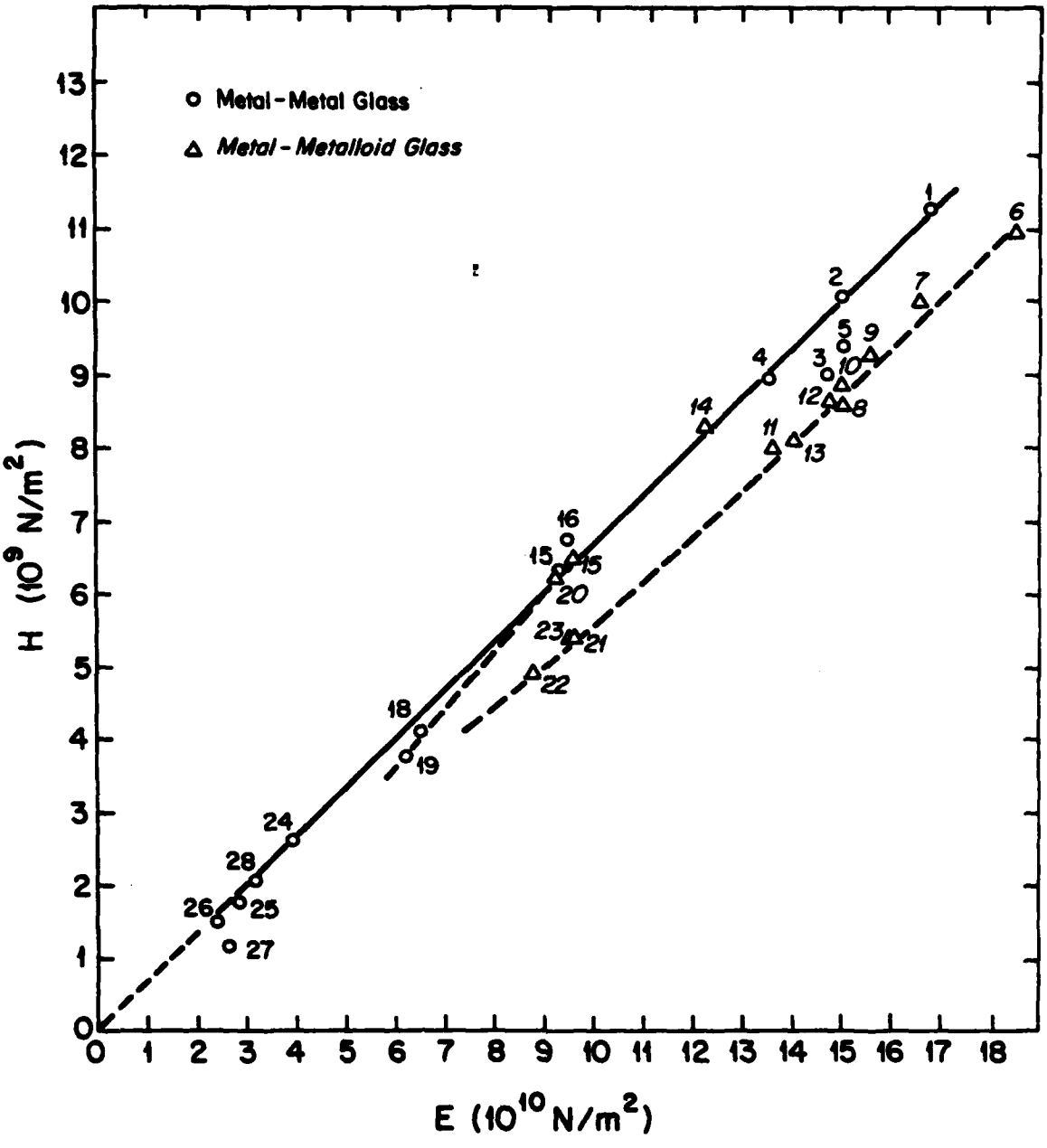

Figure 1 - Plot of Vickers microhardness H against Young's modulus E for various amorphous metals. Numbers correspond to compositions given in Table 1. Data points shown as circles are for alloys containing only metals; data points shown as triangles are for alloys containing metalloids.

since the hardness of crystalline metals depends strongly on the microstructure and degree of crystal perfection, i.e. dislocation content, the H/E value of any given crystalline alloy is not even uniquely determined. Also, H/E values for crystalline metals can be much lower, e.g. ≈0.003 for pure fcc Rh (13) (covalently bonded materials can have much higher H/E values, e.g. H/E ≈0.24 for diamond).

The fact that shear must be present in plastic flow and the observations noted in Ref. 3 suggest that a correlation between H and G may be even stronger than the observed one between H and E. If future observations of G indeed demonstrate a constant shear yield strain, the observed constant tensile yield strain would imply a constant Poisson's ratio $\nu=\frac{E}{2G}-1$ for all M-M glasses studied here; it may be noted that ν is also nearly constant for crystalline metals (14).

Metal-Metalloid Glasses: As suggested in Ref. 1, the data for selected metal-metalloid (M-X) glasses shown in Fig. 1 exhibit lower ν values for a given E, compared to the correlation for M-M glasses. Fe-Co-Ni glasses of high metalloid content, such as $Fe_{.78}Si_{.10}B_{.12}$, $Ni_{.78}Si_{.10}B_{.12}$, $Co_{.78}Si_{.10}B_{.12}$, $Fe_{.75}B_{.25}$, $Fe_{.80}B_{.20}$ and $Fe_{.85}B_{.15}$ form a "lower boundary" in Fig. 1, represented by the dashed line. Other high-metalloid glasses including Pt-X and Pd-X alloys also follow this correlation. However, the separation of M-M and M-X behavior is not complete; Ti_{10}-M-Si glasses follow the M-M correlation and, among the alloys with low B content, $Fe_{.84}Zr_{.08}B_{.08}$ lies on the M-X curve while $Zr_{.45}Cu_{.45}B_{.10}$ is on the M-M curve. Also at lower E and H values the distinction between both curves is lost in the experimental uncertainty, e.g. for Ca-M glasses. Further, we note that the approximate M-X curve, unlike that in Ref. 1, does not appear to intersect the M-M curve at high H and E values.

We have considered the question whether there might be a common master curve for the M-M and M-X hardness values if both were given in terms of G rather than E. Our present H-E data do not suggest a joint relation of H and G for both families of glasses. While we have not studied the Poisson's ratios of the M-M glasses presented here, it is a fact that for transition metals ν varies only over a relatively small range of 0.3 ± 0.05 (14) and it is not likely that M-M glasses have ν values of magnitude and variation required to place all of the data on one H vs. G master curve. For example, the Pd-Cu-Si data point in Fig. 1 has the lowest H/E value of the M-X glasses; this glass also has a rather high ν of ~0.40 (15). For a (hypothetical) M-M glass of equal hardness as Pd-Cu-Si lying on the dashed M-M line to have the G value required to coincide with the H vs. G point of Pd-Cu-Si, ν for this M-M glass (and for all other M-M glasses if the M-M glasses were to have a direct H vs. G proportionality) would need to be ~0.16, which would be an unusually low value (14). It is thus likely that for H vs. G as well as H vs. E there would not be a common master curve for M-M and M-X glasses.

While it is likely that the bonding character of the glasses is responsible for the differences between M-M and M-X glasses, we feel that at this time there are not enough data (especially H-G data) available for a detailed discussion of potentially contributing factors such as directionality of M-X bonds, degree of d-bonding, etc.

ACKNOWLEDGEMENT

In this paper, data from a number of prior studies have been compiled and evaluated. We are pleased to acknowledge support of the individual studies by the Army Research Office Durham, the Office of Naval Research, and the National Science Foundation.

REFERENCES

1. L.A. Davis, Metallic Glasses, J.J. Gilman and J.H. Leamy Editors, p. 190, ASM Metal Park, Ohio (1976).
2. L.A. Davies, Scripta Met., 9 (1975) 431.
3. C.-P. Chou, L.A. Davis and M.C. Narasimhan, Scripta Met., 11 (1977) 417.
4. L.A. Davis, Rapidly Quenched Metals, N.J. Grant and B.C. Giessen, Editors, p. 369, MIT Press (1976).
5. L.A. Davis, C.-P. Chou, L.E. Tanner and R. Ray, Scripta Met., 10 (1976) 937.
6. S.H. Whang, L.T. Kabacoff, D.E. Polk and B.C. Giessen, Met. Trans., 10A (1979) 1789.
7. S.H. Whang, L.T. Kabacoff, D.E. Polk and B.C. Giessen, J. Mat. Sci., 15 (1980) 247.
8. S.H. Whang and B.C. Giessen, to be published.
9. I.W. Donald, S.H. Whang, H.A. Davies and B.C. Giessen, Proceedings of this Conference.
10. S.H. Whang and B.C. Giessen, Proceedings of this Conference and to be published.
11. R.V. Raman, S.H. Whang, D.E. Polk and B.C. Giessen, to be published.
12. J. Hong, Ph.D. Thesis, Northeastern University, Boston, Mass., Oct., 1979.
13. J.J. Gilman, Science of Hardness Testing, J.H. Westbrook and H. Conrad, Editors, ASM Metal Park, Ohio (1973).
14. K.A. Gschneidner, Jr., Solid State Physics, 16 (1964) 275.
15. H.S. Chen, J.T. Krause and E. Coleman, J. Non-Cryst., Solids 18 (1975) 157.

ALLOY CHEMICAL COMPARISON OF THE REFRACTORY METAL - NOBLE METAL PHASE DIAGRAMS T_5-T_{10} (T_5 = V, Nb, Ta; T_{10} = Pd, Pt)*

R. Waterstrat
American Dental Association Health Foundation Research Unit. National Bureau of Standards, Washington, D. C.
and

B.C. Giessen
Materials Science Division, Institute of Chemical Analysis and Department of Chemistry, Northeastern University, Boston, MA

ABSTRACT

The six T_5-T_{10} metal alloy phase diagrams containing Pd or Pt have now all been established. The alloy phases occurring in these systems are tabulated and reviewed here with respect to their structures.

An extensive study of the T-x phase diagrams of the binary alloy systems composed of combinations of the refractory T_5 metals, V, Nb, Ta, on the one side and the noble T_{10} metals, Pd and Pt, on the other side has recently been concluded [1-5] by completion of work on the system Nb-Pt; this was the last remaining, undetermined phase diagram of this group. (The system V-Pd had been previously studied [6].) These studies were undertaken to establish definitively the presence or absence of certain alloy phases in these systems and to determine alloy constitution as a function of temperature and concentration; in the process of this work, alloy chemical information on structures, lattice parameters, etc., has also been gathered. A comparative compilation of the salient alloy chemical features of these systems is therefore possible and is given in the following.

The alloy phase data are arranged into an overview, Table I (which contains data for the alloy chemically related T_5-Ni systems) and four individual Tables II-V, according to phase type and stoichiometry [1-10]. While most of the alloy chemical features are obvious from these Tables, we point out some details in the following.

The tetrahedrally close packed (TCP) phases (also known as Frank-Kasper phases) include Cr_3O (A 15) type, σ type, and μ type phases. Of these, Cr_3O and σ are T_5-rich; μ phases occur only in Ni systems and have AB stoichiometry. Cr_3O and σ-type phases occur together only in two systems, in six systems only one of these types is found, and one system (Nb-Pd) has no TCP phase.

At or near AB, there are high temperature phases in all systems of Nb and Ta with Pd and Pt; while structures have been determined after quenching only in two of them (Nb-Pd and Ta-Pd), all of these phases are assumed to have disordered Cu type structures which are derived from the terminal Pd or Pt solid solutions. Where ordered AB structures exist, they are distorted phases based on the hcp Mg type structure (VPt and NbPt) or the bcc W type structure (TaPd).

---

*Communication No. 164 of the Institute of Chemical Analysis at Northeastern University, Boston, Massachusetts 02115, USA.

Mat. Res. Soc. Symp. Proc. Vol. 19 (1983)

Table I: Intermetallic Phases in T_5-T_{10} Systems (including Ni)

System	T_5-Rich TCP Phases		(Structure Type in Parenthesis) AB		AB_2		AB_3		Ref.
	A_3B	σ	HT	LT	HT	LT	HT	LT	
V-Ni	V_3Ni (Cr_3O)	σ (σ)	Ni s.s.		Ni s.s.	VNi_2 ($MoPt_2$)	Ni s.s.	VNi ($TiAl_3$)	[7]
V-Pd	V_3Pd (Cr_3O)	-	Pd s.s.		Pd s.s.	VPd_2 ($MoPt_2$)	Pd s.s.	VPd_3 ($TiAl_3$)	[6]
V-Pt	V_3Pt (Cr_3O)	-	Pt s.s.	VPt (AuCd)	Pt s.s.	VPt_2 ($MoPt_2$)	Pt s.s.	VPt_3 ($TiAl_3$)	[3]
Nb-Ni	-	-	$NbNi$[a] (μ phase)		-		$NbNi_3$ ($TiCu_3$)		[7]
Nb-Pd	-	-	Pd s.s.	-	$NbPd_2$ ($MoPt_2$)		Pd s.s.	β-$NbPd_3$ (β-$NbPd_3$); α-$NbPd_3$ ($TiAl_3$)	[1]
Nb-Pt	Nb_3Pt	σ	Pt s.s.[b]	NbPt (AuCd)	$NbPt_2$ ($MoPt_2$)		β-$NbPt_3$ (β-$NbPt_3$); α-$NbPt_3$ ($TiCu_3$)		[4]
Ta-Ni[c]	-	-	$TaNi$[a] (μ phase)		$TaNi_2$ ($MoSi_2$)		$TaNi_3$[d] (δ-$TaPt_3$)		[7]
Ta-Pd	-	σ	Pd s.s.	TaPd (γ-TiCu)	$TaPd_2$ ($MoPt_2$)		$TaPd_3$ ($TiAl_3$)		[2]
Ta-Pt	-	σ	Pt s.s.	-	$TaPt_2$ ($TaPt_2$)		β-$TaPt_3$ (β-$NbPt_3$); α-$TaPt_3$ ($TiCu_3$)		[5]

(a) μ phase is TCP (Frank-Kasper) phase
(b) Off-stoichiometric
(c) Ta-Ni also forms Ta_2Ni (Al_2Cu)
(d) $TaNi_3$ ($TiCu_3$) has also been reported [8].

Table II: TCP (Frank-Kasper) Phases in T_5-T_{10} Systems

	Pd	Pt
V	HT:Single phase V s.s. Int.T:2 phase V s.s. + Pd s.s. Lt:V_3Pd:$T_{peritectoid}$ = 840°C Cr_3O-A15 type (cubic) a = 4.815 Å	V_3Pt:$T_{m,peritectic}$ = 1800°C Cr_3O-A15 type a = 4.817 Å (at 25 at.pct. Pt)
Nb	NONE	1. Nb_3Pt (19-28 at.pct. Pt): $T_{m,peritectic}$ = 2040° Cr_3O-A15 type a = 5.139 Å (28 at.pct. Pt): 2. "Nb_2Pt" (31-36 at.pct. Pt) $T_{m,peritectic}$ = 1800°C σ - β-U type (tetragonal) a = 9.940 Å (at 32 at.pct. Pt) c = 5.145 Å (at 32 at.pct. Pt)
Ta	σ:$T_{peritectic}$ = 2550°C σ type a = 9.978 Å c = 5.208 Å	σ:$T_{peritectic}$ ~ 2210°C σ type a = 9.95 Å c = 5.16 Å

The structures of the eight AB_2 phases were comprehensively reviewed earlier [9]. (Nb-Ni does not form an AB_2 phase.) Seven of these eight phases are isostructural ($MoPt_2$ type) and are based on the Cu type structure of the Ni, Pd, or Pt solid solutions.

All AB_3 phases are based on the same ordered, rectangular AB_3 mesh [8,10], but with different stacking sequences, ranging in length from 2 layers (hcp-like) and 3 layers (Cu type-like) to 6 and 12 layers. Of special interest is the conversion of some stacking sequences into the 3 layer type by cold work and the sensitivity of the stacking sequence to impurity content [8].

The quantitative interpretation of the structural transitions between related phases must await future theoretical developments. In terms of the ordering temperatures relative to the melting temperatures, the stability of the ordered T_{10}-rich phases increases on going from V to Ta and from Ni to Pt.

ACKNOWLEDGMENTS

The authors are grateful to the National Science Foundation, the Office of Naval Research, and the American Dental Association Health Foundation Research Unit at the NBS for support.

Table III: AB Phases in T_5-T_{10} Systems

	Pd	Pt
V	Pd s.s. (all T's)	HT: Pt s.s.:T_m ~ 1770°C; LT: VPt :T_{order} ~ 1500°C AuCd - B19 type a = 2.707 Å b = 4.747 Å c = 4.413 Å
Nb	HT: Pd s.s. $T_{m,peritectic}$ ~ 1565°C (at 60 at.pct. Pd) $T_{eutectoid}$ = 1225°C; a = 4.020 Å* LT: (< 1255°C) Two phase Nb s.s. + $NbPt_2$	HT:α'-Pt: $T_{m,peritectic}$ = 1780°C (at 57 at.pct. Pt) $T_{eutectoid}$ = 1670°C (Structure unknown, prob. Pt s.s.); HT/LT: $Nb_{1-x}Pb_{1+x}$ $T_{m,peritectic}$ ~ 1750°C AuCd - B19 type (at 50 at.pct. Pt) a = 2.780 Å b = 4.983 Å c = 4.611 Å
Ta	HT: Pd s.s. T_m ~ 1720°C, $T_{eutectoid}$ = 1550°C a = 4.006 Å;* Int.T : Two phase (c + $TaPd_2$) LT: TaPd:$T_{peritectoid}$ = 1410°C γTiCu - B'1 type a = 3.279 Å c = 6.036 Å	HT: TaPt(HT) $T_{m,peritectic}$ = 1795°C $T_{eutectoid}$ = 1635°C (Structure unknown, prob. Pt s.s.) LT Two phase (c + $TaPt_2$)

*measured on rapidly quenched alloys

They are pleased to acknowledge the superb contributions of their collaborators in this program, Prof. N.J. Grant, Drs. R.H. Kane and D.P. Parker, Ms. R. Koch, and Mr. R.C. Manuszewski.

REFERENCES

1. B.C. Giessen, N.J. Grant, D.P. Parker, R.C. Manuszewski, and R.M. Waterstrat, Met. Trans 11A, 709 (1980).

2. R.M. Waterstrat, B.C. Giessen, R. Koch, and R.C. Manuszewski, Met. Trans 9A, 643 (1978).

Table IV: AB_2 Phases in T_5-T_{10} Systems

	Pd	Pt
V	HT:Pd s.s.:T_m ~ 1360°C; LT:VPd_2:T_{order} = 905°C, $MoPt_2$ type (orthorhombic) a = 2.750 Å b = 8.250 Å c = 3.751 Å	HT:Pt s.s.:T_m ~ 1805°C, a ~ 3.868 Å; LT:VPt_2:T_{order} ~1100°C $MoPt_2$ type a = 2.730 Å b = 8.323 Å c = 3.800 Å
Nb	$NbPd_2$:T_m, peritectic ~ 1610°C $MoPt_2$ type a = 2.839 Å b = 8.376 Å c = 3.886 Å	$NbPb_2$:T_m, peritectic ~ 1990°C $MoPt_2$ type a = 2.801 Å b = 8.459 Å c = 3.951 Å
Ta	$TaPd_2$:T_m, congruent ~ 1800°C $MoPt_2$ type a = 2.896 Å b = 8.397 Å c = 3.790 Å	$TaPt_2$:T_m, congruent ~ 2245°C $TaPt_2$ type (orthorhombic) a = 8.403 Å b = 4.785 Å c = 4.744 Å

3. R.M. Waterstrat, Met. Trans. 4A, 455 (1973).
4. R.M. Waterstrat and B.C. Giessen, Met. Trans., to be published (1983).
5. B.C. Giessen, R.H. Kane, and N.J. Grant, Trans. Met. Soc. AIME 233, 855 (1965).
6. W. Koester and W.D. Haehl, Z. Metallk. 49, 647 (1958).
7. M. Hansen, Constitution of Binary Alloys (McGraw-Hill, NY 1958).
   R.P. Elliott, Constitution of Binary Alloys, First Supplement (McGraw-Hill, NY 1965).
   F.A. Shunk, Constitution of Binary Alloys, Second Supplement (McGraw-Hill, NY 1969).
8. B.C. Giessen and N.J. Grant, Acta Met. 15, 871 (1967).
9. B.C. Giessen and N.J. Grant, J. Less-Common Metals 8, 114 (1965).
10. B.C. Giessen and N.J. Grant, Acta Cryst. 17, 615 (1964).

Table V: AB_3 Phases in T_5-T_{10} Systems

	Pd	Pt
V	HT: Pd s.s.:T_m ~ 1375°C; LT: VPd_3:T_{order} = 815°C, $TiAl_3$ type (3ℓ) (tetragonal) a = 3.847 Å c = 7.751 Å.	HT:Pt s.s.:T_m ~ 1800°C a ~ 3.879 Å LT:VPt_3:T_{order} = 1015°C $TiAl_3$ type (3ℓ) a = 3.861 Å c = 7.824 Å.
Nb	HT:α-Pd s.s.:T_m ~ 1625°C; LT:(<~ 1600°C) β-$NbPd_3$:β-$NbPd_3$ type (6ℓ) (orthorhombic) a = 5.486 Å b = 4.845 Å c =13.602 Å; α-$NbPd_3$:$TiAl_3$ type (3ℓ) a = 3.895 Å c = 7.913 Å.	$NbPt_3$:$T_{m,congruent}$ ~ 2040°C β-$NbPt_3$:β-$NbPt_3$ type (12ℓ) (monoclinic) a = 5.537 Å α = 90°32' b = 4.870 Å c = 27.33 Å. α-$NbPt_3$:$TiCu_3$-DO_a type (2ℓ) (orthorhombic) a = 5.534 Å b = 4.873 Å c = 4.564 Å.
Ta	$TaPd_3$:$T_{m,congruent}$ = 1770°C $TiAl_3$ type (3ℓ) a = 3.880 Å c = 7.978 Å.	$TaPt_3$:$T_{m,congruent}$ = 2065°C β-$TaPt_3$:β-$NbPt_3$ type (12ℓ) a = 5.537 Å α = 90°32.4' b = 4.869 Å c =27.33 Å; α-$TaPt_3$:$TiCu_3$ type (2ℓ) a = 5.538 Å b = 4.874 Å c = 4.560 Å.

CRYSTAL CHEMISTRY OF METASTABLE ALLOY PHASES*

B. C. Giessen
Materials Science Division, Institute of Chemical Analysis and Department of Chemistry, Northeastern University, Boston, Massachusetts 02115 USA

EXTENDED ABSTRACT

Knowledge of the metastable crystalline alloy phases that can be prepared from the liquid or vapor by non-equilibrium methods is useful because the descriptive crystal chemistry of an alloy system should include metastable phases stable with respect to the components but unstable respective to other intermediate phases [1]. Alloy phases within a certain range of positive free energy of formation are also of interest, especially for systems without equilibrium phases. Accordingly, there have been some systematic "hunts" for metastable alloy phases (MAP's) that can be prepared by rapid liquid quenching, reviewed in Refs. 2-7. The principal results of these studies on disordered (element-like) and ordered MAP's and some additional data are presented here.

Phase Diagrams: The phase diagram representation of MAP's is discussed in Ref. 4; typically, MAP's are presented in: a "quenched phase plot" showing the composition ranges of MAP's prepared by quenching; an augmented T-x phase diagram modified by incorporating metastable phases; an augmented free energy diagram; and an operational plot showing those phases retained by quenching to a specific supercooling temperature ΔT_s or by quenching at a given cooling rate.

Disordered MAP's: Many B-metal phases of this type containing elements of the Cu, Zn, Al, Si and As (B1 to B5) groups have been prepared by quenching to -196°C [2,5,8,9,10]. Some of the findings were:

Metastable Hume-Rothery (HR) phases (VEC controlled) based on Ag and Au can be prepared in systems in which the characteristic sequence α, β (or ε), γ is incomplete, such that a metastable HR phase is retained with the structure and VEC of the first "missing" HR phase [10].

Many alloys of Zn, Cd, Ga, Sn, Pb, Bi and other low melting normal B-metals form MAP's with the Cu type (fcc), In type (tetragonal, c/a ≲1), γ (HgSn δ-10) type (simple hexagonal), β-Sn type (tetragonal) and π(α-Po) type (simple cubic). These alloy phases lie in phase fields (characterized qualitatively by ranges of the average VEC and average potential) containing many stable and metastable alloys with different combinations of components and identical crystal structures. Many of these structures have gradual or discontinuous transitions to other stable or metastable phases or connect isolated, isostructural regions, e.g., in the Cd-In system [8]. The occurrence of these phases can be understood in terms of pseudopotential theory [2].

In B-metals, some MAP's are structurally related to high pressure (HP) phases. Thus, in the (simple eutectic) Al-Ga system, a MAP with the In type is isostructural with a HP phase of Ga; conversely, the MAP may have the (hypothetical) equilibrium structure of hydrostatically "expanded" Al [11].

Some recent results are: A (Ga-Zn) MAP [12] is related to another HP form of Ga. An unexpected, elemental crystal structure was found in the Hg-In system, where a MAP with the actinide structure of β-U was formed [9]. An ω type phase is formed by partial equilibration of a Zr-rich Zr-Cu glass [13].

---

*Communication # 165 of the Institute of Chemical Analysis at Northeastern University, Boston, Massachusetts 02115, USA.

Mat. Res. Soc. Symp. Proc. Vol. 19 (1983)

Ordered MAP's: Ordered MAP's were comprehensively reviewed in 1976 [7]; since then, many additional ordered MAP's were reported. Classification of ordered MAP's [7] is based on their crystal chemical relationships to stable phases or other metastable phases in the same system or in chemically related ones.

Some ordered MAP's have very complex crystal structures: thus, metastable Au_4Si has a tetragonal subcell with 10 atoms/cell and a supercell where at least one cell edge is 3 times that of the subcell [14]. Ordered MAP's are often formed as transition phases during equilibration of metallic glasses; a recent example is m-BeTi [15].

Ordered MAP's appear somewhat unpredictably in rapidly quenched alloys, especially T metal alloys. Since as yet there is no generally recognized theory for the correlation and structural prediction of ordered alloy phases, an understanding of the numerous ordered MAP's interspersed between equilibrium phases must also await the development of such a theoretical framework.

ACKNOWLEDGMENT

Parts of this work have been supported by the NSF and the ONR to whom I am grateful for sponsorship. It is also a pleasure to thank recent collaborators in this program, especially Drs. R. St. Amand, T.X. Mahy, R. Raman and M. Segnini and Mr. D. Szymanski.

REFERENCES

1. A.K. Jena, B.C. Giessen, M.B. Bever, and N.J. Grant, Acta Met., 16, 1047 (1968).
2. B.C. Giessen, in Adv. in X-Ray Analysis, C.S. Barrett, G.R. Mallett, and J.B. Newkirk, Eds., Vol. 12 (Plenum Press, New York, 1969), 23.
3. B.C. Giessen, in Developments in the Structural Chemistry of Alloy Phases, B.C. Giessen, Ed. (Plenum Press, New York, 1969), 227.
4. B.C. Giessen and R.H. Willens, in Phase Diagrams; Materials Science and Technology, Vol. III, A.M. Alper, Ed. (Academic Press, New York, 1970), 103.
5. W.B. Pearson, The Crystal Chemistry and Physics of Metals and Alloys (Wiley-Interscience, New York, 1972), 287.
6. A.K. Sinha, B.C. Giessen and D.E. Polk, in Treatise on Solid State Chemistry, N.B. Hannay, Ed., Vol. III (Plenum Press, New York, 1979), 1.
7. B.C. Giessen, in Proc. Second Internat. Conf. on Rapidly Quenched Metals, Section I, N.J. Grant and B.C. Giessen, Eds. (MIT Press, Cambridge, MA, 1976), 351.
8. P.K. Srivastava, B.C. Giessen and N.J. Grant, Acta Met., 16, 1199 (1968).
9. T.X. Mahy, Ph.D. Thesis, Northeastern University, Boston, MA, 1978.
10. B.C. Giessen, Z. Met., 59, 805 (1968).
11. B.C. Giessen, U. Wolff, and N.J. Grant, J. Appl. Cryst., 1, 30 (1968).
12. D. Szymanski, J.C. Barrick and B.C. Giessen, J. Sol. State Chem., 30, 55 (1979).
13. R. Raman, Ph.D. Thesis, Northeastern University, Boston, MA, 1979.
14. B.C. Giessen and J.C. Barrick, unpublished results.
15. B.C. Giessen and L. Tanner, Met. Trans., 9A, 67 (1978).